Electronic Precompensation of Dispersion and Nonlinearities in Fibre-Optic Transmission Systems

vorgelegt von
Diplom-Ingenieur
Christian Weber
aus Quedlinburg

Von der Fakultät IV - Elektrotechnik und Informatik
der Technischen Universität Berlin
zur Erlangung des akademischen Grades

Doktor der Ingenieurwissenschaften
Dr.-Ing.

genehmigte Dissertation

Promotionsausschuss:

Vorsitzender:	Prof. Dr.-Ing. Hans-Joachim Grallert
Berichter:	Prof. Dr.-Ing. Klaus Petermann
Berichter:	Prof. Dr.-Ing. Werner Rosenkranz

Tag der wissenschaftlichen Aussprache: 8.1.2010

Berlin 2010
D 83

Danksagung

Den Erfolg dieser Arbeit habe ich vielen Menschen zu verdanken. Ich möchte sie an dieser Stelle erwähnen.

Mein besonderer Dank gilt Herrn Prof. Petermann für seine ausgezeichnete Betreuung der Promotion. Sein tiefes Verständnis für optische Nachrichtentechnik, sein Scharfsinn sowie sein geduldiger und offener Geist förderten und formten diese Arbeit maßgeblich. Es war mir eine Ehre, unter seiner Leitung zu promovieren.

Des Weiteren danke ich Prof. Rosenkranz für die Erstellung des Gutachtens und Prof. Grallert für seine Arbeit als Vorsitzender des Promotionsausschusses.

Bei meinem zweitem Betreuer Christian Bunge möchte ich mich ganz besonders bedanken. Er hat das Projekt initiiert und mit seinen Ideen und Beiträgen immens vorangetrieben. Herzlich gedankt sei auch allen Mitarbeitern des Fachgebiets Hochfrequenztechnik: den Technologen im ersten Stock, allen technischen Mitarbeitern, Frau Hamer und natürlich den Kollegen des dritt3n Stocks. Ich danke ganz besonders Stefan Warm, Johannes Fischer und Marcus Winter für die freundschaftliche Arbeitsatmosphäre und die zahlreichen guten Ideen, die sie eingebracht haben. Ihr habt einen großen Anteil am Gelingen der Arbeit! Es war ein Privileg, mit so engagierten und klugen Kollegen zusammenzuarbeiten. Marcus danke ich zusätzlich für seine Ratschläge zum Layout und zur Typographie dieses Buches.

Ohne Finanzierung geht bekanntlich gar nichts. Daher möchte ich mich hiermit für die Förderung durch das Eibone-Projekt[1] des Bundesministeriums für Bildung und Forschung (BMBF) bedanken.

Außerdem möchte ich mich ganz besonders herzlich bei meiner Familie und meinen Freunden bedanken. Ihr habt mir Kraft für diese Arbeit gegeben, indem ihr mich in allen Dingen unterstützt habt und indem ihr einfach da ward. Danke dafür!

Als Christ danke ich zum Abschluss meinem Herrn Jesus Christus für die Kraft, Ausdauer, Weisheit und Freude, die er mir für diese Arbeit geschenkt hat. Ihm gebührt alle Ehre.

Christian Weber

Berlin, 14. Januar 2010

[1] Eibone - Efficient Integrated Backbone

Abstract

Fibre-optic transmission at high bit rates is limited by several optical impairments such as chromatic dispersion and fibre nonlinearities. The compensation of these effects was typically carried out completely in the optical domain, e.g. using dispersion compensating fibres (DCF) and dispersion management. However, optical components have several disadvantages including high cost, physical size, additional loss, latency and lack of adaptability. Recent advances in high speed digital signal processing have enabled high bit rate electronic impairment mitigation in the transmitter or receiver electronics as an attractive alternative to optical compensation, allowing for adaptability, cost savings and a simplified link design.

This thesis focuses on the mitigation of chromatic dispersion and fibre nonlinearities at the transmitter in long-haul 10 and 40 Gbit/s/channel wavelength division multiplexing transmission over standard single mode fibre using direct detection. In particular, fundamental limitations due to nonlinearities are studied using numerical simulations by assuming an ideal precompensating transmitter and unrestricted hardware complexity. We pay special attention to the role of the bit pattern length and the statistical nature of interchannel nonlinearities. In addition, practical limitations due to realistic hardware components are investigated by modelling the nonlinear digital filter based on look-up tables, the digital-to-analog conversion (DAC) and the field modulator.

We consider three cases: electronic predistortion (EPD) of chromatic dispersion, EPD of intrachannel nonlinearities and combined EPD of dispersion and intrachannel nonlinearities. The EPD systems are compared to conventional optically dispersion compensated (ODC) systems. Generally, it is found that 10 Gbit/s EPD systems suffer from severe degradations due to intra- and interchannel nonlinearities compared to optical dispersion compensation (ODC). At 40 Gbit/s, however, the limitations of EPD due to nonlinearities are less critical in comparison to ODC, showing that the nonlinear tolerance of EPD improves at higher bit rates.

The analysis of the hardware limitations at 40 Gbit/s reveals that a DAC sampling rate of at least 60 GSa/s with 4 bit resolution and a triple Mach–Zehnder modulator (MZM) are required. Further, we show that precompensation of dispersion introduces a large channel memory that requires digital filters with a long impulse response in the precompensating transmitter. As an alternative, we combine EPD of intrachannel nonlinearities and optical dispersion compensation in ODC systems with a resonant dispersion map, thus allowing for a reduced channel memory. A significantly increased nonlinear tolerance is demonstrated.

Zusammenfassung

Hochbitratige Glasfaserübertragungssysteme werden durch verschiedene optische Effekte wie chromatische Dispersion und Fasernichtlinearitäten begrenzt. Die Kompensation dieser Effekte wird typischerweise durch rein optische Techniken erreicht, z.B. dispersionskompensierende Fasern (DCF), Dispersionsmanagement oder optimierte Modulationsformate. Allerdings weisen optische Komponenten einige Nachteile auf: hohe Kosten, physische Größe, zusätzliche Verluste, Signallaufzeitverzögerungen und fehlende Adaptierbarkeit. Alternativ zur optischen Kompensation wird zunehmend elektronische Signalentzerrung in der Sende- oder Empfangselektronik untersucht, deren Einsatz in hochbitratiger Übertragung erst durch die aktuellen Fortschritte bei der Entwicklung schneller digitaler Signalverarbeitung ermöglicht wurde. Vorteile sind unter anderem die geringeren Kosten, die Adaptierbarkeit auf zeitlich veränderliche Störungen sowie die Möglichkeit zur Vereinfachung des optische Streckendesigns.

In dieser Arbeit wird die senderseitige Vorkompensation der chromatischen Dispersion und der Fasernichtlineartitäten in Weitverkehrsübertragungsstrecken bei Bitraten von 10 und 40 Gbit/s behandelt. Als optischer Empfängertyp wird Direkt-Detektion betrachtet. Das Ziel der Arbeit ist einerseits die Analyse fundamentaler Begrenzungen durch Nichtlinearitäten im Einkanal- und Wellenlängenmultiplex-Betrieb. Dazu werden numerische Simulationen präsentiert, bei denen ein ideal vorverzerrender Sender ohne Beschränkung des Hardware-Aufwands angenommen wird. Im Hinblick auf die Genauigkeit der Simulationen diskutieren wir die Rolle der verwendeten Bitsequenzlängen und berücksichtigen die Statistik der Interkanalnichtlinearitäten. Des Weiteren werden praktische Begrenzungen untersucht, die durch die Verwendung realistischer Hardware-Komponenten gegeben sind. Insbesondere werden nichtlineare digitale Filter (look-up tables), Digital-Analog-Wandler (DAC) und der verwendete Mach–Zehnder Modulatortyp (MZM) betrachtet.

Wir untersuchen drei Fälle: Elektronische Vorverzerrung (EPD) der chromatischen Dispersion, kombinierte EPD von Dispersion und Intrakanalnichtlinearitäten sowie EPD von Intrakanalnichtlinearitäten in optisch dispersionskompensierten Strecken. Die EPD Systeme werden verglichen mit konventionellen optisch dispersionskompensierten Systemen (ODC). Es zeigte sich, dass die EPD Systeme bei einer Datenrate von 10 Gbit/s im Allgemeinen stärker von Intra- und Interkanalnichtlinearitäten beeinträchtigt werden als ODC Systeme. Bei 40 Gbit/s EPD Systemen ergibt sich hingegen eine ähnliche nichtlin-

eare Schwelle wie bei ODC System. Die Toleranz gegenüber Nichtlinearitäten verbessert sich also bei einer Erhöhung der Datenrate zugunsten von EPD.

Für eine mögliche praktische Realisierung der EPD Technik sind die Hardware-Anforderungen des vorverzerrenden Senders von besonderem Interesse. Die diesbezüglichen Untersuchungen ergaben, dass für eine effiziente Kompensation der Dispersion bei 40 Gbit/s mindestens eine DAC-Wandlerrate von 60 GSa/s mit 4 Bit Auflösung und ein Dreifach-MZM benötigt werden. Weiterhin zeigen wir, dass die senderseitige Vorkompensation der Dispersion ein langes Kanalgedächtnis erzeugt, das digitale Filter mit einer langen Impulsantwort erfordert. Zur möglichen Reduzierung des Kanalgedächtnisses wenden wir die Vorverzerrung der Intrakanalnichtlinearitäten in optisch dispersionskompensierten Strecken mit resonantem Dispersionsschema an und zeigen eine deutlich erhöhte Toleranz gegenüber Nichtlinearitäten.

Contents

CHAPTER 1

Introduction

> "The Americans have need of the telephone, but we do not. We have plenty of messenger boys."
>
> *William Preece, Chief Engineer, British Post Office*[1].

Telecommunication is the exchange of information over a distance[2]. For centuries, messages were transported by messengers, or couriers. In spite of Preece's statement, telecommunications replaced the service of messengers (even in Great Britain) by mechanical telegraph in 1794, by copper wires in 1837, by electromagnetic waves in 1896, and by optical fibre around 1980 [Huurdeman2003].

Ever since the first fibre-optic communication systems were installed, the needs, the opportunities and the economic conditions of the telecommunication industry have stimulated the research and development of numerous technical advances, allowing terabits of data to be transmitted over trans-oceanic distances. The recent emergence of high-speed digital signal processing in the electronic domain to compensate for impairments caused in the optical domain is one such advance. In order to understand the evolution of fibre-optic transmission systems towards the techniques covered in this thesis, we will briefly

[1] In 1879, Preece officially reported this statement to a House of Commons committee two years after Alexander Graham Bell's telephone was first demonstrated in Great Britain [Huurdeman2003, p. 167].

[2] tele (Greek): distant, communicare (Latin): to share

review some of the relevant developments in fibre-optic transmission history based on [Agrawal2002, Huurdeman2003, Savory2007a, Abbott2008].

1.1. History of Digital Signal Processing in Fibre-Optics

The idea to use electronic signal processing for optical systems already emerged in the early days of fibre-optic transmission history. A 140 Mbit/s experimental field trial in Great Britain, reported in [Hill1977], used electronic equalisation. The first proposed electronic predistortion (EPD) transmission [Koch1985] dates back to 1985 when 4 Gbit/s transmission was the state-of-the-art technology. The authors use a time-division-multiplexing technique to optically superpose individually predistorted pulses and demonstrate the effectiveness of the approach using a proof-of-principle experiment. However, these technologies were not implemented in commercial systems since the available speed of electronic signal processors was significantly lower than required for high-bit rate optics.

In the beginning of the 1990s, the advent of optical erbium-doped fibre amplifier (EDFA) had a huge impact on the transmission system design since it allowed optical amplification over a wide optical bandwidth range without opto-electronic conversion. The so called O-E-O[3] repeaters that were used to periodically regenerate the signal in the electronic domain could be replaced by optical amplifiers, thus, simplifying the link design and saving cost. With optical amplifiers, no high-speed electronic circuits were required for signal regeneration. While the EDFA provides optical amplification over a bandwidth of a few terahertz, it requires only low-speed control circuits for operation.

The EDFA was a strong driver for the wavelength division multiplexing (WDM) technology. Using WDM, data can be transmitted over multiple wavelength channels within one fibre to utilise the fibre's vast bandwidth. The growing demand for capacity was a strong driver for the explosive growth in the terrestrial long-haul network in the time period up to the year 2000. Coincident with the implementation of WDM in commercial systems was the increase of the bit rate per channel to 10 Gbit/s. Optical impairments such as chromatic dispersion and fibre nonlinearities became an increasingly relevant factor in dense WDM systems operated at this bit rate. Compensation of dispersion and suppression of nonlinearities was carried out completely in the optical domain using, e.g., negative-dispersion fibres, dispersion management and optimised modulation formats. Compensation using optical components such as

[3] O-E-O: Optical-electrical-optical. The acronym describes the conversion from the optical to the electrical domain followed by regeneration of the data and conversion back to the optical domain.

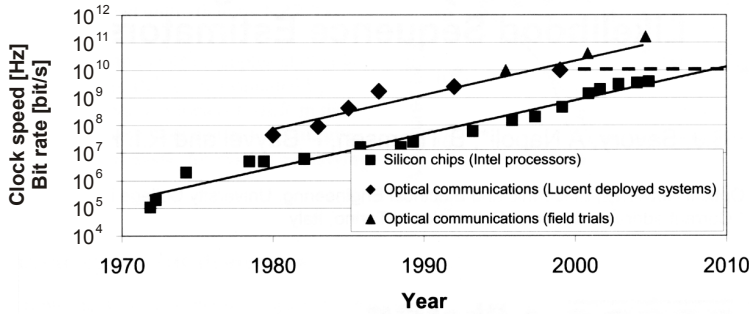

Figure 1.1. *Bit rate evolution of fibre-optic transmission system installed by Lucent and clock speeds of silicon chips fabricated by Intel. ©IEEE 2005, reproduced from [Savory2005] with kind permission from the IEEE and the author.*

negative-dispersion fibres have several disadvantages, e.g. high cost, physical size, additional loss, additional latency and lack of adaptability.

In order to illustrate the evolution of fibre-optic transmission systems and digital signal processing, Fig. 1.1 shows a graph of the channel bit rates in commercial optical systems (installed by Lucent) and the speed of processor chips by Intel [Savory2005]. It can be seen that the bit rate in optics and the chip speed have increased in parallel. The increasing speed of electronics, however, shows a delay of approximately 12 years compared to optics. This explains why complex digital signal processing functions could not be applied to fibre-optic transmission until recently.

The collapse of the telecommunications market near the end of 2000 put an end to the demand for increasing bit rate. After the economic downturn, cost reduction was the driver instead of capacity growth. As a result, the introduction of 40 Gbit/s to commercial systems was delayed and the bit rate stayed at 10 Gbit/s for a decade, indicated by the dashed line in Fig. 1.1. This created an opportunity for the development of digital signal processors to reach the clock speeds required for impairment equalisation of fibre-optic transmission links.

The new generation of digital signal processing components in optics was marked by a maximum likelihood sequence estimation (MLSE) chip for receiver side equalisation operating at a sample rate of 25 GSa/s [Färbert2004] and by a transmitter side processor carrying out electronic dispersion precompensation combined with a pair of 20 GSa/s digital-to-analog converters (DAC) [McNicol2005]. Both chips improve the system performance of optical 10 Gbit/s transmission links by digitally mitigating optical signal degradations. More pre-

cisely, MLSE and EPD compensate for accumulated chromatic dispersion and may therefore replace negative-dispersion fibres in the link allowing for simplified link designs and thus cost savings. In addition, electronic compensation can be made adaptive to cope with time varying impairments. A series of developments in high-speed electronic digital signal processing technology followed which, according to [Shtaif2008] and [Cartledge2009], created a new paradigm in optical communications. The realisation of high-speed digital-to-analog converter (DAC) and analog-to-digital converter (ADC) devices, and digital signal processors have allowed to overcome optical distortions and enabled the adoption of more spectrally efficient modulation formats.

As a general classification, signal processing electronics are either implemented at the transmitter or at the receiver. Electronic equalisation schemes use post-detection linear and nonlinear filtering, e.g. feed-forward equaliser (FFE) and decision feedback equaliser (DFE) filter structures in the receiver. Compensation of the effects of chromatic dispersion and polarisation mode dispersion (PMD) was demonstrated [Bülow2002]. However, the loss of the phase information after square-law detection limits the maximum accumulated dispersion that can be compensated electronically using signal processing to approximately 150 km standard single mode fibre (SSMF) in 10 Gbit/s transmission [Watts2005]. Theoretically, longer uncompensated transmission of several hundreds of kilometers may be possible using MLSE [Bosco2006] and nonlinear Volterra filters [Xia2007].

Recently, coherent detection has attracted renewed attention for receiver side impairment mitigation. Before the advent of the EDFA in 1989, coherent detection was already discussed as a potential technology to improve the receiver sensitivity. However, research into coherent detection decreased after the invention of the EDFA because comparable sensitivities were achieved by optically preamplified direct detection using an EDFA.

The recently revived interest in coherent detection is explained by the fact that it allows to transfer both the amplitude and the phase information to digital receiver electronics, thus, substantially extending the electronic mitigation possibilities. In particular, the linear effects of chromatic dispersion and PMD can be implemented easily by adaptive electronic filtering at the receiver [Shtaif2008]. Therefore, advanced coherent receiver technologies are currently investigated as a potential candidate for future 100 Gbit/s transmission driven by signal processing technologies that were not available a decade ago and by the demand for spectrally more efficient modulation formats such as quadrature phase shift keying (QPSK) [Savory2007, Sun2008, Nelson2009].

At the transmitter, an optical field modulator such as the Cartesian modulator [Griffin2002] allows to control the amplitude and phase of the transmitted

field. Driving the modulator with appropriate drive signals enables predistortion of the optical field to precompensate for fibre impairments, such as chromatic dispersion and fibre nonlinearities. This technique is referred to as EPD. It combines the advantages of using a simple direct detection receiver and having access to both the phase and the amplitude of the optical field using a complex field modulator. Alternatively, electronic dispersion precompensation has been demonstrated using a directly modulated laser, eliminating the need for a costly external modulator [Warm2008]. However, we focus the following discussion on EPD for long-haul applications over several hundred to thousand kilometers which is only feasible using external modulation.

Electronic precompensation for chromatic dispersion over more than 5000 km has been proposed and demonstrated for systems operating at 10 Gbit/s in 2005 and 2006 [ElSaid2005, Killey2005, O'Sullivan2005, Birk2006]. In fact, Nortel Networks developed a commercial solution for electronic domain compensation of dispersion and proclaimed that "optical dispersion compensation is obsolete" [Roberts2005]. Controversial discussions were stimulated, in particular at the ECOC 2005, where the EPD technique was experimentally demonstrated [O'Sullivan2005] while other authors raised concerns about the reduced tolerance to nonlinearities at 10 Gbit/s [Essiambre2005a, Winzer2005].

Although there are a number of published successful experiments of EPD at 10 Gbit/s, e.g. [Birk2006, Watts2007a], scaling of this technique to higher bit rates of 40 Gbit/s and above has not been addressed in great detail. It has been stated that the linear filters required for dispersion precompensation can be scaled to 40 Gb/s and on to 100 Gb/s as the evolution of the CMOS process provides more gates [Roberts2008]. However, the impact of fibre impairments, e.g. the Kerr nonlinearities, and the requirements on transmitter hardware, e.g. the DAC sampling rate, in such precompensated high bit rate transmission systems require further investigation.

1.2. Aims and Overview of the Thesis

This thesis presents a study on electronic precompensation of dispersion and nonlinearities in high bit rate direct-detection fibre-optic transmission systems. In particular, fundamental limitations due to fibre nonlinearities and practical limitations due to realistic hardware components are explored.

The thesis is organised as follows. Chapter 2 introduces the theoretical background of fibre-optic transmission systems required for the rest of the thesis. Linear and nonlinear fibre impairments which affect the transmission are explained. Modulation formats and the corresponding transmitter and receiver

structures are discussed. In addition, methods for characterising the nonlinear tolerance of a transmission system are presented.

Chapter 3 considers only linear precompensation of chromatic dispersion. If dispersion is precompensated, fibre nonlinearities will present a fundamental limit to the performance. The impact of intra- and interchannel nonlinear effects is analysed at 10 and 40 Gbit/s. The results are compared to a conventional optically dispersion compensated system. Practical requirements of digital signal processors and digital-to-analog converters are studied. The nonlinear tolerance of a precompensated system is compared to an inline compensated system using realistic system conditions in single channel and WDM operation at 40 Gbit/s.

Electronic predistortion of fibre nonlinearities will be addressed in Chapter 4. Improvements in the nonlinear tolerance are shown for systems using a combination of dispersion and nonlinearity precompensation at 10 Gbit/s in the single channel and WDM case. We find that implementing this technique at 40 Gbit/s leads to an enormous complexity increase and discuss an alternative predistortion scheme which uses a combination of electronic predistortion of nonlinearities and optical inline compensation. It is shown that this scheme achieves effective compensation of intrachannel nonlinearities.

Finally, the thesis is summarised in Chapter 5. We draw conclusions concerning the impact of nonlinearities in precompensated transmission systems at bit rates of 10 and 40 Gbit/s. The perspectives of EPD, recommendations for further research and possible alternatives for electronic signal processing in future high bit rate systems are discussed.

1.3. Original Contributions

The following list shows the original contributions of my research during the thesis work and the corresponding publications.

- Digital electronic precompensation of intrachannel nonlinearities was proposed in a transmission system which consists of 100% dispersion-compensated spans [Weber2006a]. The impact of different Mach–Zehnder transmitter structures was compared [Weber2006]. Simulation results demonstrate that effective compensation of intrachannel nonlinearities is achieved. This study is part of Chapter 4.
- A numerical investigation on various advanced modulation formats for EPD of intrachannel nonlinearities was carried out in a collaboration with the Technische Universität München [Hellerbrand2007].

- The implications of the channel memory length for electronic mitigation of dispersion and nonlinearities was studied using an MLSE receiver and a precompensating transmitter [Weber2007]. It was shown that the processor memory requirements for look-up table (LUT) based nonlinearity compensation and MLSE equalisation increase drastically if the bit rate is changed from 10 to 40 Gbit/s. The implications for nonlinearity predistortion are discussed in Chapter 4.
- The impact of intrachannel nonlinearities in linearly dispersion precompensated 10 and 40 Gbit/s single channel transmission was studied. While EPD at 10 Gbit/s suffers from severe degradations, the 40 Gbit/s results assuming an ideal EPD transmitter show that no significant reduction of the nonlinear tolerance is expected compared to optical inline dispersion compensation [Weber2008]. Chapter 3 contains these investigations.
- Fundamental nonlinear limitations of WDM systems using linear electronic dispersion precompensation are studied at high bit rates. The statistical distributions of cross-phase modulation (XPM) induced penalties were considered at 10 and 40 Gbit/s. In contrast to 10 Gb/s systems, only a small performance degradation due to XPM was found at 40 Gb/s [Weber2009], cf. Chapter 3.
- A comprehensive study on the impact of intra- and interchannel nonlinearities in high bit rate EPD systems was carried out and published in [Weber2009a]. The simulations take into account realistic EPD transmitter hardware as well as the additional optical loss and nonlinearities of dispersion compensating fibre in optical dispersion compensation (ODC) systems. Using the realistic system modelling, it is shown that EPD is expected to achieve a nonlinear tolerance which is only slightly worse than that of conventional ODC systems. This study is part of Chapter 3.

CHAPTER 2

Theory of Fibre-Optic Transmission Systems

This chapter provides the theoretical background of fibre-optic transmission systems which is required for the rest of the thesis. First, a complete transmission system is presented to give an overview of the typical components. Next, the sources of impairments are described including noise, linear fibre effects such as chromatic dispersion and nonlinear fibre impairments such as the Kerr effect. For ideal compensation of chromatic dispersion and fibre nonlinearities, the theory of phase conjugation is presented in Section 2.6. Finally, the receiver model including the estimation of the bit error rate (BER) is described in Section 2.7.

2.1. Overview

The generic setup of a fibre-optic point-to-point transmission system is shown in Fig. 2.1. In the transmitters (Tx), the data bits are modulated on optical carriers at wavelengths $\lambda_1 \ldots \lambda_N$ using a specific modulation format. A multiplexer performs optical bandpass filtering of the individual wavelength channels and combines them into a single optical fibre.

The optical field carrying the wavelength division multiplexing (WDM) signal propagates along the transmission fibre. During propagation the signal is affected by several linear and nonlinear fibre impairments such as attenuation, chromatic dispersion and fibre nonlinearities. Depending on the required

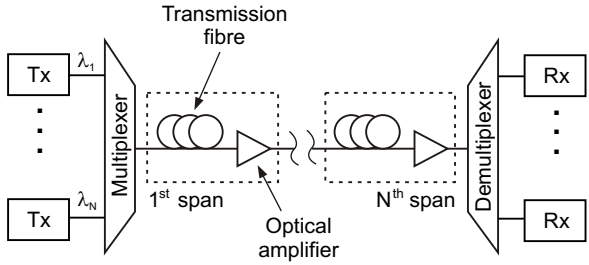

Figure 2.1. *Basic setup of a WDM optical line transmission system.*

Table 2.1. *Transmission distances of WDM systems [Winzer2006, Green2001].*

System	Distance
Access	$<$ 100 km
Metro	$<$ 300 km
Long-haul	$>$ 300 km
Ultra long-haul	$>$ 3,000 km

transmission distance, the transmission line consists of fibre spans which include the transmission fibre, an optical amplifier, and, if necessary, some form of inline dispersion compensation. Inline dispersion compensation may be omitted if alternative dispersion compensation schemes are employed such as electronic dispersion compensation which will be discussed in Chapter 3. Further, it depends on the data rate and the transmission distance if dispersion compensation is required. Table 2.1 lists typical transmission distances of optical communication networks [Winzer2006, Green2001]. This thesis focuses on long-haul systems operated at data rates of 10 Gbit/s and above where chromatic dispersion and fibre nonlinearities are the important impairments.

After transmission over the fibre spans, the WDM signal is split into the individual wavelength channels by the demultiplexer which acts as an optical bandpass filter. Each wavelength is detected using a receiver (Rx) where the signal is demodulated to recover the transmitted information.

In the next sections, we will discuss modelling aspects and important characteristics of the system components.

2.2. Transmitter and Modulation Formats

The transmitter encodes the digital binary information on the optical field waveform. The optical field is described by its time domain electrical field vector

$$\mathbf{E}(t) = \mathrm{Re}\left\{\underline{A}(t)\exp(j\omega_0 t)\right\}\mathbf{e}(t) \tag{2.1}$$

where $\mathbf{e}(t)$ is a unit vector indicating the polarisation, $\underline{A}(t)$ is the complex amplitude, ω_0 is the angular frequency corresponding to the WDM channel's carrier wavelength $\lambda_0 = 2\pi c/\omega_0$. The complex amplitude phasor may be written as

$$\underline{A}(t) = A(t)\exp(j\varphi(t)) \tag{2.2}$$

where $\varphi(t)$ is the time-dependent phase. The amplitude is assumed to be normalised such that $|\underline{A}|^2$ represents the optical power P. From (2.1) it follows that the optical wave offers three physical properties that can be modulated with information: amplitude $A(t)$, phase $\varphi(t)$ and polarisation $\mathbf{e}(t)$.

Amplitude modulation also referred to as amplitude-shift keying (ASK) is used in the majority of current commercial transmission systems since ASK modulated signals are easily detectable using a photo diode. In the simplest form of ASK, binary data is modulated onto a wave by switching the light on and off depending on the transmitted bits which is therefore named on-off keying (OOK). Encoding the data on the phase of the optical field is referred to as phase shift keying (PSK). It is an attractive modulation scheme used for advanced formats such as differential phase shift keying (DPSK). Polarisation shift keying (Pol-SK) being the third choice of encoding data on an optical field plays a minor role in optical communication due to the difficulties of maintaining a polarisation over a long transmission fibre.

In Chapter 4, we will investigate the impact of the chosen modulation format on the predistortion of fibre nonlinearities. Therefore, the characteristics of the modulation formats and the transmitter structures are briefly introduced in the following sections. A comprehensive discussion of modulation formats in optical communication can be found in [Winzer2006].

2.2.1. Optical Modulator

The optical modulator converts the transmitted data from the electrical domain to the optical domain by modulating the physical properties of an optical field. As stated above, amplitude and phase are the physical quantities relevant for fibre-optic transmission. There are several modulator technologies such as directly modulated lasers, electro-absorption modulators and Mach–Zehnder

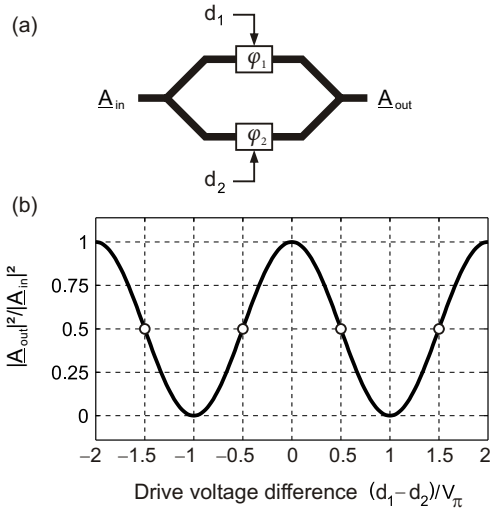

Figure 2.2. *Mach–Zehnder modulator: (a) interferometric structure, (b) power transfer characteristic. The open circles indicate 50% transmission (quadrature point).*

modulators, differing in complexity and achievable performance. The standard solution for long-haul transmission is the Mach–Zehnder modulator (MZM) as it allows for chirp-free modulation, i.e. pure amplitude modulation without phase modulation. A MZM is also referred to as an external modulator since the laser itself is operated as a continuous-wave (CW) laser with constant power and is then modulated using an external interferometer.

Fig. 2.2(a) shows the structure of a Mach–Zehnder interferometer with two drive electrodes (dual-drive MZM). The incoming signal $\underline{A}_{in}$ is split equally into the two arms of the interferometer. In each of the two arms, the optical fields experience a phase shift φ_1 and φ_2 which are controlled by the drive voltages d_1 and d_2, respectively,

$$\varphi_{1,2} = \pi \frac{d_{1,2}}{V_\pi} \tag{2.3}$$

where V_π is the voltage required for a π phase shift. The voltage controlled phase modulator is most conveniently realised by utilising the linear electro-optic effect (*Pockels effect*) in materials such as $LiNbO_3$ or III-V compound semiconductors (see, e.g., [Li2003]).

At the output coupler, the two waves recombine and interfere to give the output signal

$$\underline{A}_{out} = \frac{\underline{A}_{in}}{2}\left[\exp(j\varphi_1) + \exp(j\varphi_2)\right] . \tag{2.4}$$

By defining an average phase $\bar{\varphi} = (\varphi_1 + \varphi_2)/2$ and a phase difference $\Delta\varphi = \varphi_1 - \varphi_2$ and substituting into (2.4) we can write the complex field transfer function of the MZM

$$\frac{\underline{A}_{out}}{\underline{A}_{in}} = \cos(\Delta\varphi/2)\exp(j\bar{\varphi}) , \tag{2.5}$$

and the power transfer function

$$\frac{|\underline{A}_{out}|^2}{|\underline{A}_{in}|^2} = \frac{1}{2} + \frac{1}{2}\cos(\Delta\varphi) = \frac{1}{2} + \frac{1}{2}\cos\left(\pi\frac{d_1 - d_2}{V_\pi}\right) . \tag{2.6}$$

The power transfer function is plotted in Fig. 2.2(b). Equation (2.5) describes the basic principle of the MZM, i.e. the conversion of a phase difference into amplitude modulation by an interferometer.

The dual-drive MZM allows for both optical amplitude and optical phase modulation depending on the relationship between the drive voltages. If the voltages are chosen equal, i.e. $d = d_1 = d_2$, the MZM is operated in the *push-push mode*. In this case, the MZM acts as a pure phase modulator since the amplitude term in (2.4) vanishes for $\Delta\varphi = 0$. Setting the voltages equal but with opposite sign, i.e. $d = d_1 = -d_2$, the MZM is operated in *push-pull mode* allowing for chirp-free amplitude modulation since the phase term in (2.5) vanishes for $\bar{\varphi} = 0$. Due to this flexibility and the possibility for integration, the MZM is widely used for the generation of various ASK and PSK modulation formats.

In addition to conventional ASK or PSK modulation, the dual-drive MZM can be used to generate optical waveforms with arbitrary amplitude and phase. This is achieved by driving the MZM with two independent drive signals $d_1(t)$ and $d_2(t)$. By inserting (2.3) into (2.5) and rearranging we find that the drive voltages required for a desired field at the output $\underline{A}_{out}(t) = |\underline{A}_{out}(t)|\exp(j\varphi(t))$ are given by

$$d_1(t) = \frac{V_\pi}{\pi}\left(\varphi(t) + \cos^{-1}\left(\frac{|\underline{A}_{out}(t)|}{|\underline{A}_{in}(t)|}\right)\right) \tag{2.7}$$

$$d_2(t) = \frac{V_\pi}{\pi}\left(\varphi(t) - \cos^{-1}\left(\frac{|\underline{A}_{out}(t)|}{|\underline{A}_{in}(t)|}\right)\right) \tag{2.8}$$

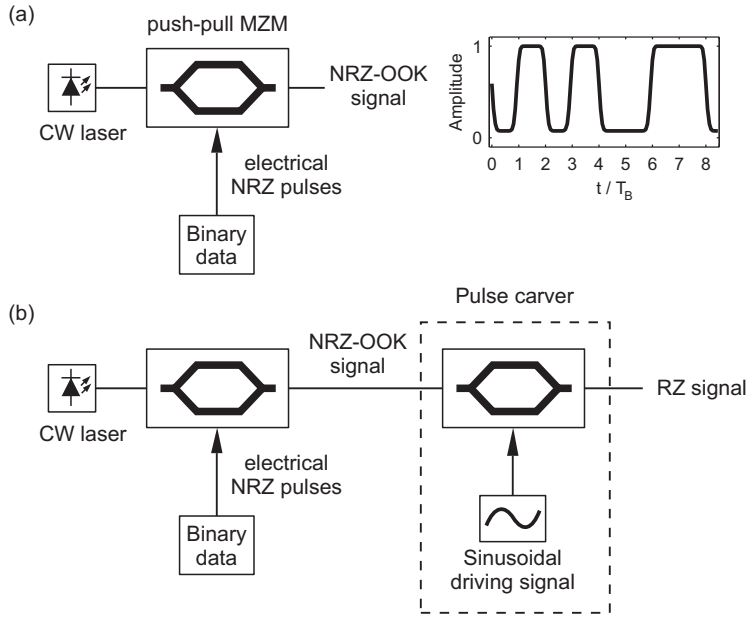

Figure 2.3. *Transmitter configuration for the generation of optical ASK modulated signals: (a) NRZ, (b) RZ.*

where the field at the input of the MZM $\underline{A}_{in}(t)$ is the output of a CW laser. This mode of operating a dual-drive MZM will be used in Chapter 4 to generate the predistorted optical waveform.

2.2.2. Amplitude Shift Keying (ASK)

Chirp-free amplitude shift keyed signals are generated using a push-pull MZM biased at the *quadrature point* that is indicated by the open circles in Fig. 2.2. For OOK modulation, the MZM is driven from minimum to maximum transmission such that the drive voltage signal is imprinted onto the amplitude of the optical field. Depending on the pulse shape and pulse width, we distinguish between nonreturn-to-zero (NRZ) and three return-to-zero (RZ) variants (33%, 50% and 67% RZ).

NRZ-OOK is generated using the transmitter configuration shown in Fig. 2.3(a). The binary data source feeds the electrical NRZ signal to the MZM which modulates the electrical signal on the CW laser light. A realistic electrical NRZ signal has a finite rise and fall time due to bandwidth limitations of the driving electronics. For the simulations presented in this thesis, the electrical

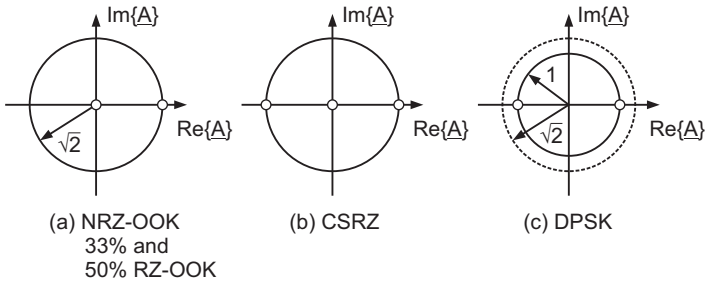

Figure 2.4. *Constellation diagrams for different modulation formats.*

NRZ pulses are generated by filtering ideal rectangular pulses using an electrical low-pass filter with a Gaussian-shaped frequency response to band-limit the pulse spectrum. After such filtering, the NRZ pulses have a specified rise time from 10% to 90% of the amplitude. We used an electrical rise time of $T_B/4$ throughout all simulations where T_B is the bit period. A typical NRZ-OOK waveform is shown in Fig. 2.3(a).

Alternatively, the NRZ-OOK signal may be visualised in the complex plane using the *constellation diagram*, Fig. 2.4(a). To obtain the constellation diagram, the complex signal $\underline{A}(t)$ is sampled at the centre of the bit slot, and the samples are represented as open circles in the complex plane. The reason for the arbitrary amplitude normalisation to $\sqrt{2}$ will be discussed in the following section on DPSK.

Generation of *RZ* signals requires a more complex transmitter structure shown in Fig. 2.3(b). After the data modulation section which is identical to the NRZ transmitter, a pulse carver section is included which consists of a push-pull MZM driven by a sinusoidal signal generator. Depending on the bias point and frequency of the sinusoidal driving signal, all three RZ pulse shape variants can be generated. The principle of the pulse carver is illustrated in Fig. 2.5. The bottom graph in Fig. 2.5 shows the three different possibilities for the sinusoidal driving signal resulting in three different pulse shapes as shown by the upper right graph.

33% RZ: The driving signal is biased at the maximum transmission point of the MZM as indicated by the open circle in the upper left graph in Fig. 2.5. Driving the MZM at half the bit rate between two transmission minima, i.e. using a peak-to-peak amplitude of $2V_\pi$, produces RZ pulses with a duty cycle of 33% of the bit slot.

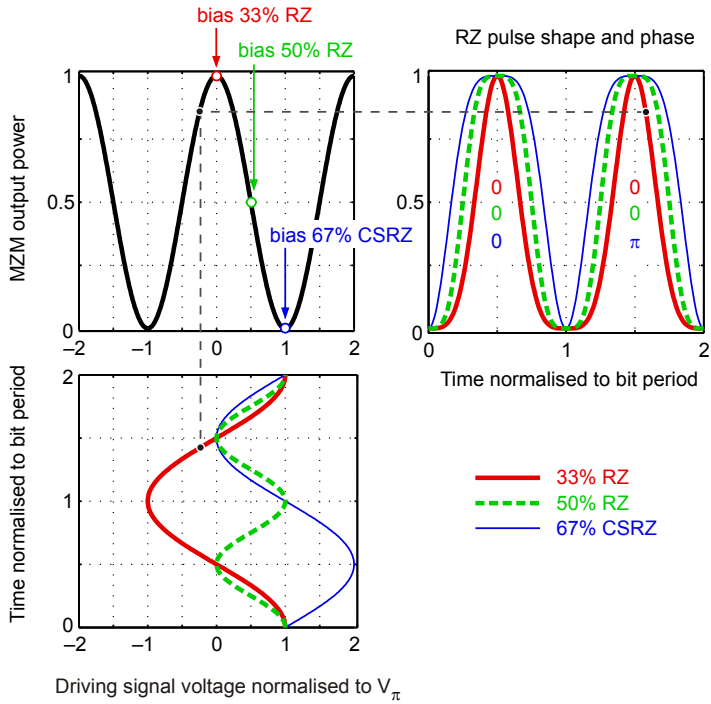

Figure 2.5. *Pulse carving of 33% RZ, 50% RZ and 67% CSRZ using a sinusoidally driven MZM.*

50% RZ: Biasing the driving signal at the quadrature point of the MZM and using a sinusoid with a frequency equal to the bit rate and a peak-to-peak amplitude of V_π produces 50% RZ pulses.

67% CSRZ: The 67% duty cycle RZ pulses are generated using a sinusoidal driving signal with a frequency of half the bit rate biased at the minimum transmission point with a peak-to-peak amplitude of $2V_\pi$. By driving the MZM between its maxima, the phase is switched between 0 and π since the MZM field transfer function changes its sign at each transmission minimum [cf. (2.5)]. This leads to a change of sign between adjacent bits in the resulting pulse train. The optical field envelope averages to zero, thus suppressing the carrier at the optical center frequency. Therefore this format is also referred to as carrier-suppressed return-to-zero (CSRZ).

The constellation diagrams of 33% and 50% RZ are essentially the same as for NRZ-OOK [Fig. 2.4(a)]. The only difference is that the peak amplitude values are different if the average signal power is kept constant. CSRZ, however, being

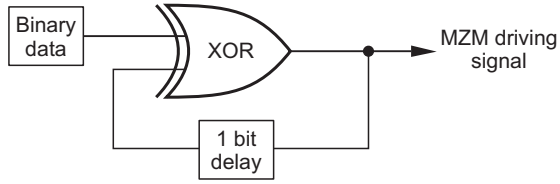

Figure 2.6. *DPSK precoder.*

a *pseudo-multilevel modulation format* shows a constellation diagram with the symbols -1, 0 and $+1$ [Fig. 2.4(b)]. The term pseudo-multilevel format is used since the third symbol does not carry more information. Instead, after square-law detection, the symbols -1 and $+1$ are mapped to the same receiver photo current values.

The performance differences between RZ and NRZ modulation formats, in particular in systems using electronic predistortion, will be discussed in Chapter 4.

2.2.3. Differential Phase Shift Keying (DPSK)

In DPSK, the data bits are encoded on the phase difference between two adjacent symbols. For differential binary PSK, a "one" bit is encoded to a phase change of π whereas for a "zero" bit the phase does not change between two adjacent pulses.

DPSK can be implemented using NRZ and RZ formats. Hence, the transmitter structures for NRZ-DPSK and RZ-DPSK are identical to Fig. 2.3 with two modifications:

1. To obtain the phase modulated waveform, the push-pull MZM is biased at the minimum transmission point and driven between the two maxima [cf. Fig. 2.2(b)]. Thus, the MZM acts as a phase switch changing the phase from 0 to π depending on the data.

2. In order to convert the data bits to the differential MZM driving signal, a precoder is required as shown in Fig. 2.6. It consists of an XOR gate with a delayed feedback loop.

The DPSK constellation diagram in Fig. 2.4(c) illustrates the symbols in the complex plane. Note that the amplitude maximum of the DPSK symbols, i.e. the radius of the constellation circle, is reduced by a factor of $\sqrt{2}$ compared to the corresponding OOK format for the same average optical power. Thus, the symbol distance in the DPSK constellation diagram is increased by a factor of

$\sqrt{2}$. This is explained by the fact that in a DPSK signal all bit slots are filled with pulses (RZ-DPSK) or with constant power (NRZ-DPSK) whereas in an OOK signal, on average, only half of the bit slots are filled. The increased symbol distance is the reason for the 3-dB increase in receiver sensitivity if balanced detection is employed [Gnauck2005]. This is one of the main advantages of DPSK over OOK formats.

2.3. Linear Impairments

While the optical field propagates along the transmission link, it is subject to various impairments which will degrade the signal. Those impairments may be classified into linear and nonlinear impairments. In this section the most important linear effects will be discussed.

2.3.1. Fibre Attenuation

Scattering and absorption of light in the fibre causes loss of optical power during propagation. Consequently, the average signal power, $\bar{P}(z)$, is attenuated according to

$$\bar{P}(z) = \bar{P}(0)\exp(-\alpha z) \tag{2.9}$$

where α in units 1/km is the attenuation coefficient[1] and $\bar{P}(0)$ is the average launch power at the input of the fibre.

The fibre attenuation parameter is wavelength-dependent, showing a minimum of approximately 0.2 dB/km around 1550 nm in modern silica optical fibre (see, e.g., [DiGiovanni2002]). The extremely low attenuation over several THz of bandwidth was one of the key factors leading to the widespread deployment of optical fibre in telecommunications. Nevertheless, the power level needs to be amplified periodically after a certain transmission distance.

2.3.2. Amplification and Optical Noise

The distance between amplifiers depends on the total system length. In terrestrial long-haul systems with link lengths below 3000 km, amplifier sites are spaced 80 to 100 km apart, whereas in submarine systems shorter span lengths near 50 km are used [Agrawal2002, p. 266]. Fig. 2.1 shows a typical optical transmission line consisting of a certain number of fibre spans.

The most widely used amplifier in fibre-optic transmission systems is the erbium-doped fibre amplifier (EDFA). It consists of an erbium-doped silica

[1] Typically, the attenuation coefficient of a fibre is specified in dB/km which is given by $\alpha_{[\mathrm{dB/km}]} = 10\alpha/\log 10 = 4.343\alpha$

fibre which is pumped by an external laser to achieve a population inversion. Thus, the incoming optical signal is amplified by stimulated emission. Typically, EDFA provide a gain of 20 to 30 dB over a bandwidth of 30 nm (4 THz).

In addition to amplification by stimulated emission, an EDFA produces amplified spontaneous emission (ASE) which manifests itself as noise and decreases the optical signal-to-noise ratio (OSNR). The OSNR is defined as the average optical signal power divided by the ASE power measured in both polarisations and in a bandwidth of $\Delta\lambda = 0.1$ nm (equivalent[2] to $\Delta\nu = 12.5$ GHz at $\lambda_0 = 1550$ nm). The OSNR degradation by an amplifier is expressed through its noise figure F which is defined as

$$F = \frac{(\mathrm{OSNR})_{\mathrm{in}}}{(\mathrm{OSNR})_{\mathrm{out}}} \,. \tag{2.10}$$

Due to the quantum nature of photons, the maximum achievable OSNR is fundamentally limited by quantum noise. Therefore, we assume a quantum noise limited input signal with an average optical power of P_{in}, whose $(\mathrm{OSNR})_{\mathrm{in}}$ is given by

$$(\mathrm{OSNR})_{\mathrm{in}} = \frac{P_{\mathrm{in}}}{h\nu\Delta\nu} \tag{2.11}$$

where h is Planck's constant and ν is the photon frequency. Note that the term $h\nu\Delta\nu$ represents the noise power of the quantum noise for the two polarisations. For $\nu = 193.6$ THz ($\lambda = 1550$ nm) and $\Delta\nu = 12.5$ GHz, we have $h\nu\Delta\nu = 1.6\,\mathrm{nW} = -58$ dBm.

At the output of the EDFA, the signal is amplified by G according to $P_{\mathrm{out}} = GP_{\mathrm{in}}$ and ASE noise is added. Thus, we obtain an output $(\mathrm{OSNR})_{\mathrm{out}}$

$$(\mathrm{OSNR})_{\mathrm{out}} = \frac{GP_{\mathrm{in}}}{h\nu\Delta\nu + P_{\mathrm{ASE}}} \tag{2.12}$$

with the ASE noise power given by [Agrawal2002]

$$P_{\mathrm{ASE}} = 2n_{sp}(G-1)h\nu\Delta\nu \tag{2.13}$$

where the parameter n_{sp} is called the spontaneous-emission factor (or the population-inversion factor). It describes the ratio of spontaneous and stimulated emission in the amplifier. Its theoretical minimum is $n_{sp} = 1$. Us-

[2] The bandwidths in terms of frequency and wavelength are related by

$$\Delta\nu = \frac{c}{\lambda_0^2}\Delta\lambda$$

where c is the speed of light in vacuum and λ_0 is the reference wavelength.

ing (2.10)-(2.13) we obtain the EDFA noise figure

$$F = \frac{1}{G}(1 + 2n_{sp}(G-1)) \approx 2n_{sp} \,. \tag{2.14}$$

This equation demonstrates that even an ideal amplifier with $n_{sp} = 1$ will degrade the OSNR by 3 dB. For practical amplifiers, F is around 4–8 dB.

In a transmission link that consists of multiple amplified spans (Fig. 2.1), ASE noise accumulates during propagation along the link. This is described by the received OSNR at the end of the transmission link

$$\mathrm{OSNR} = \frac{P_{\mathrm{in}}}{h\nu\Delta\nu F_{\mathrm{tot}}} \tag{2.15}$$

where F_{tot} is the total noise figure of the transmission link. For the simple case of N fibre spans having equal length L and attenuation α, the gain of each EDFA is set to compensate for the fibre loss, $G = \exp(\alpha L)$. The total noise figure is then given by

$$F_{\mathrm{tot}} = 1 + N(GF - 1) \approx N\,G\,F = N\exp(\alpha L)\,F \,. \tag{2.16}$$

By substituting (2.16) into (2.15) and converting to dB, we arrive at the well-known formula to estimate the achievable OSNR of a transmission system

$$\mathrm{OSNR}_{[\mathrm{dB}]} = 58\ \mathrm{dB} + P_{in[\mathrm{dBm}]} - \alpha_{[\mathrm{dB/km}]}L - F_{[\mathrm{dB}]} - 10\log(N) \tag{2.17}$$

where $h\nu\Delta\nu = -58$ dBm was used.

Equation (2.17) describes the noise limit of a fibre-optic transmission system including only attenuation and noise as degrading effects. It shows that the achievable OSNR may be increased using a higher launch power. However, the maximum allowed launch power is limited by fibre nonlinearities as we will discuss in Section 2.4.

2.3.3. Chromatic Dispersion

Chromatic dispersion is a result of the frequency dependence of the refractive index $n(\omega)$ of a silica fibre. It plays an important role for the propagation of optical pulses since the spectral components of a signal travel at different speeds leading to temporal pulse distortions. This section briefly reviews the linear pulse propagation in optical fibre with a frequency dependent refractive index. For a comprehensive analysis refer to, e.g., [Agrawal2001].

For the majority of fibre-optic long-haul transmission systems, the transmission fibre is a standard single mode fibre (SSMF). By modelling the fibre as a

cylindrical dielectric waveguide and solving the wave equation, it can be shown that it supports two orthogonal linearly polarised propagating modes. In general, the propagating wave of a guided mode is given by

$$\mathbf{E}(x, y, z, t) = \mathbf{e}(t)\, F(x, y) E(z, t) \tag{2.18}$$

where $F(x, y)$ represents the transverse modal distribution. For a cylindrical fibre, $F(x, y)$ is the distribution of the fundamental LP_{01} mode which is often approximated by a Gaussian function. The unit vector $\mathbf{e}$ specifies the polarisation of the wave. It is referred to as the Jones vector.

In (2.18), the term relevant for chromatic dispersion is the field $E(z, t)$. Dispersive propagation is conveniently calculated in the frequency domain using the Fourier transform

$$\underline{E}(z, j\omega) = \int_{-\infty}^{\infty} E(z, t) \exp(-j\omega t) dt\,. \tag{2.19}$$

The wave propagation along the positive z-coordinate is then described by

$$\underline{E}(z, j\omega) = \underline{E}(0, j\omega) \exp(-j\beta(\omega) z) \tag{2.20}$$

where $\beta(\omega)$ is the frequency-dependent propagation constant which depends on the refractive index of the fibre material and the design parameters such as core diameter and core-cladding index difference [Agrawal2001, p. 11]. It can be expanded in a Taylor series around a reference angular frequency $\omega_0 = 2\pi c/\lambda_0$

$$\beta(\omega) = \beta_0 + \beta_1(\omega - \omega_0) + \frac{\beta_2}{2}(\omega - \omega_0)^2 + \frac{\beta_3}{6}(\omega - \omega_0)^3 + \ldots \tag{2.21}$$

where the series coefficients are defined by

$$\beta_n = \left(\frac{d^n \beta}{d\omega^n}\right)_{\omega=\omega_0}\,. \tag{2.22}$$

The first term of (2.21) represents a frequency-independent phase rotation and can be neglected for the propagation of pulses. The second coefficient $\beta_1 = \tau = 1/v_{gr}$ is equal to the group delay per length τ and the inverse of the group velocity v_{gr}. The third term describes first-order chromatic dispersion, also called group-velocity dispersion (GVD). The parameter $\beta_2 = d\tau/d\omega$ is the GVD parameter or chromatic dispersion parameter and characterises the change of the group delay with frequency. It is also common to specify chromatic dispersion

in wavelength units by the parameter

$$D = \frac{d\tau}{d\lambda} = -\frac{2\pi c}{\lambda_0^2}\beta_2 \tag{2.23}$$

where D is usually quoted in units ps/nm/km. A typical value in SSMF at $\lambda_0 = 1550$ nm is $D_{\mathrm{SMF}} = 16$ ps/nm/km and $\beta_2 = -20$ ps^2/km. There are two physical origins of chromatic dispersion in optical fibres: *material dispersion* as a result of the frequency dependence of the core and cladding materials, and *waveguide dispersion* due to the refractive index profile. The total dispersion parameter is given by the sum of the material and waveguide dispersion,

$$D = D_M + D_W\,. \tag{2.24}$$

For SSMF at 1550 nm, the waveguide contribution D_W is small compared to the material dispersion D_M. However, D_W may be modified by careful design of the fibre core diameter and the refractive index profile. This is used for a dispersion compensating fibre (DCF) which has a large value of negative dispersion, typically around $D_{\mathrm{DCF}} = -100$ ps/nm/km to enable cancellation of accumulated dispersion as will be discussed later.

The fourth term in (2.21) is the second-order chromatic dispersion or dispersion slope with the parameter $\beta_3 = d\beta_2/d\omega$. The dispersion slope is also often expressed in terms of wavelength using the parameter

$$S = \frac{dD}{d\lambda} = \left(\frac{2\pi c}{\lambda_0^2}\right)^2 \beta_3 - \frac{2}{\lambda_0} D \tag{2.25}$$

where the slope parameter S is usually quoted in units ps/nm^2/km. A typical value in SSMF at $\lambda_0 = 1550$ nm is $S_{\mathrm{SMF}} = 0.08$ ps/nm^2/km.

While (2.20) fully describes the electro-magnetic wave propagation, one is often interested in the evolution of the slowly varying pulse amplitude $A(z, t)$ in the baseband notation. The slowly varying field envelope may be separated from the field by writing

$$E(z, t) = A(z, t)\exp(-j\beta_0 z + j\omega_0 t)\,. \tag{2.26}$$

We may introduce a retarded time axis, $t' = t - \tau z$, moving with the group velocity $v_{gr} = 1/\tau$. This is valid since the effect of the group delay does not change the pulse shape. Taking the Fourier transform of the slowly varying

envelope for $t = t' + \tau z$

$$\underline{A}(z, j(\omega - \omega_0)) = \int_{-\infty}^{\infty} A(z, t' + \tau z) \exp[-j(\omega - \omega_0)t' \,] dt' \tag{2.27}$$

and using (2.20)-(2.22) yields the evolution of the slowly varying envelope in the frequency domain

$$\underline{A}(z, j\Delta\omega) = A(0, j\Delta\omega) \exp\left(-j\frac{\beta_2}{2}\Delta\omega^2 z - j\frac{\beta_3}{6}\Delta\omega^3 z\right) \tag{2.28}$$

where $\Delta\omega = \omega - \omega_0$ was used for brevity.

Finally, the time domain pulse envelope $A(z, t')$ may be found by taking the inverse Fourier transform. The partial differential equation governing the pulse propagation in the time domain is derived by differentiating (2.28) with respect to z and transforming to the time domain

$$\frac{\partial A(z, t')}{\partial z} = j\frac{\beta_2}{2}\frac{\partial^2 A(z, t')}{\partial t'^2} + \frac{\beta_3}{6}\frac{\partial^3 A(z, t')}{\partial t'^3} \,. \tag{2.29}$$

In (2.28) and (2.29), the first and second order dispersion parameters are taken into account which is sufficient for modelling WDM lightwave systems. The physical meaning of (2.28) is that each spectral component of the signal envelope acquires a phase shift depending on frequency and propagation distance. However, the optical power spectral density which is defined as the absolute magnitude squared of the optical field's Fourier transform remains unchanged by chromatic dispersion.

From (2.28), we may derive the linear transfer function $\underline{H}(z, j\Delta\omega)$ of a dispersive fibre of length z,

$$\underline{H}(z, j\Delta\omega) = \frac{\underline{A}(z, j\Delta\omega)}{\underline{A}(0, j\Delta\omega)} = \exp\left(-j\frac{\beta_2}{2}\Delta\omega^2 z\right) \tag{2.30}$$

where $\beta_3 = 0$ was assumed. The impulse response $h(z, t)$ of a fibre of length z is then given by the inverse Fourier transform of (2.30).

To understand the effect of chromatic dispersion in the time domain, we study the response of a fibre to a single unchirped Gaussian pulse with an initial pulse shape $\underline{A}(t) = A_0 \exp[-(t/T_0)^2]$ where T_0 is the half width at the 1/e amplitude. It is related to the full width at half maximum T_{FWHM} by $T_{\mathrm{FWHM}} = 2\sqrt{\ln 2}T_0$. An analytic solution to the problem of Gaussian pulse propagation is well-known [Agrawal2001, p. 67]. The calculated real part, imaginary part and absolute pulse envelope of $A(z, t)$ are shown for $z = 0 \ldots 800$ km in Fig. 2.7

for an initial pulse width of 25 ps. The Gaussian pulse maintains its Gaussian shape during propagation, but the pulse width increases with the propagation distance z according to

$$\frac{T_0(z)}{T_0} = \sqrt{1 + \left(\frac{z}{L_D}\right)^2} \tag{2.31}$$

where

$$L_D = T_0^2/|\beta_2| \tag{2.32}$$

is the dispersion length. It is defined as the length after which a pulse has broadened by a factor of $\sqrt{2}$. Thus, the dispersion length relates a signal parameter and a fibre parameter. Using (2.23) and taking into account that the initial pulse width is inversely proportional to the bit rate B, we have $L_D \propto 1/(|D|B^2)$. The product $|D|B^2$ is of fundamental importance for the analysis of dispersive nonlinear pulse propagation as we will see below.

Although defined for a Gaussian pulse, L_D is an important length scale in any high-speed fibre-optic transmission system since (2.32) shows that the broadening of signal pulses scales with the square of the bit rate. It is useful to discriminate various nonlinear transmission regimes as will be shown in the next section.

Pulse broadening due to chromatic dispersion causes pulses to spread into adjacent bit slots. Thus, the decision in a bit slot depends on the neighbouring bits. This effect is also known as intersymbol interference (ISI). If no dispersion compensation is used, the transmission distance is limited due to ISI. The dispersion limited transmission distance scales with L_D and hence with the inverse square of the bit rate. At 10 Gbit/s over SSMF, the dispersion limit is 60–70 km depending on the modulation and receiver characteristics [Gnauck1997]. Increasing the bit rate to 40 Gbit/s reduces the dispersion limit by a factor of 16 to 4 km. Longer transmission distances require dispersion compensation.

To compensate for chromatic dispersion, the majority of currently deployed long-haul systems use inline optical dispersion compensating elements such as DCF which are placed at the end of each fibre span at the amplifier sites along the link. The dispersion parameter of the DCF is around $D_{\mathrm{DCF}} = -100$ ps/nm/km. In these fibres, the dispersion slope S has the same sign as that of the transmission fiber (positive), so that the fibers will cancel dispersion completely only at one wavelength. However, since the compensation mismatch changes weakly with wavelength, operation over a wide wavelength band is possible enabling compensation of multiple wavelength channels in a WDM system. Such systems are referred to as optical dispersion compensation (ODC).

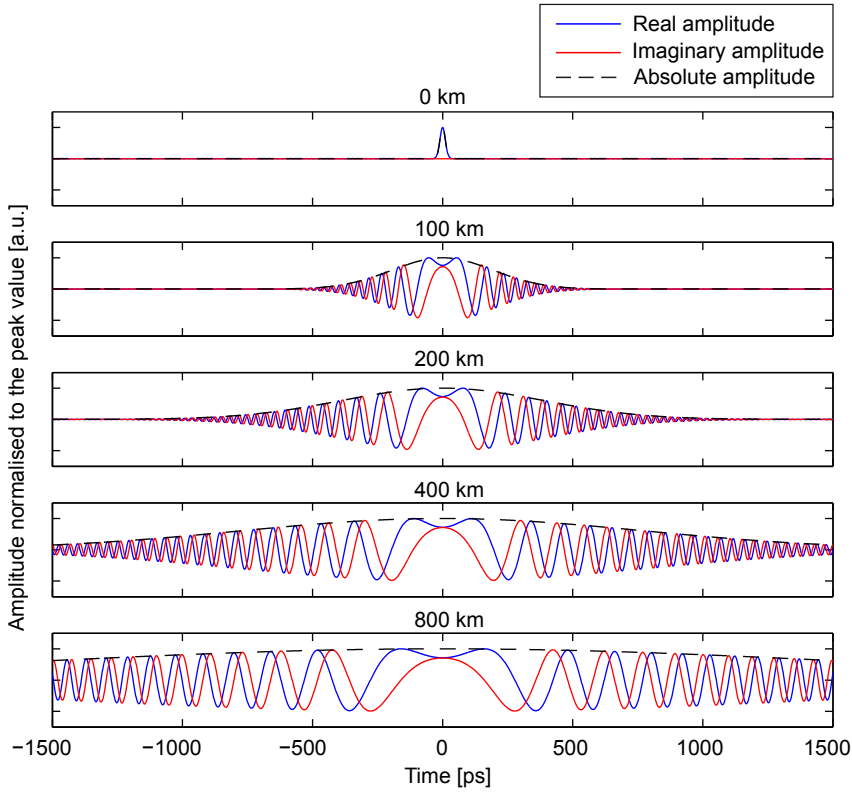

Figure 2.7. *Response of an SSMF to a Gaussian pulse with $T_{FWHM} = 25$ ps after propagation distances ranging from 0 to 800 km.*

Alternatively, chromatic dispersion may be compensated using electronic signal processing in the transmitter or receiver without the need for DCF elements along the link. Transmitter side precompensation of dispersion will be investigated in Chapter 3.

2.3.4. Linear Channel Memory

The effect of chromatic dispersion causes a *memory of a communication channel*. The memory is defined as the number of bits that affect the decision in the current bit slot including the current bit. The memory due to chromatic dispersion may be estimated by the relative time shift Δt of two spectral components with the frequency difference Δf

$$\Delta t = -DL\Delta f \frac{\lambda_0^2}{c} \tag{2.33}$$

where the product DL is often called *accumulated* or *cumulative dispersion*. More generally, the accumulated dispersion is given by integrating over the z-dependent dispersion parameter

$$D_{\mathrm{acc}}(z) = \int_0^z D(z')dz' \,. \tag{2.34}$$

Instead of propagating the signal over a dispersive fibre, an accumulated dispersion may also be applied to the signal using electronic precompensation inside the transmitter prior to transmission which will also introduce a memory. Therefore, D_{acc} is used instead of DL.

If Δf is chosen to represent the spectral width of the signal, one can estimate the memory m_{L} in terms of bit periods by multiplying (2.33) with the bit rate B yielding

$$m_{\mathrm{L}} = B\Delta t + 1 = |D_{\mathrm{acc}}|B\Delta f \frac{\lambda_0^2}{c} + 1 \,. \tag{2.35}$$

Considering that the spectral width is usually proportional to the bit rate, i.e. $\Delta f \propto B$, we have

$$m_{\mathrm{L}} - 1 \propto |D_{\mathrm{acc}}|B^2 \,. \tag{2.36}$$

The channel memory is an important parameter for the design of electronic dispersion compensation devices as will be shown in Chapter 3.

2.4. Nonlinear Fibre Impairments

By increasing the launch power of an optical signal, the field intensity in the fibre is also increased which gives rise to nonlinear effects of the fibre. Nonlinearities can be classified into two groups: nonlinear scattering effects and the power dependent refractive index. The latter is also referred to as the optical Kerr effect [Agrawal2001, p. 211ff.]. The nonlinear scattering effects are stimulated Raman scattering (SRS) [Agrawal2001, p. 298ff.] and stimulated Brillouin scattering (SBS) [Agrawal2001, p. 355ff.]. These effects will be neglected for the further discussion since SRS has a very high power threshold of around 500 mW which is far above the power used in telecommunication applications. SBS may also be neglected in high bit rate transmission systems since the signal spectral width typically exceeds the relevant bandwidth of SBS which is only a few 10 MHz. Therefore, this section presents the impairments associated with the Kerr effect in optical fibre which is the most important nonlinear fibre effect for the transmission systems considered in this thesis.

2.4.1. Intensity-Dependent Refractive Index

The refractive index n of silica increases at high field intensities giving rise to nonlinear phase modulation of the propagating waveform. The physical origin of this effect stems from the anharmonic oscillations of electrons in response to a high-intensity electromagnetic field [Boyd1992]. Nonlinear refraction as a result of the Kerr effect is accounted for by modifying the refractive index

$$n' = n + n_2 \frac{P}{A_{\text{eff}}} \tag{2.37}$$

where n_2 is the nonlinear-index coefficient, and A_{eff} is the effective mode area. The nonlinear-index coefficient of silica fibre is $n_2 = 2.6 \times 10^{-20}$ m^2/W. As a result of the intensity-dependent refractive index, the propagation constant also becomes intensity dependent [Agrawal2002, p. 64]

$$\beta' = \beta + \gamma P \tag{2.38}$$

where $\gamma = 2\pi n_2/(A_{\text{eff}}\,\lambda_0)$ is the nonlinearity coefficient. For SSMF, a typical value is $\gamma_{\text{SSMF}} = 1.31$ W^{-1}km^{-1}. Modifying the pulse propagation equation (2.29) to including the nonlinearity coefficient yields the nonlinear Schrödinger equation (NLSE)

$$\frac{\partial A(z,t)}{\partial z} + \frac{\alpha}{2}A(z,t) - j\frac{\beta_2}{2}\frac{\partial^2 A(z,t)}{\partial t^2} = -j\gamma|A|^2 A(z,t) \tag{2.39}$$

where we neglected third-order dispersion and added the loss term containing α. The NLSE is a nonlinear partial differential equation which describes the propagation of the slowly varying amplitude of a signal over a nonlinear fibre. Clearly, the right-hand side of (2.39) represents the nonlinearity. The NLSE is of fundamental importance for the analysis of fibre-optic transmission systems. The solution for an arbitrary input signal is usually obtained numerically using the *split-step Fourier algorithm* [Agrawal2001]. For this thesis, the commercially available software VPItransmissionMaker was used which implements the split-step algorithm.

While the Kerr effect is the common physical reason for the nonlinear refractive index related effects in fibre, it is useful to further classify the different effects in a high bit rate WDM transmission system into *intrachannel* and *interchannel* nonlinearities. Intrachannel nonlinearities describe the nonlinear effects in a single wavelength channel and interchannel nonlinearities refer to the nonlinear effects between neighbouring wavelength channels. We demonstrate the difference using the NLSE (2.39) by assuming a signal $A(z, t)$ containing two wavelength channels, i.e. $A = A_1 + A_2$. Substituting this into the nonlinear part $|A|^2A$ of (2.39) yields the terms

$$\underbrace{|A_1|^2A_1 + |A_2|^2A_2}_{\text{intrachannel}} + \underbrace{\underbrace{2(|A_2|^2A_1 + |A_1|^2A_2)}_{\text{XPM}} + \underbrace{A_1^2A_2^* + A_1^*A_2^2}_{\text{FWM}}}_{\text{interchannel}} . \tag{2.40}$$

The first two terms represent the intrachannel nonlinearities in the first and second wavelength channel, respectively. We discuss intrachannel effects in the following sections. The remaining terms are interchannel effects leading to nonlinearities in one channel induced by the signal in the other channel. We may further classify interchannel nonlinearities into cross-phase modulation (XPM) and four-wave mixing (FWM) as indicated in (2.40). These effects are reviewed in Sections 2.4.7 and 2.4.6.

2.4.2. Intrachannel Nonlinear Effects

Assuming that only a single wavelength channel signal A_1 is transmitted, an analytic solution to (2.39) can be found in the special case of a fibre without dispersion [Agrawal2001, p. 98]. The solution shows that after propagating over the distance L, the signal $A_1(L, t)$ has experienced a nonlinear phase shift

$$\varphi_{\text{NL}}(L, t) = \gamma P(0, t) \int_0^L \exp(-\alpha z) dz \tag{2.41}$$

where $P(0,t)$ is the instantaneous power of the launched signal. The integral in (2.41) represents an important characteristic length scale which is referred to as the *effective length* L_{eff},

$$L_{\text{eff}} = \int_0^L \exp(-\alpha z)dz = \frac{1-\exp(-\alpha L)}{\alpha} \approx \frac{1}{\alpha}\,. \tag{2.42}$$

The approximation $1/\alpha$ is valid for typical fibre lengths of several tens of kilometers. For an SSMF of 80 km length with $\alpha = 0.21$ dB/km, (2.42) yields $L_{\text{eff}} = 21$ km. Physically, the effective length can be interpreted as the length of an equivalent fibre with $\alpha = 0$ that causes the same nonlinear phase shift.

A phase shift alone would not lead to signal degradation in OOK systems since the signal phase is lost after the photo diode at the receiver and only the intensity is detected. In fibres with $\beta_2 \neq 0$, however, the dispersion following the nonlinear phase modulation results in the conversion of this phase modulation to intensity distortions which will eventually degrade the OOK signal. The effect of nonlinear signal distortion is a result of the combined effects of chromatic dispersion and fibre nonlinearities. Depending on the number of overlapping pulses within a certain length, different propagation regimes can be distinguished.

2.4.3. SPM in the Solitonic Transmission Regime

If no pulse overlap occurs within the effective length, the pulse power will modulate the phase of itself which is called *self-phase modulation*. This is the case, e.g., in a single channel optically inline dispersion compensated 10 Gbit/s system using standard single mode fibre (SSMF). In this regime, the signal evolves relatively slowly due to chromatic dispersion and the pulses do not broaden significantly within the effective length. This may be expressed by the number of overlapping bits in the effective length, or more precisely, the memory m_{L} defined in (2.35) for $L = L_{\text{eff}}$. As an example, we choose a 10 Gbit/s signal, $\Delta f = 10$ GHz, over SSMF with $D = 16$ ps/nm/km. Equation (2.35) then yields a memory after $L_{\text{eff}} = 21$ km of $m_{\text{L}} = 1.3$ bit, showing that each bit only affects itself through self-phase modulation (SPM)[3].

With normal dispersion ($\beta_2 > 0, D < 0$), SPM induces a chirp on the signal that leads to an increased pulse broadening, hence increased ISI. In contrast, SPM followed by anomalous dispersion ($\beta_2 < 0, D > 0$), may result in pulse compression because the SPM-induced chirp and the dispersion-induced chirp

[3] Note that the memory m_{L} is defined in (2.35) to include the current bit. Even in the absence of accumulated dispersion which means no pulse overlap, we have $m_{\text{L}} = 1$ bit.

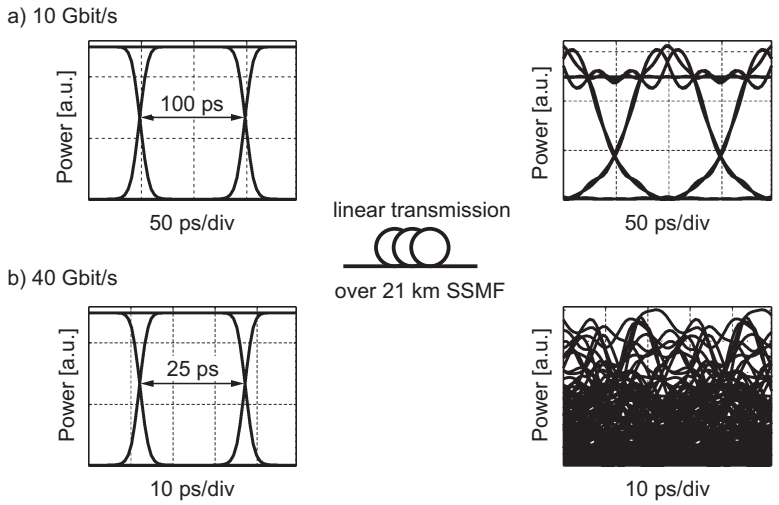

Figure 2.8. *Eye diagrams of the optical power before and after linear transmission over 21 km SSMF for a) 10 Gbit/s and b) 40 Gbit/s.*

cancel out partially or even completely. The latter case is referred to as optical soliton transmission. Although solitons are of less practical relevance in current high bit rate fibre-optic transmission, the term *solitonic transmission regime* is sometimes used for the case of low pulse overlap in the effective length such as for 10 Gbit/s OOK transmission over SSMF [Essiambre2002].

Fig. 2.8(a) shows the eye diagrams of the 10 Gbit/s transmitted signal (left) and the signal with an accumulated dispersion equal to 21 km SSMF to illustrate the waveform evolution due to dispersion after the effective length of the fibre. Clearly, the 10 Gbit/s NRZ pulses have only slightly broadened after the effective length. Thus, nonlinear phase modulation will only affect each pulse itself.

Next to SPM, the WDM signal transmission in the solitonic regime is strongly affected by interchannel nonlinearities such as XPM and FWM. The principle of these types of nonlinearities will be presented in Sections 2.4.7 and 2.4.6.

2.4.4. IXPM and IFWM in the Pseudo-linear Regime

In current high-speed transmission systems, the bit rate is increased to 40 Gbit/s and above. This significantly changes the impact of chromatic dispersion and fibre nonlinearities compared to 10 Gbit/s transmission because the pulse spreading scales with the square of the bit rate, cf. (2.36). Considering a bit rate of 40 Gbit/s and a signal bandwidth of 40 GHz, the pulse overlap within the ef-

fective length over SSMF increases to $m_L = 5.3$ bit according to (2.35). This is clearly observed in Fig. 2.8(b) which shows the eye diagram of a 40 Gbit/s signal after linear transmission over 21 km SSMF. Pulses strongly overlap and the amplitude profile of individual pulses is lost. In contrast to the solitonic regime, the impact of nonlinearity on a single isolated pulse (SPM) is small in high-speed transmission. Instead, a number of pulses belonging to the same wavelength channel overlap and interact through nonlinearity. These intrachannel nonlinear effects among neighbouring pulses are the dominant source of signal degradation in the so called *pseudo-linear transmission regime* [Essiambre2002].

Another important characteristic of the pseudo-linear regime is the fast waveform evolution with accumulating dispersion. Since the waveform resulting from a number of overlapping pulses is given by the sum of the fields of these pulses rather than the sum of their powers, a small phase change due to dispersion strongly affects the resulting amplitude. This fast waveform variation combined with large pulse overlap causes a redistribution of any nonlinear phase distortions among many pulses. Thus, nonlinear effects are averaged and their effect on pulse distortion is reduced. This phenomenon is the basis for pseudo-linear transmission [Essiambre2002].

More specifically, the dominant intrachannel nonlinearities in the pseudo-linear regime are classified into two effects: intrachannel cross-phase modulation (IXPM) and intrachannel four-wave mixing (IFWM). This follows from the NLSE in exactly the same way as demonstrated in (2.40). The only difference is that the fields A_1 and A_2 are not interpreted as two different wavelength channels, but as two overlapping pulses in the time domain. The terms $2(|A_2|^2 A_1 + |A_1|^2 A_2)$ then describe IXPM whereas the terms $A_1^2 A_2^* + A_1^* A_2^2$ represent IFWM. Self-phase modulation in the individual pulses (intrapulse SPM) also occurs, however with negligible impact.

The process of IXPM is schematically illustrated in Fig. 2.9 [Bayvel2002]. Two neighbouring pulses which are initially separated in time will overlap while propagating along the transmission fibre. The time derivative of the pulse power of one pulse edge causes a nonlinear frequency shift of the other pulse. In Fig. 2.9, the pulse drawn with a dashed line modulates the pulse drawn with a solid line[4]. As a result of the frequency difference between pulses, the pulses propagate at slightly different velocities. When the dispersion is compensated the pulses are recompressed, but the nonlinear distortions remain, which manifest as a timing jitter in the case of IXPM.

Next to IXPM, there is a second intrachannel effect called IFWM. The basic principle of IFWM is shown in Fig. 2.10 [Shake1998]. The upper left-hand

[4] Of course, both pulses modulate each other, but for clarity only one of the IXPM processes is shown.

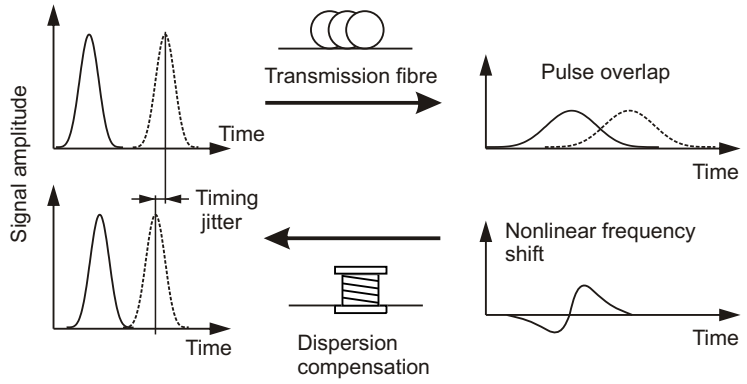

Figure 2.9. *Schematic illustration of IXPM.*

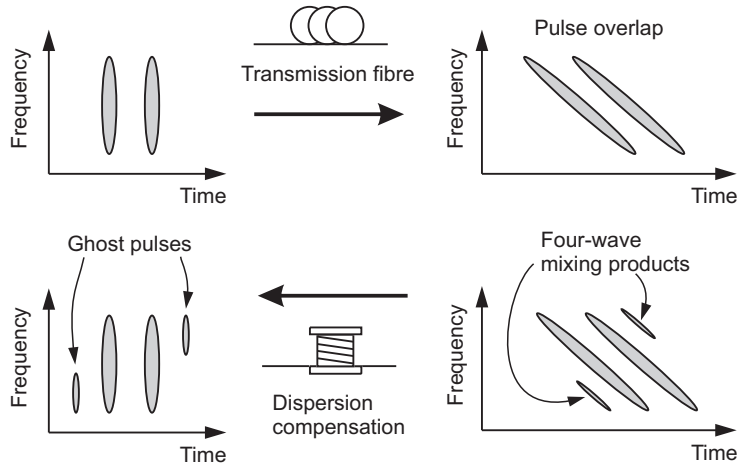

Figure 2.10. *Schematic illustration of IFWM.*

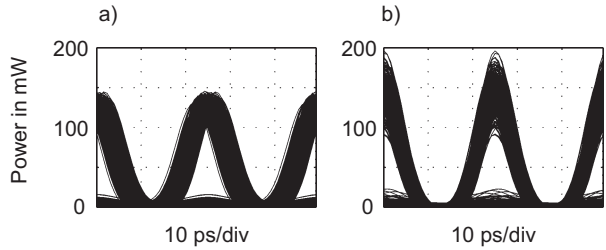

Figure 2.11. *Optical eye diagrams of a 40 Gbit/s RZ-33 signal after nonlinear transmission over 80 km fully dispersion compensated SSMF and noise-free amplification (a) without dispersion precompensation, D_{pre} =0, and (b) with dispersion precompensation of $D_{pre} = -400$ ps/nm.*

graph shows the time-resolved spectra (spectrogram [Hlawatsch1992]) of two pulses before transmission. This spectrogram illustrates the frequency components belonging to an individual pulse. In this representation, the effect of chromatic dispersion manifests as a tilt of the two pulse spectrograms since different frequency components travel at different speed. As a result, the pulse spectrograms overlap in the time domain. The overlapping frequency components of both pulses interact through the Kerr nonlinearity and the four-wave mixing effect occurs which generates the mixing products shown in the lower right-hand graph. If dispersion is compensated, the tilt is reversed, i.e. the pulses are recompressed in the time domain, but the mixing products remain visible in the signal as amplitude variations. If the mixing product falls into an empty bit slot, i.e. a "zero" bit, the IFWM effect generates so called *ghost pulses*, lower left-hand graph in Fig. 2.10. In the case of a bit slot with a "one" bit, the amplitude is distorted. However, the ghost-pulses generally have a far more detrimental impact on the bit error rate than the amplitude fluctuations of the "ones". This allows to identify a worst-case bit pattern for the effect of IFWM which is given by an isolated "zero" bit between long series of successive "one" bits [Essiambre1999]. In the isolated "zero" bit slot, many IFWM mixing products accumulate to a strong ghost pulse. We will use this bit pattern in Chapter 3 to analyse the impact of intrachannel nonlinearities in precompensated systems.

As an example for the impact of IXPM and IFWM, the signal propagation over a 40 Gbit/s transmission system consisting of a single span SSMF is calculated numerically using the NLSE (2.39). An RZ-33 modulated signal is launched with an average power of 14 dBm which is sufficiently high to induce nonlinear effects over 80 km of SSMF. At the receiver, the accumulated dispersion of the signal and the SSMF loss are perfectly compensated using a linear DCF and a

noise-free EDFA, respectively. The optical eye diagram of the received signal is shown in Fig. 2.11(a). The pulses are significantly affected by timing jitter due to IXPM. In addition, ghost pulses on the "zero" level are visible. Fig. 2.11(b) shows the received signal if the transmitted signal is dispersion precompensated by $D_{\text{pre}} = -400$ ps/nm while maintaining net zero dispersion at the receiver. As reported in [Killey2000], dispersion precompensation can be used to adjust the relative impact of each of the intrachannel effects. With values as large as $D_{\text{pre}} = -400$ ps/nm, IFWM has the dominant impact. Clearly, the IFWM-induced amplitude fluctuations on the "ones" and the ghost pulses on the "zeros" dominate over the IXPM-induced timing jitter.

2.4.5. Nonlinear Channel Memory

The pseudo-linear regime is characterised by a significant pulse overlap and nonlinear interaction of these overlapping pulses. Since the overlap itself is a result of chromatic dispersion which is a linear effect it can be completely compensated using dispersion compensating elements. However, the nonlinear distortions are not compensated. Similar to the linear channel memory (cf. Section 2.3.4), we may define a *nonlinear channel memory* as a result of the combined effect of dispersion and intrachannel nonlinearities.

The nonlinear memory is related to the linear memory introduced in Section 2.3.4. However, the linear memory is a function of the accumulated dispersion D_{acc} which means that by linearly compensating dispersion to achieve $D_{\text{acc}} = 0$, the linear memory vanishes. In contrast, the nonlinear memory characterises the nonlinear signal distortions that remain in the signal after linear dispersion compensation to achieve $D_{\text{acc}} = 0$. Similar to (2.35), the nonlinear memory m_{NL} is defined by

$$m_{\text{NL}} = \max(|D_{\text{acc}}|) B \Delta f \frac{\lambda_0^2}{c} + 1 \,. \tag{2.43}$$

where $\max(|D_{\text{acc}}|)$ is the maximum accumulated dispersion at a position in the transmission link where the power is sufficiently high to induce nonlinear effects. Typically this position is found at $z = 0$ or within the effective length.

The nonlinear memory has two consequences. The first is related to the bit pattern length for the accurate simulation of nonlinear systems and will be discussed in Chapter 3 and 4. Secondly, the nonlinear memory has some importance for the required hardware complexity in transmission systems using predistortion of nonlinearities also presented in Chapter 4.

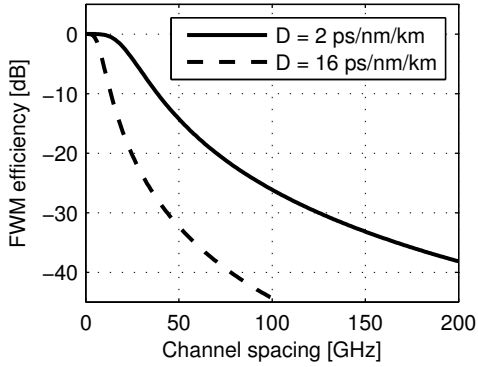

Figure 2.12. *FWM efficiency as a function of the channel spacing after transmission over 100 km for two different fibre dispersion parameters.*

2.4.6. Four-Wave Mixing

In WDM transmission the beating between wavelength channels leads to the generation of waves at new wavelengths. If three channels copropagate at angular frequencies ω_i, ω_j and ω_k, a new wave is generated at

$$\omega_{ijk} = \omega_i + \omega_j - \omega_k \,. \tag{2.44}$$

This will cause signal crosstalk if the frequency ω_{ijk} falls within the band of an existing WDM channel. The cases where $\omega_i \neq \omega_j = \omega_k$ or $\omega_j \neq \omega_i = \omega_k$ are referred to as degenerate FWM.

In contrast to SPM or XPM, the FWM process is sensitive to the phase of the waves. This may be described by the FWM efficiency η which is a measure for the power of the generated new wave relative to the power of the existing waves. Assuming the channels are copolarised, η is given by [Bayvel2002]

$$\eta = \left| \frac{1 - \exp(-[\alpha + j\Delta\beta]L)}{(\alpha + j\Delta\beta)L} \right|^2 \tag{2.45}$$

where L is the propagation distance and $\Delta\beta$ is the difference in the phase constants between the channels as a result of the fibre dispersion

$$\Delta\beta = \beta_2(\omega_i - \omega_k)(\omega_j - \omega_k) \,. \tag{2.46}$$

The quantity $\Delta\beta$ characterises the *phase matching* between the interacting channels. Fig. 2.12 shows a plot of the FWM efficiency versus the channel spacing

$\Delta f = \sqrt{(\omega_i - \omega_k)(\omega_j - \omega_k)}/(2\pi)$ after $L = 100$ km with $\alpha = 0.21$ dB/km for two different fibre dispersion parameters corresponding to SSMF ($D = 16$ ps/nm/km) and dispersion-shifted fibre ($D = 2$ ps/nm/km), respectively. The efficiency is normalised to the value at $\Delta f = 0$ where perfect phase match is achieved. Clearly, the efficiency takes the highest value where perfect phase matching occurs, e.g. in a fibre without chromatic dispersion. The phase matching is decreased for higher fibre dispersion and for larger channel spacing. While FWM is the dominant degradation in systems that use dispersion-shifted fibre with a local dispersion of only a few ps/nm/km, it is usually less important in SSMF-based transmission. In SSMF systems, however, another interchannel effect becomes apparent as the dominant impairment, namely cross-phase modulation.

2.4.7. Cross-Phase Modulation (XPM)

The XPM effect causes a phase modulation of the signal in one channel by the intensity of the signals in the other channels [Bayvel2002]. It is modelled by the terms $2|A_2|^2A_1$ and $2|A_1|^2A_2$ in (2.40). Considering the XPM effect of channel 2 on channel 1, the phase shift in channel 1 induced by channel 2 over the propagation distance Δz is given by

$$\Delta\varphi_{\mathrm{XPM}} = 2\gamma|A_2|^2\Delta z \tag{2.47}$$

assuming copolarised channels. If the channels have different states of polarisation, the phase shift will be reduced. Orthogonal polarisation of the channels reduces the factor from 2 to 2/3 in (2.47).

In contrast to FWM, the effect of XPM itself is not a function of the channel spacing. Considering the case of one probe channel surrounded by many pump channels, this means that the XPM phase shift of channels closer to the probe channel is the same as for channels further away from the probe channel. However, the impact of XPM is a result of both the phase shift and the group velocity difference between interacting channels. Key to understanding is the concept of the *walk-off* between channels as a result of different group velocities due to chromatic dispersion.

The walk-off is defined as the distance-dependent time shift between the signals in two channels. It is characterised by the walk-off parameter

$$d_{12} = \frac{1}{v_{gr,1}} - \frac{1}{v_{gr,2}} = D\Delta\lambda = 2\pi\beta_2\Delta f = -D\Delta f\frac{\lambda_0^2}{c} \tag{2.48}$$

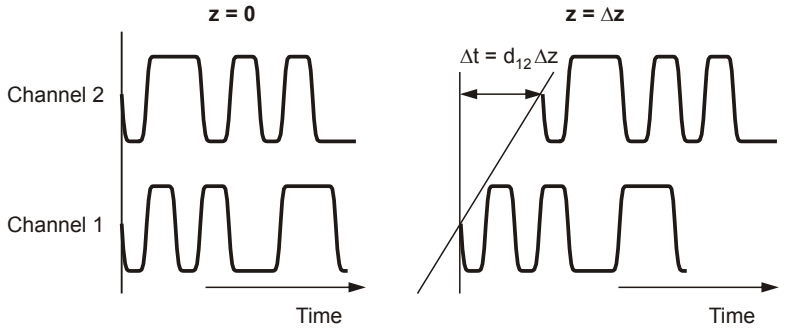

Figure 2.13. *Walk-off between two wavelength channels in a WDM system.*

where $\Delta\lambda$ and Δf are the channel spacing in terms of wavelength and frequency, respectively. Fig. 2.13 illustrates the walk-off. On the left-hand side of the figure, the time-dependent intensity of two wavelength channels is shown at the position $z = 0$ in the fibre. The two channels are modulated with different data and for clarity they are temporally aligned to the same position within the bit slot[5]. After propagation over the distance Δz, channel 2 has experienced a time shift $\Delta t = d_{12}\Delta z$ relative to channel 1. As a result of the walk-off, the time and distance-dependent XPM phase shift on channel 1 (probe channel) induced by the intensity in channel 2 (pump channel) is given by

$$\varphi_{\mathrm{XPM}}(z,t) = 2\gamma \int_0^z |A_2(z', t + d_{12}z')|^2 \exp(-\alpha z')dz' \tag{2.49}$$

where the expression $|A_2(z', t + d_{12}z')|^2$ accounts for the temporal shift of the pump channel intensity due to walk-off. It has been shown that the worst case, i.e. the largest XPM penalty, occurs if the walk-off vanishes while increasing the walk-off reduces the impact of XPM [Kikuchi1997]. This is attributed to an averaging of the XPM-induced phase shifts in the presence of walk-off.

The number of bits over which the averaging extends between two channels spaced Δf apart after propagation over distance z is given by

$$N_{12}(z) = d_{12}Bz \tag{2.50}$$

where OOK modulation using the bit rate B was assumed. The dominant contribution to the XPM phase shift is generated over the effective length $z = L_{\mathrm{eff}}$ defined in (2.42). By substituting (2.48) into (2.50) and introducing the spectral

[5] In practical WDM systems, this is not the case. In fact, the timing between channels is completely random since the channels are independently modulated.

efficiency $S = B/\Delta f$, we have the number of averaged bits in the effective length

$$N_{12}(L_{\text{eff}}) = |D|\frac{B^2}{S}\frac{\lambda_0^2}{c}L_{\text{eff}}\,. \tag{2.51}$$

Clearly, the number of bits and thus the amount of averaging scales with $|D|B^2$ assuming constant spectral efficiency. To give an example, in a 10 Gbit/s system using SSMF and a channel spacing of $\Delta f = 50$ GHz (spectral efficiency $S = 0.2$ bit/s/Hz) we have $N_{12}(L_{\text{eff}}) = 1.3$ bit. At 40 Gbit/s and $\Delta f = 200$ GHz (same spectral efficiency), this increases to $N_{12}(L_{\text{eff}}) = 21.5$ bit. Consequently, XPM has a stronger impact at 10 Gbit/s than at 40 Gbit/s.

2.5. Dispersion Management

An effective method to minimise the impact of both intra- and interchannel nonlinearities is achieved by using an optimally designed link dispersion profile, also referred to as *dispersion management* [Forghieri1997] or *dispersion mapping* [Essiambre2002]. Typically, a number of spans made of transmission fibre, such as SSMF, are periodically compensated for dispersion and loss using DCF and amplifiers, respectively. Fig. 2.14(a) shows a typical setup of a dispersion managed transmission system, and Fig. 2.14(b) shows the corresponding dispersion map diagram which is given by the accumulated dispersion $D_{\text{acc}}(z)$ [cf. (2.34)] as a function of the transmission distance. The first fibre following the transmitter introduces a certain amount of *dispersion precompensation* denoted by D_{pre}. In the link, an inline DCF is placed after each transmission fibre. The accumulated dispersion of the inline DCF is not necessarily equal to the accumulated dispersion of the transmission fibre. Under- or overcompensation is possible leading to a *residual dispersion per span* denoted by D_{res}. Before the receiver, the accumulated dispersion of the signal is compensated leaving a certain amount of net residual dispersion, D_{nrd}. It is desirable that all spans are identical. In this case, the dispersion map is characterised by the three parameters precompensation, residual dispersion per span and net residual dispersion. By varying these parameters the nonlinear tolerance of the system is optimised. Precise dispersion management becomes increasingly important at higher bit rates of 10 and 40 Gbit/s. However, the optimal dispersion map for 10 Gb/s is generally sub-optimal for 40 Gb/s and vice versa.

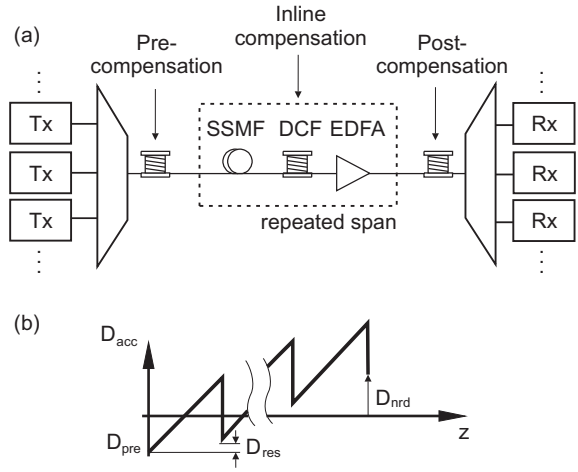

Figure 2.14. *Dispersion-managed transmission system using pre-, post- and inline dispersion compensation: (a) system setup, (b) dispersion map diagram.*

2.6. Optical Phase Conjugation

In 1979, Yariv *et al.* proposed a dispersion compensation scheme employing optical phase conjugation [Yariv1979]. Later, the concept was extended by Fisher *et al.* who showed that an ideal broadband phase conjugator also compensates for the combined effect of group velocity dispersion and the Kerr effect [Fisher1983]. Interest in the use of phase conjugation for optic transmission systems started in the 1990s. Using optical phase conjugation in fibre optic transmission systems is often referred to as mid-span spectral inversion. It was first experimentally demonstrated by [Watanabe1993]. Interest in this technique revived again in recent years for the upgrade of existing lower bit rate infrastructure to higher bit rates and novel modulation formats [Jansen2005].

The principle of distortion compensation through optical phase conjugation can be shown by taking the complex conjugate of the NLSE in (2.39). An analysis of the resulting equation (see [Breuer1996] for details) reveals that distortions from chromatic dispersion and nonlinearities can be undone by generating the complex conjugate of the distorted complex pulse amplitude in the middle of the transmission link. Optical phase conjugation is typically achieved using a nonlinear phenomenon such as four-wave mixing.

For compensation of chromatic dispersion induced distortions, the principle becomes intuitively clear since taking the complex conjugate of the time domain signal corresponds to reflecting the frequency spectrum about the origin,

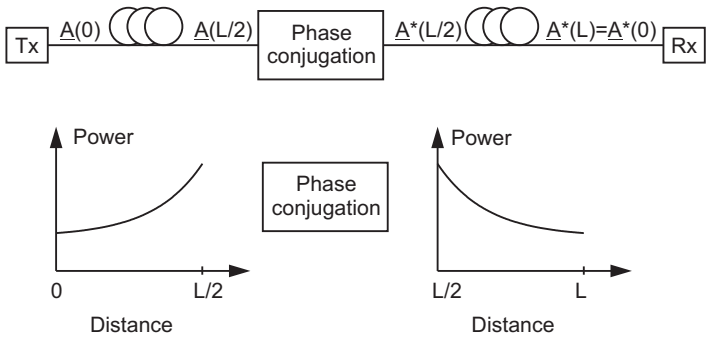

Figure 2.15. *Principle of phase conjugation for compensation of chromatic dispersion and fibre nonlinearities.*

i.e. the frequency axis is inverted. After the conjugating element, the dispersion in the second half of the link will then completely cancel the time shift that each frequency component has acquired from the dispersion of the first half of the span. Similarly, the nonlinear phase shift of the first half is compensated in the second half after the phase conjugation, if the power distribution of the second half of the span is symmetrical with respect to the position of the conjugating element. This condition is illustrated in Fig. 2.15 [Breuer1996] for a transmission system consisting of two spans with a phase conjugating element in the middle of the link. The complex envelope $\underline{A}(0)$ of the launched signal travels along the first fibre of length $L/2$ whose power distribution is assumed to be exponentially increasing. The signal is distorted by chromatic dispersion and nonlinearities of the fibre. After ideal phase conjugation, the signal $\underline{A}^*(L/2)$ propagates along the second fibre with the same dispersion and nonlinearity parameter, but with exponentially decreasing power. This power distribution is required for ideal compensation of distortions such that at the end of this link, the signal $\underline{A}^*(L)$ is equal to the complex conjugate of the signal at the input of the fibre, $\underline{A}^*(0)$.

Nonlinear optical phase conjugation is the theoretical basis for the predistortion technique presented in Chapter 3 and 4. By using digital signal processing to calculate the propagation and the phase conjugation, the first half of the transmission link is implemented in the transmitter electronics while the second half of the link is the physical transmission link. More specifically, the calculation starts with the desired waveform at the receiver $\underline{A}(0)$. Then, the propagation and phase conjugation of this signal is calculated to obtain the waveform $\underline{A}^*(L/2)$ that is predistorted for the distortions due to dispersion and nonlinearities. Eventually, this waveform is transmitted over the actual transmission

link. In the absence of noise and other additional impairments, the predistortion evolves into the desired waveform $\underline{A}^*(0)$ at the receiver.

2.7. Receiver Model

After a signal has propagated along the optical transmission link, the receiver in a WDM system demultiplexes the WDM signal to obtain the individual wavelength channels. Subsequently, the waveform of each channel is detected and demodulated to an electrical signal for digital processing and recovering of the transmitted data. The majority of current fibre-optic transmission system uses optically preamplified direct detection receivers or balanced receivers. Therefore, we focus on such receivers in this section. Employing the proposed predistortion technique introduces all the complexity at the transmitter while the receiver in such systems remains the same as in conventional direct detection or balanced detection receiver schemes.

2.7.1. Direct Detection Receiver

On-off keyed signals are detected using a direct detection receiver with a single photo diode. A block diagram of the direct detection receiver model is shown in Fig. 2.16. The signal $A(t)$ represents the noise-free linearly polarised optical waveform after transmission over the link. In the simulation carried out for this thesis, we assume noise-free inline amplifiers. The accumulated ASE noise is treated analytically in the receiver model based on [Forestieri2000]. This is valid since in preamplified direct-detection systems, ASE noise dominates over other noise sources. In the following, we present the key characteristics of the receiver model. The first element of the receiver model shown in Fig. 2.16 is the preamplifier. It adds to the signal white Gaussian ASE noise $n(t) = n_{||}(t) + n_{\perp}(t)$ with noise components for the parallel ($||$) and orthogonal ($\perp$) polarisation, respectively. The noise power spectral density

$$\sigma^2_{\mathrm{ASE}} = \frac{d\langle n^2_{||}(t)\rangle}{df} = \frac{d\langle n^2_{\perp}(t)\rangle}{df} \tag{2.52}$$

is related to the OSNR of the link by

$$\sigma^2_{\mathrm{ASE}} = \frac{\langle |A^2(t)| \rangle}{2\mathrm{OSNR}\,\Delta\nu} \tag{2.53}$$

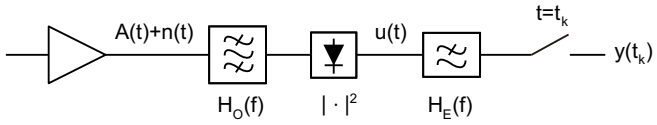

Figure 2.16. *Block diagram of a direct detection receiver.*

where $\Delta\nu$ is the resolution bandwidth of the OSNR, typically equivalent to $\Delta\lambda = 0.1$ nm (at $\lambda_0 = 1550$ nm $\Delta\nu = 12.5$ GHz), and $\langle\cdot\rangle$ denotes the average value. The term $\langle|A^2(t)|\rangle$ represents the average optical power of the signal.

The optical band-pass filter is used to filter the desired channel out of the received WDM spectrum. In addition, ASE noise is suppressed by optical filtering. The photo current after the photo diode $u(t)$ may be written as

$$u(t) = \left|[A(t) + n_{||}(t)] * h_O(t)\right|^2 + |n_{\perp}(t) * h_O(t)|^2 \tag{2.54}$$

where $h_O(t)$ is the time impulse response of the optical bandpass filter and $*$ denotes the convolution operation. The current after the electrical low-pass filter at the sample time $t = t_k$ is given by

$$y(t_k) = u(t) * h_E(t)|_{t=t_k} \tag{2.55}$$

where $h_E(t)$ is the time impulse response of the electrical low-pass filter.

2.7.2. Balanced Receiver

Differential phase shift keyed modulation formats such as DPSK cannot be received with direct detection since the phase would be lost. In this case, a delay interferometer is required to convert the phase modulation to amplitude modulation. As shown in Fig. 2.17, the optical signal is split equally to the arms of the delay interferometer. After the field in one arm is delayed by one bit period, the two fields interfere at the output coupler. Depending on the phase change between adjacent pulses the signal will emerge at the constructive or destructive port. Using balanced detection, i.e. detecting both output ports of the interferometer using two photo diodes and subtracting the photo currents, the 3 dB sensitivity advantage of the DPSK format is obtained [Gnauck2005].

The photo current $u(t)$ of the DPSK receiver is easily derived by describing the signals at the output ports of the delay interferometer. Let $B(t)$ be the input signal of the interferometer. The output at the constructive and destructive port is then given by $[B(t) - B(t - T)]/2$ and $[B(t) + B(t - T)]/2$, respectively. Assuming a linearly x-polarised field at the receiver, the x- and y-components

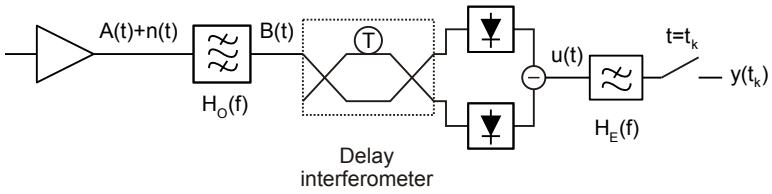

Figure 2.17. *Block diagram of a balanced DPSK receiver.*

of the field at the input of the delay interferometer are given by $B_x(t) = A(t) + n_{||}(t)$ and $B_y(t) = n_{\perp}(t)$, respectively.

2.7.3. Bit Error Rate Estimation

The received sample $y(t_k)$ is compared to a decision threshold y_{th} to recover the transmitted bits. If $y(t_k) < y_{\text{th}}$, the received sample will be detected as a logical "zero", otherwise as a logical "one". The performance of the transmission link is typically assessed using the bit error rate (BER) which is given by the ratio of incorrectly detected bits to the total number of transmitted bits.

A straightforward way to determine the BER is to simulate the transmission system including the noise of the link components using a sufficient number of bits and to count the incorrectly detected bits at the receiver. This method is referred to as a Monte Carlo estimation of the BER. While the Monte Carlo method is generally valid, it requires long simulation times for lower BER. The reason is that for a sufficiently high accuracy of the Monte Carlo result, the number of required error observations scales with 1/BER. Currently, the lowest BER available by Monte Carlo simulations with acceptable computation time is in the range of 10^{-3} to 10^{-4}.

Estimation of lower BER requires analytical or semi-analytical methods. The aim of such methods is to find an approximate solution for the probability density function $\text{pdf}_k(y)$ of each received signal sample y_k in order to calculate the error probability which is then used as an estimate of the BER.

Throughout this thesis we used a receiver model presented in [Forestieri2000] which was implemented by Randel, cf. [Randel2005]. It models the ASE noise as additive white Gaussian noise before the receiver and takes into account the effect of square-law detection and arbitrary optical and electrical filtering. Using a Karhunen–Loève series expansion of the combination of signal and noise it can be shown that the photocurrent may be expressed as a weighted sum of squared Gaussian random variables where each individual photocurrent sample obeys a noncentral chi-square distribution [Forestieri2000]. From the theory of

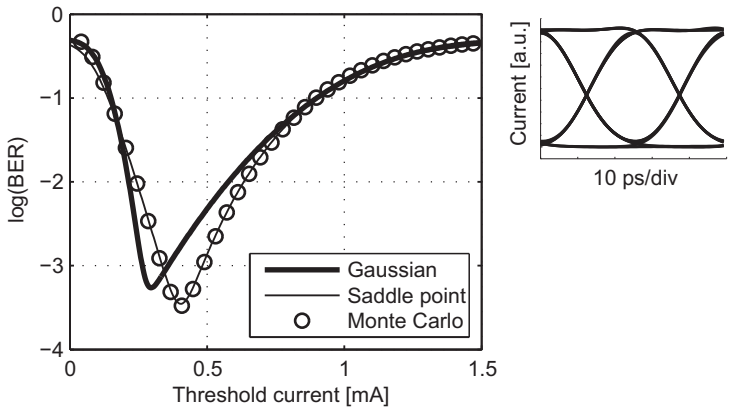

Figure 2.18. *BER as a function of the threshold current using different BER estimation methods. The signal used in this example was a 40 Gbit/s NRZ modulated waveform in back-to-back configuration. The received OSNR was set to 15 dB. Inset: Electrical eye diagram of the NRZ-OOK signal.*

probability distributions it is known that the resulting pdf of a sum of statistically independent random variables can be calculated using the moment generating function $\Phi_k(j\omega)$ which is given by the Fourier transform of the pdf,

$$\Phi_k(j\omega) = \mathcal{F}\left\{\mathrm{pdf}_k(y)\right\} \ . \tag{2.56}$$

There are two options for the estimation of the BER from the resulting moment generating function differing in computational effort and accuracy.

- By calculating the mean and the variance from the moment generating function Φ_k, the pdfs of the sampled photocurrent can be approximated by a Gaussian distribution which is equivalent to assuming post-detection Gaussian noise statistics. It is well known that in this case the BER is easily calculated analytically [Marcuse1991].
- Alternatively, the BER may be derived as an integral of the moment generating function. The resulting line integral is then evaluated approximately using the saddle-point approximation [Forestieri2000].

A comparison with respect to the computation time showed that the first method which uses Gaussian statistics is very fast while determining the saddle points using the second method requires a considerable amount of computation time. One would prefer the Gaussian method if the accuracy were suffi-

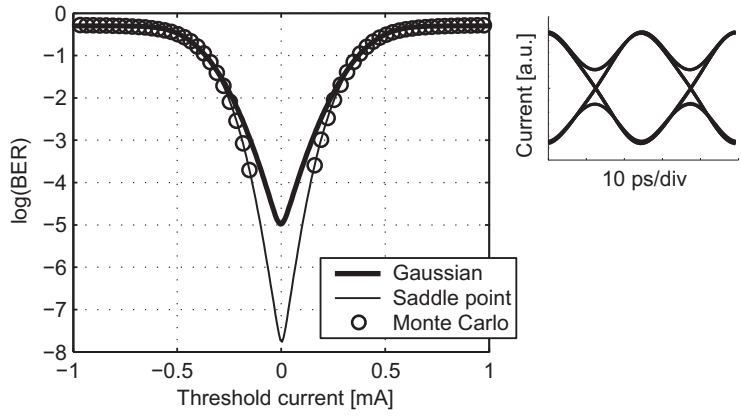

Figure 2.19. *BER as a function of the threshold current using different BER estimation methods. The signal used in this example was a 40 Gbit/s RZ-DPSK modulated waveform in back-to-back configuration. The received OSNR was set to 15 dB. Inset: Electrical eye diagram of the RZ-DPSK signal.*

cient. Therefore, we need to compare the accuracy of the two methods for the relevant system scenarios.

The accuracy of each method depends on various system parameters including the modulation format. To give an example, we study the BER of a 40 Gbit/s transmission system in the back-to-back configuration, i.e. without a fibre between the transmitter and the receiver. Fig. 2.18 shows the BER versus the decision threshold for a 40 Gbit/s NRZ-OOK signal received using a direct detection receiver shown in Fig. 2.16. The optical signal is filtered by a second-order Gaussian optical band-pass, having 3-dB bandwidth of 80 GHz, detected using an ideal photodiode, and filtered by an electrical low-pass fifth-order Bessel filter, having a 3-dB cut-off frequency of 28 GHz. The received OSNR was set to 15 dB. As a reference, the BER was first calculated using Monte Carlo error counting. The results in Fig. 2.18 show that the results obtained using the saddle point approximation agree very well with the Monte Carlo simulation. In contrast, the Gaussian approximation does not match the Monte Carlo points at all. The optimal threshold is very different. However, the optimal BER obtained using the Gaussian approximation is only slightly larger than the exact optimal BER. For this reason, the Gaussian approximation is valid in OOK transmission and was used for such simulations in this thesis since it significantly speeds up the simulations compared to the saddle point method.

Next, we compare the three BER estimation methods for DPSK transmission. The receiver setup shown in Fig. 2.17 was used with the same filters as for OOK. The BER as a function of the threshold current is shown in Fig. 2.19. Clearly, the Gaussian approximation fails to predict the correct BER value. The Monte Carlo results show that the tails of the chi-square like density function fall off much steeper than predicted by the Gaussian approximation. In contrast, the saddle point approximation shows good agreement with the Monte Carlo results. The fact that a DPSK receiver has to be modelled using the moment generating function instead of simple Gaussian statistics is well-confirmed by published results [Gnauck2005]. Therefore, for the DPSK transmission simulations, we will use the saddle point approximation based on the moment generating function.

The limitation of the BER estimation method used here lies in the fact that it does not take into account nonlinear interactions of the signal and the noise along the transmission fibre since noise is only considered additive in the receiver. In DPSK transmission, however, a phenomenon called *nonlinear phase* noise or *Gordon-Mollenauer effect* is important [Gordon1990]. Random amplitude fluctuations due to ASE noise lead to random nonlinear phase rotations through the Kerr effect which is harmful for phase-shift keyed modulation formats such as DPSK. The impact of the Gordon-Mollenauer effect is particularly severe in systems operating at low OSNR values and showing strong intrachannel nonlinearities [Ohm2005]. In such systems nonlinear phase noise may cause additional penalties.

2.8. Characterisation of Nonlinear System Degradation

This thesis is concerned with the impact of nonlinearities in various system scenarios. The nonlinear tolerance of a transmission system determines the maximum allowable launch power which is an important characteristic of a transmission system since it affects the achievable OSNR margin and the maximum achievable transmission distance. Most fibre-optic communication systems operate in a launch power regime where nonlinearities affect the performance. Therefore, this section will present the methods to analyse the transmission performance in the presence of fibre nonlinearities.

The ultimate performance criterion of transmission systems is the BER. Commercial networks require very low BER in the range of 10^{-12} which is referred to as *error free*. Laboratory experiments used to consider a BER of 10^{-9} as error free. Current forward error correction (FEC) schemes which are capable of output BER values of 10^{-11} from an input BER in the range of 10^{-4} to 10^{-3} have allowed to operate on higher BER values [Chandrasekhar2008].

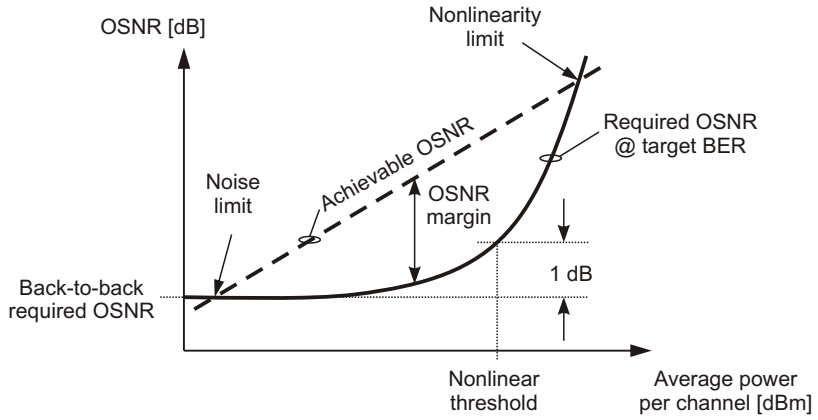

Figure 2.20. *Typical required OSNR curve.*

However, the drawback of using the BER as a performance criterion is that it depends on the received OSNR of the transmission link which is determined, amongst others, by the ASE noise power generated by the amplifiers along the link, see (2.17). It is useful to have a performance criterion that is independent of the amplifier noise figures. A commonly used criterion which fulfills this condition is the required OSNR for a certain target BER. It is computed numerically by taking the noise-free received waveform and determining the BER as a function of the received OSNR which, eventually, yields the required OSNR for a certain target BER.

A typical reference for the transmission performance is the *back-to-back required OSNR*, i.e. the value obtained if the transmitter is connected to the receiver without a piece of fibre between. The nonlinear tolerance is analysed for a fixed transmission distance by increasing the launch power into the system. A possible result is shown schematically in Fig. 2.20. A higher launch power increases the nonlinear perturbation which usually leads to an increase of the required OSNR. The *nonlinear threshold* of the transmission link may be quantified using the launch power which leads to a 1-dB increase of the required OSNR compared to back-to-back. It is a measure of the nonlinear tolerance of the transmission link.

The dashed line in Fig. 2.20 represents the achievable OSNR of the link which can be calculated according to (2.17). Clearly, the OSNR improves with increasing launch power. The difference between the achievable OSNR and the required OSNR is referred to as the *OSNR margin*. In practice, a transmission

system is designed with a certain OSNR margin which is chosen sufficiently large to accommodate the penalties due to various time varying effects such as polarisation mode dispersion, aging of components or future channel rate upgrades.

As shown in Fig. 2.20, the OSNR margin is positive between the limits given by the two intersections of the achievable and the required OSNR curves. On the low launch power side, the transmission is limited by the accumulation of ASE noise. If the achievable OSNR is lower than the required OSNR, the transmission is not possible for the target BER. On the high launch power side, the transmission is limited due to nonlinearities. Larger nonlinear degradations lead to a higher required OSNR such that the OSNR margin shrinks to zero which again makes transmission at the specified error rate impossible. Between these two limits, there is a launch power for which the OSNR margin is maximum. Optimally, the system is operated around this launch power.

CHAPTER 3

Electronic Precompensation of Chromatic Dispersion

Compensation of chromatic dispersion becomes a necessity for long-haul transmission at high bit rates of 10 Gbit/s and above. As stated in Section 2.3.3, the majority of currently deployed long-haul systems use inline optical dispersion compensating elements, mostly dispersion compensating fibre (DCF). They are placed periodically at the end of each fibre span on the amplifier sites along the link. Systems using such a dispersion compensation scheme will be referred to as optical dispersion compensation (ODC) systems in this work. Although the use of negative-dispersion fibres is a commercially advanced technique, there are several disadvantages including high cost (several thousand dollar per coil), physical size, additional loss, additional latency, nonlinearity and lack of adaptability.

As introduced in Chapter 1, novel transmitter and receiver based digital signal processing technologies emerged in recent years to overcome dispersion in a more flexible and cost-effective way. We will focus on the transmitter-based technique that uses electronic predistortion (EPD) of the launched signal to compensate for chromatic dispersion.

In this chapter, we present a comprehensive study on the nonlinear limitations of EPD in single channel and wavelength division multiplexing (WDM) systems with non-return to zero on-off keying (NRZ-OOK) modulation. The impact of intra- and interchannel nonlinear effects is analysed at 10 and 40 Gbit/s. The results are compared to an ODC system with an optimised dispersion map.

Section 3.1 introduces the system setups used for EPD and ODC. First, we investigate the EPD system under ideal conditions, i.e. by assuming that the perfectly predistorted field is transmitted causing no implementation penalty. This allows to study fundamental nonlinear limitations of EPD which is presented in Section 3.2.

The theoretically achievable performance is further limited by a practical implementation of the EPD transmitter. The required ideal predistorted waveform is degraded due to imperfect components such as the digital signal processor, the optical field modulator and the digital-to-analog converter. Therefore, more realistic system models are employed in Section 3.3 to account for limited sampling and quantisation in the EPD transmitter. It will be shown that EPD at 10 Gbit/s suffers from strong nonlinear degradations compared to ODC whereas at 40 Gbit/s, the realistic EPD system achieves an optical signal-to-noise ratio (OSNR) margin performance similar to that of ODC.

3.1. System Setups

In this section, the two dispersion compensation schemes are introduced: optical dispersion compensation (ODC) using inline DCF and electronic predistortion of dispersion at the transmitter. The two presented system setups are used for the majority of the numerical simulations throughout this thesis. The optimised ODC system is the conventional technique to compensate dispersion and mitigate nonlinear degradations. Its performance, therefore, serves as a reference to which the EPD system may be compared.

3.1.1. ODC System

The block diagram of the ODC transmission system is shown in Fig. 3.1(a). We consider a multi-span system of 800 km length (10 $\times$ 80 km spans). Each span consists of an standard single mode fibre (SSMF), a dispersion compensating fibre (DCF) and an erbium-doped fibre amplifier (EDFA). The fibre parameters are given in Table 3.1. The amplifier gain equals the span loss of 16.8 dB.

Fig. 3.1(a) shows a five-channel WDM system. Prior to transmission, the channels are multiplexed at the transmitter using a second-order Gaussian band-pass filter for each channel whose center frequency is the carrier frequency of the channel and whose 3-dB bandwidth is given in Table 3.1 for 10 and 40 Gbit/s, respectively. At the receiver, the central channel is demultiplexed using a second-order Gaussian band-pass filter. The bandwidths for 10 and 40 Gbit/s are given in Table 3.1. The values are the result of a numerical optimisation detailed in Appendix A. It should be noted that the demultiplexer bandwidths do not sim-

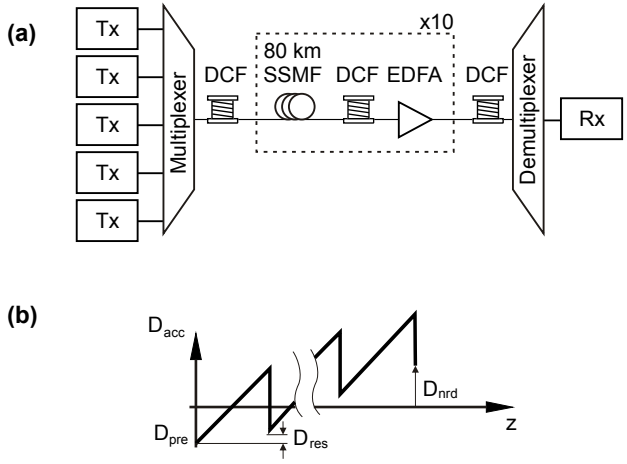

Figure 3.1. *(a) System setup for the optically dispersion compensated system. (b) Corresponding dispersion map diagram.*

ply scale with the bit rate since a higher spectral efficiency of 0.4 bit/s/Hz was used for 40 Gbit/s instead of 0.2 bit/s/Hz at 10 Gbit/s.

The electrical postdetection filter is a fifth-order Bessel low-pass having a 3-dB cut-off bandwidth of $0.7 \times B$ which is consistent with optimum values in published literature, cf. e.g. [Winzer2001]. Then the signal is detected using an ideal square-law photo diode which converts the optical intensity to an electric current. The performance is evaluated using the required OSNR in a bandwidth of 0.1 nm for a bit error rate (BER) of 10^{-4}, cf. Section 2.7. The direct detection receiver is the same in both the ODC and the EPD system.

For the single channel simulations presented in Section 3.2.1 and 3.2.3, only the central channel was transmitted using the same multiplexer and demultiplexer filters as in the WDM case.

The accumulated dispersion of the SSMF is postcompensated by the DCF as shown by the dispersion map diagram in Fig. 3.1(b). The impact of fibre nonlinearities in ODC systems may be effectively reduced by optimising the dispersion map, cf. [Essiambre2002] and Section 2.5. In this chapter, a singly-periodic dispersion map is used [Fig. 3.1(b)]. At the transmitter, a dispersion precompensation D_{pre} is introduced and the inline dispersion compensating fiber modules leave a residual dispersion per span D_{res}. The third parameter is the net residual dispersion at the receiver D_{nrd}. All three parameters have been optimised

Table 3.1. *Simulation parameters*

Bit rate	10 Gbit/s	40 Gbit/s
Channel spacing	50 GHz	100 GHz
Optical mux filter	20 GHz	120 GHz
Optical demux filter	20 GHz	44 GHz
Electrical low pass filter	7 GHz	28 GHz
D_{pre} in ODC system	−1000 ps/nm	−300 ps/nm
D_{res} in ODC system	100 ps/nm	20 ps/nm
D_{nrd} in ODC system	150 ps/nm	0 ps/nm
Modulation format	NRZ-OOK	
Number of WDM channels	5	
Number of spans N_{sp}	10	
Span length L_{SMF}	80 km	
Attenuation α_{SMF}	0.21 dB/km	
SSMF dispersion D_{SMF}	16 ps/nm/km	
Nonlinear coefficient γ_{SMF}	1.31 $\text{W}^{-1}\text{km}^{-1}$	

for the NRZ-OOK format using numerical simulations to maximise the nonlinear tolerance. A detailed description of the optimisation process is given in Appendix B. The optimum values for the 10 and 40 Gbit/s dispersion maps are given in Table 3.1.

In Section 3.2, we assume linear and lossless DCF and a single-stage EDFA to obtain the theoretical maximum of the achievable ODC performance. A more realistic ODC system model is used in Section 3.3 where lossy and nonlinear DCF and dual-stage EDFA are assumed.

3.1.2. EPD System

Electronic predistortion employs digital signal processing in the transmitter that precompensates the transmitted field for the accumulated chromatic dispersion of the transmission link to obtain a desired field at the receiver. Fig. 3.2(a) shows the investigated EPD system that is considered in this chapter. The difference to the ODC system is that the inline dispersion compensating modules along the link are replaced by a predistorting transmitter.

The sources of degradations of an EPD system can be classified into two categories: the accuracy of the EPD waveform synthesis in real time, and the effect of linear and nonlinear fibre impairments. The former limitations are related to the hardware implementation of the EPD transmitter and lead to an implementation penalty. In order to study implementation penalties arising from

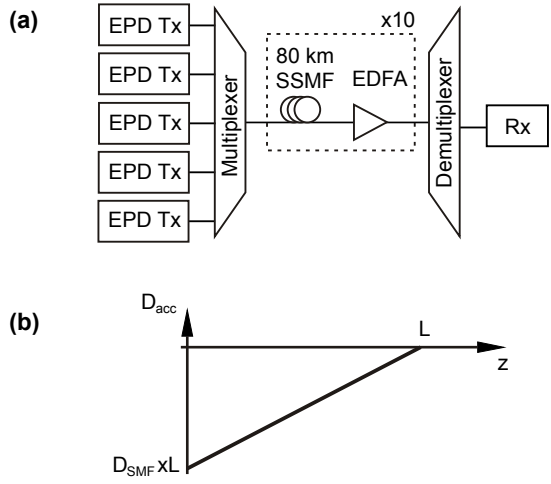

Figure 3.2. *(a) System setup for the electronically predistorted system. (b) Dispersion map diagram.*

imperfections of the components, a realistic model of the EPD transmitter is introduced in Section 3.3. In principle, the implementation penalty could be overcome by technological improvements of hardware components. Therefore, the fundamental limitations of EPD due to fibre impairments are of particular interest. For the system-level simulations presented in Section 3.2, we assume an ideal implementation of the transmitter that is equivalent to a linear lossless negative-dispersion fibre at the transmitter. This models the case of zero implementation penalty. It allows to quantify the theoretically maximum achievable performance.

More specifically, the effect of dispersion precompensation is modelled using the inverse transfer function of a linear lossless negative-dispersion fibre in the frequency domain, cf. (2.30) in Section 2.3.3. The inverse transfer function is given by

$$\underline{H}^{-1}(L, j\Delta\omega) = \exp\left(-j\frac{D_{\mathrm{SMF}}}{4\pi c}\lambda_0^2\Delta\omega^2 L\right) \tag{3.1}$$

where L is the entire length of the transmission link, $\Delta\omega = \omega - \omega_0$ is the angular frequency relative to the optical carrier frequency ω_0, λ_0 is the carrier wavelength, D_{SMF} is the fibre dispersion parameter in units ps/nm/km at wavelength λ_0. The ideal complex predistorted field $\underline{A}_{\mathrm{TX}}(t)$ is then calculated from the de-

sired target field at the receiver $\underline{A}_{\mathrm{RX}}(t)$ using

$$\underline{A}_{\mathrm{TX}}(t) = \mathcal{F}^{-1}\left\{\mathcal{F}\left\{\underline{A}_{\mathrm{RX}}(t)\right\}\underline{H}^{-1}(L, j\Delta\omega)\right\} \tag{3.2}$$

where $\mathcal{F}\{\cdot\}$ and $\mathcal{F}^{-1}\{\cdot\}$ denote the Fourier transform and the inverse Fourier transform, respectively. This approach can be used for any target modulation format. All simulations in this chapter are carried out using unchirped NRZ-OOK with 10%-90% rise and fall time of a quarter of the bit period.

The implementation of (3.2) in the simulations is as follows. The sampled field in the time domain is transformed to the frequency domain using the fast Fourier transform (FFT). The frequency domain representation of the field is multiplied by $\underline{H}^{-1}(L, j\Delta\omega)$ and subsequently transformed to the time domain, again using an FFT.

As for ODC, transmission over 10×80 km SSMF is considered using the fibre parameters given in Table 3.1. The resulting dispersion map diagram of the ideal EPD system is shown in Fig. 3.2(b). For the single channel simulations, only the central channel is active. The WDM simulations were performed using five co-polarised channels all of which are individually predistorted. Multiplexer and demultiplexer filters are the same as for ODC. In the WDM simulations, the performance of the central channel is evaluated.

3.2. Fundamental Nonlinear Limitations in EPD Systems

If chromatic dispersion is ideally compensated, fibre nonlinearities will impose a fundamental limit on the maximum launch power of the system. The impact of nonlinearities in 10 Gbit/s single channel and WDM transmission using EPD has been studied extensively in recent years [ElSaid2005, O'Sullivan2005, Killey2005b, Essiambre2005a, Klekamp2006, Chandrasekhar2006, Jansen2007]. It was shown that 10 Gbit/s EPD systems are more strongly degraded by intra- and interchannel fiber nonlinearities than conventional ODC systems. As a result, the maximum launch power in 10 Gbit/s EPD systems is significantly reduced limiting the maximum reach and the OSNR margin [Jansen2007]. However, a recent comparison on optical versus electronic dispersion compensation at the receiver showed that at symbol rates of 25 GBaud, ODC no longer has an advantage with respect to nonlinearities [Carena2008]. This raises the question, to what extent the bit rate affects the nonlinear tolerance of EPD systems. Therefore, we will analyse the nonlinear tolerance of ODC and EPD systems at 10 and 40 Gbit/s for single channel and WDM operation.

The nonlinear tolerance is characterised by calculating the required OSNR as a function of the launch power per channel, cf. Section 2.8. For an accurate pre-

diction of the nonlinear system performance in a single channel system, it is important to use a sufficiently long bit sequence depending on the dispersion map of the system [Wickham2004]. Here, we use De Bruijn binary sequence (DBBS) of order m with length 2^m. A DBBS contains every possible bit pattern of m bits. A DBBS is similar to the well-known pseudo-random binary sequence (PRBS) with the only difference that a DBBS also contains the pattern of m consecutive zeros which is missing in a PRBS.

According to [Wickham2004], the required value of m for accurate characterisation of nonlinear effects can be estimated by the nonlinear channel memory, m_{NL}, given by (2.43) in Section 2.4.5. We will discuss the length of the required DBBS for each considered case.

3.2.1. 10 Gbit/s Single Channel

For the 10 Gbit/s ODC system, using (2.43) with the values of Table 3.1, $\max(|D_{\mathrm{acc}}|) = |D_{\mathrm{pre}}| = 1000$ ps/nm, $B = 10$ Gbit/s and $\Delta f = 10$ GHz yields $m_{\mathrm{NL}} = 2$ indicating the low channel memory of the system. The 10 Gbit/s EPD system with $\max(|D_{\mathrm{acc}}|) = 12.8$ ns/nm has $m_{\mathrm{NL}} = 12$, a value significantly higher than for ODC due to the large number of pulses overlapping at the transmitter.

The ODC and EPD transmission were simulated using DBBS of order $m = 10$ and $m = 13$ with corresponding sequence lengths of 2^{10} and 2^{13} bits, respectively. The predistorted signal was calculated using (3.2). The required OSNR for a BER of 10^{-4} versus the launch power is shown in Fig. 3.3. In the linear transmission regime, i.e. at low launch power, the ODC and EPD systems show the same required OSNR performance since the ideal EPD transmitter perfectly compensates for chromatic dispersion and no implementation penalty occurs. The back-to-back required OSNR for a BER of 10^{-4} is 9.9 dB. Increasing the launch power above -4 dBm leads to a rapidly increasing required OSNR in the EPD system. The curves for DBBS lengths 2^{10} and 2^{13} have converged showing that intrachannel nonlinear effects are accurately captured. The nonlinear threshold, defined as the launch power for a 1-dB OSNR penalty compared to back-to-back, is reached at -1.4 dBm for EPD. In contrast, the nonlinear threshold of the 10 Gbit/s ODC system is reached at approximately 10 dBm launch power, confirming the substantially larger intrachannel nonlinear tolerance of optimised ODC systems compared to EPD, which was also found in [Essiambre2005a, Killey2005b, Klekamp2006].

It should also be noted that in the ODC case, the required OSNR first decreases with increasing launch power and reaches a minimum around -4 dBm. The reason is that the self-phase modulation induced chirp and the chirp caused

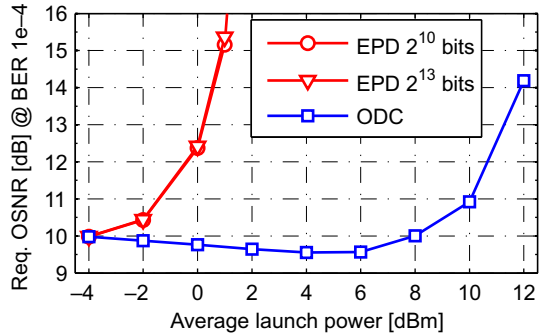

Figure 3.3. *Required OSNR for BER of 10^{-4} in single channel 10 Gbit/s systems with ODC and ideal EPD of chromatic dispersion after transmission over 10×80 km SSMF.*

by dispersion postcompensation ($D_{\text{nrd}} = 150$ ps/nm, see Table 3.1) partially cancel out which improves the signal quality even above that of the back-to-back case, cf. Section 2.4.3. The condition for the so called solitonic effect is that the pulses do not broaden significantly within the effective length such that each pulse mainly affects itself through self-phase modulation (SPM). In other words, the nonlinear channel memory, m_{NL}, must be close to 1, thereby maintaining the deterministic nature of the self-phase modulation. If however, $m_{\text{NL}} \gg 1$, as in the case of EPD, many pulses overlap and interact through the intrachannel nonlinearity. The resulting nonlinearity induced chirp cannot be compensated using linear dispersion postcompensation. Hence, the required OSNR curve for the EPD system increases monotonically and shows no improvement for larger launch powers.

3.2.2. ODC to EPD Transition at 10 Gbit/s

The ideal EPD system can be understood as an ODC system with 100% precompensation of $D_{\text{pre}} = 12.8$ ns/nm, and a residual dispersion per span equal to the accumulated dispersion of the span, i.e. $D_{\text{res}} = 1.28$ ns/nm. By varying D_{pre} from 0 to 12.8 ns/nm and D_{res} from 0 to 1.28 ns/nm, accordingly, we study the gradual transition between the dispersion maps associated with ODC and EPD. For each value of D_{res}, D_{pre} was chosen such that

$$D_{\text{pre}} = -N_{\text{sp}} D_{\text{res}} \tag{3.3}$$

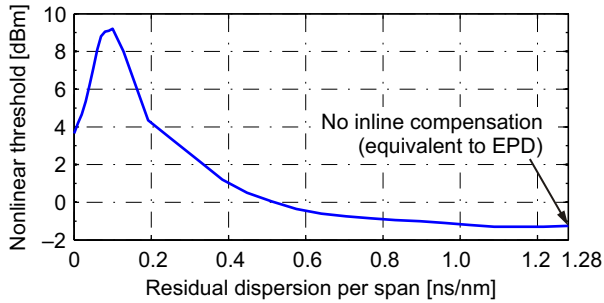

Figure 3.4. *Nonlinear threshold (BER = 10^{-4}) of single channel 10 Gbit/s transmission over 10×80 km SSMF versus the residual dispersion per span D_{res}. The precompensation for each value of D_{res} is chosen such that the net residual dispersion at the receiver is zero.*

where N_{sp} is the number of spans, here $N_{\mathrm{sp}} = 10$. This will ensure that for each value of D_{res}, the net residual dispersion at the receiver is zero. As a result, the saw-tooth shaped dispersion map [Fig. 3.1(b)] will gradually evolve into the monotonically increasing dispersion map of the EPD system [Fig. 3.2(b)]. This allows more insight into the effect the dispersion map on the system's nonlinear tolerance.

The nonlinear threshold obtained from required OSNR results at a BER of 10^{-4} versus the residual dispersion per span is shown in Fig. 3.4. The value $D_{\mathrm{res}} = 1.28$ ns/nm corresponds to no inline compensation (EPD), values below correspond to ODC. For the resonant dispersion map, $D_{\mathrm{pre}} = D_{\mathrm{res}} = 0$, the nonlinear threshold is 4 dBm. Increasing the residual dispersion up to $D_{\mathrm{res}} = 0.1$ ns/nm, which means that the precompensation is decreased to $D_{\mathrm{pre}} = -1.0$ ns/nm, will improve the nonlinear threshold to 9 dBm. This dispersion map is close to optimum. In agreement with previous studies on 10 Gbit/s precompensation [Berntson1996, Forghieri1997] it was found that precompensation and residual dispersion per span mitigate SPM, cf. Section 2.4.3. It should be noted that the maximum nonlinear threshold in Fig. 3.4 is slightly lower than that of the optimised ODC system due the restricted choice of D_{pre} and D_{res} given by (3.3). Further increasing the residual dispersion, and decreasing the precompensation accordingly, reduces the nonlinear threshold. At $(D_{\mathrm{pre}}, D_{\mathrm{res}}) = (12.8, 1.28)$ ns/nm, the dispersion map is equivalent to EPD where the nonlinear threshold is reduced to -1.4 dBm. This dispersion map causes many pulses to overlap, thereby making the nonlinear distortions random as a result of the random bit sequence. In addition, it was shown that

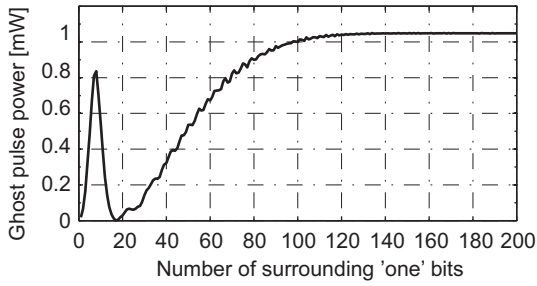

Figure 3.5. *Power of the ghost pulse at the receiver generated by a number of surrounding 40 Gbit/s NRZ 'one' bits with fixed peak power of 4 dBm after EPD transmission over 10×80 km SSMF.*

a larger amount of accumulated dispersion leads to a larger phase-modulation (PM) to intensity-modulation (IM) conversion, which degrades the signal quality of intensity modulated signals [Schüppert2009]. This amplifies the effect of SPM.

3.2.3. 40 Gbit/s Single Channel

The simulation of 40 Gbit/s EPD systems is challenging due to the increased channel memory caused by a large number of overlapping bits at the transmitter. Using (2.43) with $\max(|D_{\text{acc}}|) = 12.8$ ns/nm, $B = 40$ Gbit/s and $\Delta f = 40$ GHz yields $m_{\text{NL}} = 165$, whereas for the 40 Gbit/s ODC system using the value of Table 3.1, $\max(|D_{\text{acc}}|) = |D_{\text{pre}}| = 300$ ps/nm, we have $m_{\text{NL}} = 5$ only. According to [Wickham2004], accurate prediction of the impact of intrachannel nonlinear effects for EPD would require a DBBS of length 2^{165} which is, however, unrealistic. Nevertheless, the large channel memory of a 40 Gbit/s EPD system can be illustrated by considering the worst-case pattern of intrachannel four-wave mixing. It is known that a strong ghost pulse is generated at the position of an isolated 'zero' bit between long series of consecutive 'one' bits [Serena2007]. In order to analyse the channel memory of the EPD system, we transmit special 40 Gbit/s test sequences over the EPD system. The sequences consist of a single 'zero' bit and a number of 'one' bits with fixed peak power on either side of the 'zero'. The peak power was set at 4 dBm.

Fig. 3.5 shows the peak power of the generated ghost pulse at the receiver versus the number of neighboring 'ones'. The results show that the ghost pulse power only saturates if more than 100 'one' bits are used. Simulations using DBBS lengths shorter than $\sim 2^{100}$ bits will not account for the complete chan-

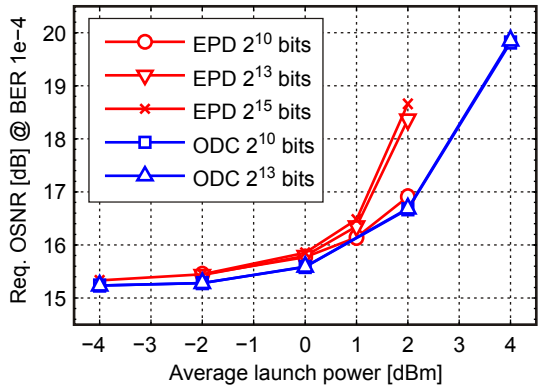

Figure 3.6. *Required OSNR for BER of 10^{-4} in a single channel 40 Gbit/s systems with ODC and ideal EPD of chromatic dispersion after transmission over 10×80 km SSMF.*

nel memory since the four-wave mixing worst case patterns are not included in shorter DBBS. Unfortunately, the computer hardware used for the simulations limited the maximum bit sequence length to $2^{15} = 32,768$ bits for single channel and 2^{11} for WDM simulations.

However, a recent study [Antona2008] on this issue used Monte Carlo simulations to present evidence that the required sequence lengths for a target BER in the order 10^{-2} to 10^{-5} are significantly shorter than predicted by (2.43). It was found that a pseudo-random bit sequence of length 2^{15} is sufficient for a BER of 10^{-5} in a highly dispersive 43 Gbit/s nonreturn-to-zero (NRZ) system. Supported by these results, we analyse the 40 Gbit/s EPD system at a BER of 10^{-4} using DBBS sequence lengths from 2^{10} to 2^{15} bits.

The calculated required OSNR as a function of the launch power is shown in Fig. 3.6. The back-to-back required OSNR is 15.3 dB. Although the EPD results fluctuate by several dB at 2 dBm launch power depending on the DBBS length, the 1-dB penalty point and, thus, the nonlinear threshold of $\sim$ 1 dBm remain relatively stable. Remarkably, there is only a small nonlinear threshold difference of less than 1 dB between EPD and ODC at 40 Gbit/s, quite in contrast to the results at 10 Gbit/s. The ODC curves for DBBS lengths of 2^{10} and 2^{13} bits are identical showing that the channel memory is accurately captured. These results were published in [Weber2008].

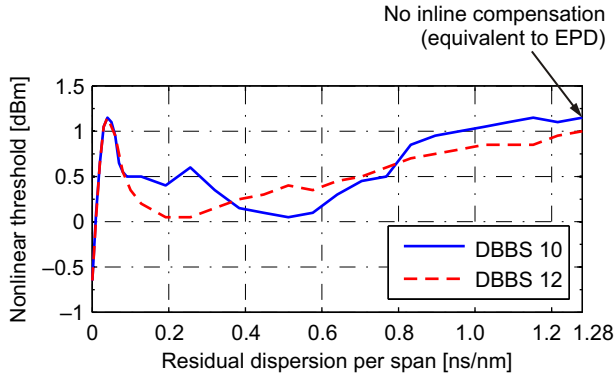

Figure 3.7. *Nonlinear threshold (BER = 10^{-4}) of single channel 40 Gbit/s transmission over 10× 80 km SSMF versus the residual dispersion per span D_{res}. The precompensation for each value of D_{res} is chosen such that the net residual dispersion at the receiver is zero.*

The difference between 10 and 40 Gbit/s single channel performance could be explained by the number of pulses that overlap and interact through nonlinearity, and by the degree of averaging of such nonlinear pulse interactions. In 10 Gbit/s EPD, a large number of overlapping pulses combined with slow waveform change rate leads to an accumulation of nonlinear interactions between overlapping pulses. In ODC systems at 10 Gbit/s, however, there is negligible pulse overlap and the pulses maintain their shape during transmission. In contrast, at 40 Gbit/s pulse overlap occurs both in ODC and EPD. In addition, signals at 40 Gbit/s change much more rapidly during propagation and nonlinear effects are averaged. Hence, their impact saturates for large pulse overlap. Still, a precise description of nonlinearities in the highly dispersive regime is a matter of ongoing research.

3.2.4. ODC to EPD Transition at 40 Gbit/s

In order to gain insight into the impact of the dispersion map on the nonlinear tolerance, we consider the gradual transition from a resonant ODC map to a DCF-less EPD map. The simulation procedure at 40 Gbit/s is the same as presented for 10 Gbit in Section 3.2.2.

The nonlinear threshold obtained from required OSNR results at a BER of 10^{-4} versus the residual dispersion per span is shown in Fig. 3.7. For the resonant dispersion map, i.e. $D_{\text{pre}} = D_{\text{res}} = 0$, the nonlinear threshold

is -0.6 dBm. Increasing the residual dispersion up to $D_{\text{res}} = 40$ ps/nm ($D_{\text{pre}} = -400$ ps/nm) will improve the nonlinear threshold to 1.1 dBm. Previous research on intrachannel nonlinearities in 40 Gbit/s transmission has shown that the optimum strategy is to minimize the pulse overlap over the effective length [Killey2000]. The optimum dispersion map parameters were found at $D_{\text{pre}} = -300$ ps/nm and $D_{\text{res}} = 20$ ps/nm, cf. Appendix B. The maximum in Fig. 3.7 is close to this optimum.

Increasing the residual dispersion above 40 ps/nm, and decreasing the precompensation accordingly, reduces the nonlinear threshold similar to what was observed for 10 Gbit/s in Section 3.2.2. Further increasing D_{res} and decreasing D_{pre} causes the nonlinear threshold to take a minimum and then to increase again. At $(D_{\text{pre}}, D_{\text{res}}) = (12.8, 1.28)$ ns/nm, the dispersion map contains no inline dispersion compensation which is equivalent to EPD where the nonlinear threshold is around 1 dBm depending on the used DBBS length. The effects of intrachannel nonlinearities seem to be less sensitive to the link's dispersion map than at 10 Gbit/s.

In order to emphasize the critical role of the DBBS length, the simulations were performed for two DBBS lengths: DBBS 10 using a sequence length of 2^{10} bits and a DBBS 12 using a sequence length of 2^{12} bits. Clearly, the two curves diverge above 90 ps/nm demonstrating inaccuracies in the nonlinear threshold. As explained in the previous section, we have some confidence that the nonlinear threshold is still sufficiently accurate if operating at a low BER of 10^{-4} [Antona2008]. Nevertheless, the numerical simulation of highly dispersive transmission at high bit rates requires further attention.

3.2.5. 10 Gbit/s WDM Transmission

In addition to intrachannel nonlinearities, the nonlinear interactions between multiple wavelength channels will further degrade the nonlinear tolerance. The impact of interchannel nonlinearities in EPD WDM systems, most importantly cross-phase modulation (XPM), is studied using a simulation technique first proposed in [Essiambre2005a] where the performance variation resulting from random time shifts between WDM channels is analysed. Using this technique, a wide range of waveform alignments are considered which are necessary for a realistic prediction of the impact of XPM. It was shown that EPD leads to fluctuations in the required OSNR due to a stronger impact of XPM caused by high power peaks in the waveforms associated with large precompensation and with the large accumulated dispersion of the EPD dispersion map [Essiambre2005a].

The simulation setup is shown in Fig. 3.8. In order to account for the statistical nature of the XPM effect, the required OSNR was calculated using 100

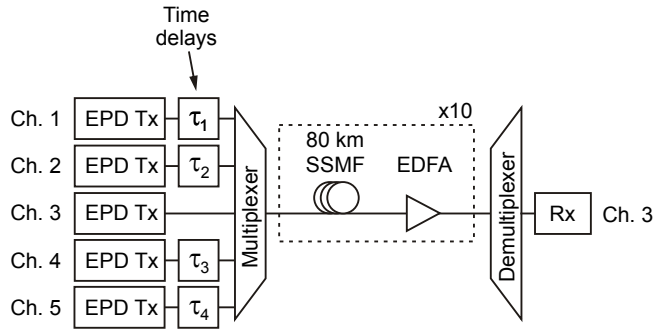

Figure 3.8. *EPD WDM system setup with five channels which are individually predistorted for the chromatic dispersion of the link. The time delay elements are used to analyse the XPM statistics in WDM operation.*

random realisations of different time shifts between the channels for a range of launch powers per channel in the 10 Gbit/s ODC and EPD systems, respectively. Parallel polarisation of the channels along the entire link has been assumed since this is the worst-case. Each channel was individually predistorted for the chromatic dispersion of the link using the ideal linear channel inversion (3.1). The bit sequence in each channel was the same De Bruijn binary sequence of order 10, i.e. the sequence length was 2^{10} bits. From the resulting histograms of the required OSNR, the 10^{th} and 90^{th} percentiles are calculated. In this case, the P-th percentile is the required OSNR value below which P percent of all values are found. Large performance variations cause a large difference between the 10^{th} and the 90^{th} percentiles.

The results are shown in Fig. 3.9. In the linear regime, at a power of -4 dBm, there is almost no difference between the system using linear EPD of chromatic dispersion (CD EPD) and the ODC system. Increasing the power leads to the spreading of the required OSNR for EPD caused by XPM as mentioned above. The maximum launch power before significant spreading occurs is -2 dBm for CD EPD. The inset shows the histogram of the required OSNR for CD EPD at 0 dBm launch power indicating severe fluctuations. Investigations into the physical reasons of the observed performance fluctuations have shown that they are due to high intensity values occurring in the predistorted waveform combined with the large accumulated dispersion of the link [Essiambre2006].

In contrast, the ODC system shows negligible spreading up to a launch power as large as 8 dBm. Above 8 dBm, however, significant spreading can also be observed for ODC. As an example, the histogram of the ODC system at 9 dBm

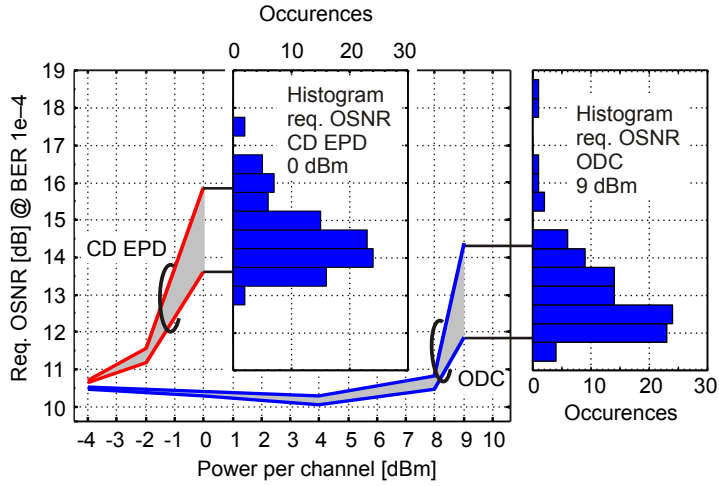

Figure 3.9. *Required OSNR distributions for BER of 10^{-4} in 5×10 Gbit/s WDM systems as a function of the average launch power per channel after 800 km with ODC and linear EPD of chromatic dispersion (CD EPD). The 10^{th} and 90^{th} percentile of the distributions are shown as a result of 100 simulations with random time delays between WDM channels. Inset: Histograms of the required OSNR for ODC at 9 dBm and EPD at 0 dBm.*

power per channel is plotted in the inset of Fig. 3.9 showing a few occurrences of large required OSNR values of up to 19 dB.

Additionally, the results in Fig 3.9 demonstrate a lower XPM tolerance of EPD compared to ODC. A theoretical study on the origins of XPM impairments[1] has investigated the effect using pump-probe simulations which have revealed that the main cause of the low XPM tolerance of EPD is the increased PM-IM conversion due to the large amount of accumulated dispersion following the nonlinear cross-phase modulation [Schüppert2009].

3.2.6. 40 Gbit/s WDM Transmission

For ODC systems it is well understood that 40 Gbit/s transmission over SSMF is mainly limited by intrachannel nonlinear effects, whereas the impact of nonlinear WDM channel interactions are less damaging [Bayvel2002]. This is a characteristic of the pseudo-linear regime, cf. Section 2.4.4. It is not clear, however, whether this is still valid for EPD transmission at a bit rate of 40 Gbit/s. Therefore, we analyse the impact of interchannel nonlinear effects in 40 Gbit/s WDM systems using the same simulation technique as for 10 Gbit/s. The parameters for the 40 Gbit/s WDM simulations are given in Table 3.1. Note that we chose a channel spacing of 100 GHz corresponding to a spectral efficiency of 0.4 bit/s/Hz whereas at 10 Gbit/s an efficiency of 0.2 bit/s/Hz was considered. For all WDM simulations, a DBBS length of 2^{11} bits was used. Although desirable for EPD simulations, the use of longer sequences is prohibitive due to the enormous computation time.

As in the previous section, the required OSNR performance of the 40 Gbit/s EPD and ODC system was calculated using 100 sets of random time shifts between the channels for different channel launch powers. The performance fluctuations at each launch power value are characterised by the 10^{th} and 90^{th} percentile of the required OSNR distributions.

The results for ODC and EPD are plotted in Fig. 3.10. As expected, the ODC system shows almost no spreading of the required OSNR because interchannel effects have negligible impact. For EPD, however, the 10^{th} and 90^{th} percentiles of the required OSNR distribution start to diverge from 0 dBm power per channel and above as a result of interchannel effects. The inset shows a required OSNR histogram at 2 dBm launch power. Required OSNR values up to nearly 20 dB may occur in the EPD WDM system at 2 dBm compared to 18.6 dB in the single channel case, cf. Fig. 3.2.3. In contrast, the ODC system has the same required OSNR for single channel and WDM which is explained by the pseudolinear transmission regime, cf. Section 2.4.4. In 40 Gbit/s ODC systems, the dominant

[1] The study was part of the diploma thesis [Schüppert2009] supervised by this author.

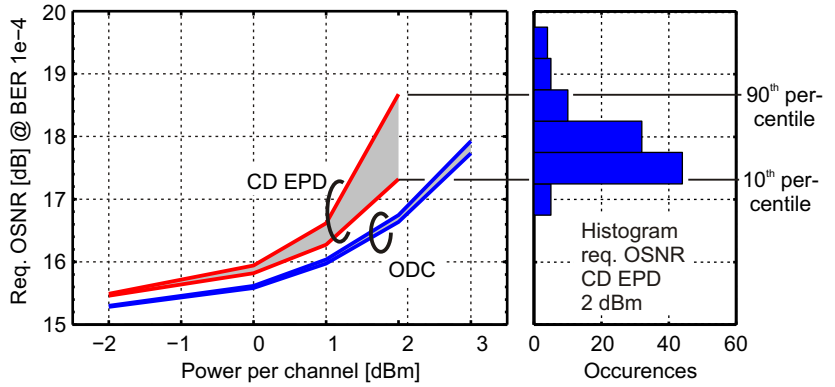

Figure 3.10. *Required OSNR distributions for BER of 10^{-4} in 5×40 Gbit/s WDM systems as a function of the average launch power per channel after 800 km with ODC and linear EPD of chromatic dispersion. The 10^{th} and 90^{th} percentile of the distributions are shown as a result of 100 simulations with random time delays between WDM channels.*

nonlinear impairment is caused by intrachannel effects whereas interchannel effects between WDM channels are negligible.

The results demonstrate that interchannel effects may not be neglected in EPD systems at 40 Gbit/s. Although these interchannel effects are present, their impact is reduced compared to 10 Gbit/s EPD despite using a higher spectral efficiency of 0.4 bit/s/Hz at 40 Gbit/s. The nonlinear threshold of the EPD system is only reduced by $\sim$ 1 dB compared to ODC.

These results show that the fundamental nonlinear limitations of EPD WDM transmission performance are similar to that of optimised ODC systems. The reason for the reduced impact of XPM in 40 Gbit/s systems is that the interfering signals walk off relatively quickly, thus causing a thorough averaging of distortions, cf. Section 2.4.7.

In conclusion, EPD becomes more attractive from a system performance point of view at 40 Gbit/s than at 10 Gbit/s. Comparing 40 Gbit/s EPD and ODC revealed that the relative difference due to fibre nonlinearities is less critical than at the lower bit rate of 10 Gbit/s. However, the practical implementation of an EPD transmitter at 40 Gbit/s is challenging due to the required bandwidth of electronic components, signal processing, modulator and digital-to-analog converters (DAC) and the large number of required finite impulse response (FIR) filter taps. Some of these issues will be addressed in the following section.

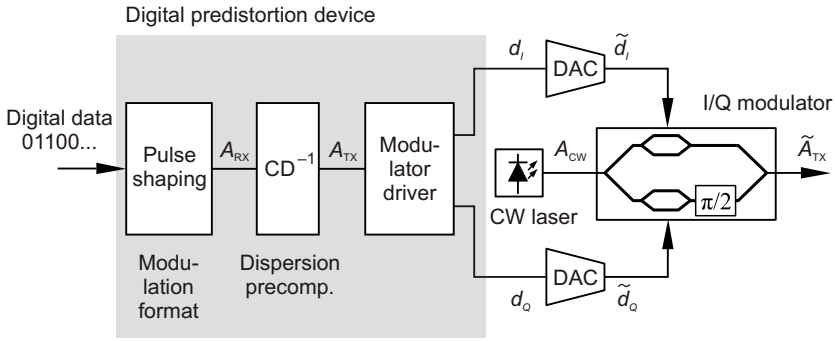

Figure 3.11. *Block diagram of the EPD transmitter.*

3.3. Realistic EPD versus ODC at 40 Gbit/s

In this section, a more realistic comparison of EPD and ODC systems at 40 Gbit/s is conducted. Three modifications of the system modelling described in Section 3.1 will be implemented: (1) In this section, the losses and nonlinearities of the DCF will be included in the simulations since linear lossless DCF overestimate the OSNR margin of ODC. (2) In practical ODC systems, the DCF is placed between the two stages of a dual-stage EDFA. The span design will be modified to include the additional amplifier stage. (3) Ideal precompensation in EPD systems overestimates the nonlinear tolerance since, in a real EPD system based on digital signal processing (DSP), a field modulator and limited sampling and quantisation of a digital-to-analog converter (DAC) will cause an implementation penalty. Therefore, we will include the model of a Mach–Zehnder field modulator and account for DAC limitations.

3.3.1. EPD Transmitter

In practical real-time EPD systems, the theoretically achievable performance presented in the previous sections will be degraded by imperfect hardware components used for the implementation of an EPD transmitter. In this section, we will present a possible transmitter implementation and account for several hardware constraints.

The EPD transmitter model used for the following simulations is shown in Fig. 3.11. The aim of the device is to produce the predistorted complex field $\underline{A}_{\mathrm{TX}}(t)$ at the output of the transmitter. However, imperfect hardware components cause signal distortions such that the ideal waveform may not be perfectly

synthesised. In order to distinguish between the desired and the real-time delivered waveform at the output of the modulator, we denote the delivered waveform by $\tilde{A}_{\mathrm{TX}}$.

The digital predistortion device converts the digital data at the input into digital (sampled and quantised) drive voltages at the output. The predistortion device is programmed for a specified amount of dispersion precompensation. The digital samples are then converted to analog drive voltages by a pair of DAC which drive an optical field modulator to synthesize the predistorted optical waveform. In the following sections, we provide a detailed description of the transmitter modelling.

The Pulse Shaping Block

The role of the pulse shaping block in Fig. 3.11 is to apply the desired target modulation format to the digital data bits. For the investigations presented in this chapter, the target modulation format was 40 Gbit/s unchirped NRZ-OOK with 10%-90% rise and fall time of 6.25 ps (a quarter of the bit period). The result is a target waveform $\underline{A}_{\mathrm{RX}}(t)$.

Dispersion Precompensating Filter

The dispersion precompensating filter generates the predistorted field waveform $\underline{A}_{\mathrm{TX}}$ from the target field $\underline{A}_{\mathrm{RX}}$. We did not investigate a particular filter structure. Instead, the block "CD^{-1}" in Fig. 3.11 represents the inverse transfer function for chromatic dispersion, $\underline{H}^{-1}(L, j\Delta\omega)$ introduced in (3.1). The field $\underline{A}_{\mathrm{TX}}$ is calculated according to (3.1) and (3.2) with an accumulated dispersion $D_{\mathrm{acc}} = D_{\mathrm{SMF}}L$ matched to the transmission link (here $D_{\mathrm{SMF}}L = 12.8$ ns/nm).

The implementation of the filter in the simulations is as follows. The sampled field in the time domain is transformed to the frequency domain using the FFT. The frequency domain representation of the field is multiplied by $\underline{H}^{-1}(L, j\Delta\omega)$ and subsequently transformed to the time domain, again using an FFT.

This filtering approach is general in that it emulates a filter that can accurately synthesise the ideal impulse response. A plot of the real and imaginary part of the complex impulse response has been shown in Fig. 2.7 in Section 2.3.3.

Although we did not implement a realistic filter structure, we will discuss some important implementation aspects in the following based on published literature. Two devices are used in practical EPD transmitter realisations to generate the required impulse responses: finite impulse response (FIR) filters or look-up tables (LUT) [ElSaid2005, Killey2005, Winzer2005]. In general, the length of the filter impulse response should be at least equal to the linear channel memory due to chromatic dispersion, m_{L}, introduced in Section 2.3.4. As a

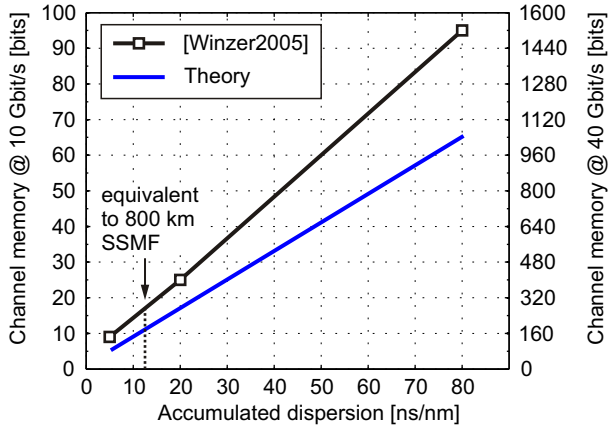

Figure 3.12. *Required channel memory for 1.5 dB implementation penalty using NRZ-OOK as the target format versus the accumulated precompensated dispersion (graph plotted from results published in [Winzer2005]) and the theoretical linear channel memory, m_L, according to* (2.35)*. The dashed line indicates the accumulated dispersion of 12.8 ns/nm (equivalent to 800 km SSMF).*

consequence, the dispersion precompensating filter requires a certain amount of processor memory depending on m_L.

In a look-up table (LUT) based implementation, the processor memory grows exponentially with the channel memory. More precisely, the total processor memory requirement of a LUT based transmitter in bits is given by $2 \times 2^{m_\mathrm{L}} \times k \times q$ (2: in-phase/quadrature parts, k is the number of samples per bit, and q is the number of quantisation bits of the DAC) [Winzer2005]. In contrast, the required processor memory of an FIR filter scales linearly with the channel memory m_L: The total memory is given by $2 \times m_\mathrm{L} \times k \times q$.

In order to estimate the required memory, we will refer to published results in [Winzer2005] which presents a comprehensive numerical simulation study on the requirements of a 10 Gbit/s EPD transmitter. In Fig. 3.12, we show the channel memory required for an implementation penalty of 1.5 dB versus the accumulated dispersion using published data from [Winzer2005]. The graph shows an estimate for the linear channel memory, m_L, which was obtained empirically by varying the length of the FIR filter until the target penalty of 1.5 dB is reached. For comparison, the theoretical linear channel memory, m_L, calculated according to (2.35) is also plotted in Fig. 3.12 where $\Delta f = B$ was used.

First, the results from [Winzer2005] reveal that the channel memory grows linearly with the accumulated dispersion[2]. The y-axis on the left-hand side represents the memory in bits at a bit rate of 10 Gbit/s. For a bit rate of 40 Gbit/s, the memory is multiplied by 16 since the channel memory scales with the square of the bit rate, cf. (2.36) in Section 2.3.4. The y-axis on the right-hand side shows the channel memory scale for 40 Gbit/s. For the 800 km transmission system considered in this chapter, the accumulated precompensated dispersion is $D_{\mathrm{acc}} = D_{\mathrm{SMF}}L = 12.8$ ns/nm. This value is marked with a dashed line in Fig. 3.12. For 10 Gbit/s, the channel memory is 17 bits whereas for 40 Gbit/s, we have 270 bits. For comparison, the values according to (2.35) are 12 and 165 bits, respectively. The relatively large difference at 40 Gbit/s indicates that the actual processor memory requirements for the 40 Gbit/s EPD transmission system remains a subject for further investigation. Using the published results, it can be concluded that a FIR filter implementation with two samples per bit would require approximately 540 taps for dispersion compensation equivalent to 800 km SSMF at a bit rate of 40 Gbit/s using NRZ-OOK modulation.

Implementing an FIR filter with hundreds of filter taps is possible with current DSP technology as shown in [Sun2008] where a real-time coherent receiver is demonstrated using a 152-tap FIR filter in a 40 Gbit/s transmission experiment. In addition, it is possible to implement the convolution operation of dispersion compensating filters in the frequency domain using the FFT algorithm, thus allowing a substantial reduction of the computational effort [Poggiolini2009]. The so called fast convolution technique is particularly efficient for large channel memories.

Therefore, we expect that the FIR filter will be a feasible filter option in high bit rate EPD transmitters. In contrast, a LUT based filter implementation for a channel memory as large as a few hundred of bits is not realistic since the LUT memory grows exponentially with the channel memory.

Field Modulator

The waveform $\tilde{A}_{\mathrm{TX}}$ is generated using an externally modulated field modulator capable of independent control of the inphase (I) and quadrature (Q) part of the field. This allows access to the amplitude and phase of the signal. Common practical implementations of such field modulators are the single dual-drive Mach–Zehnder modulator (MZM) and the triple dual-drive MZM[3]. The

[2] Note that the channel memory at 80 ns/nm is not relevant for the systems considered here. It is included to demonstrate the linear scaling.

[3] We found several different names for this device in literature: nested MZM, dual-parallel MZM, Cartesian MZM. Some publications use the term I/Q modulator which refers to the function rather than to the structure.

single dual-drive MZM has been discussed in Section 2.2.1. The disadvantage of the single MZM for linear precompensation of dispersion is that an additional (memoryless) nonlinear stage is required to linearise the transfer function [Killey2005]. In contrast, the triple MZM enables the use of linear filtering [McGhan2006]. A comparison of modulator structures for EPD of dispersion has also shown that the triple MZM is more tolerant to electrical bandwidth limitations, driving signal amplitude and delay mismatch [Yang2006]. Therefore, we concentrate on the triple MZM in this section.

The structure of the triple MZM is shown in Fig. 3.11. It consists of two inner single dual-drive MZM both driven in push-pull mode which have been discussed in Section 2.2.1. One can show that the output of the triple MZM is given by [Weber2006]

$$\underline{\tilde{A}}_{\mathrm{TX}}(t) = \frac{A_{\mathrm{CW}}}{2}\left(\cos\left(\frac{\pi\tilde{d}_I(t)}{V_\pi}\right) - j\cos\left(\frac{\pi\tilde{d}_Q(t)}{V_\pi}\right)\right) \tag{3.4}$$

where V_π is the voltage required for a π phase shift in one arm of the inner MZM and A_{CW} is the light of the continuous wave laser, $\tilde{d}_I$ and $\tilde{d}_Q$ are the modulator drive voltages at the output of the DAC for the inphase and quadrature component, respectively. The continuous-wave (CW) laser is assumed to have zero linewidth. In other words, it emits a monochromatic field with constant amplitude. In practice, this assumption means that the laser linewidth is kept sufficiently small not to cause noticeable degradations.

The drive voltages $d_I(t)$ and $d_Q(t)$ required to generate the ideal transmitted optical field $\underline{A}_{\mathrm{TX}}(t)$ are obtained from (3.4) as follows

$$d_I(t) = \frac{V_\pi}{\pi}\cos^{-1}\left(2\,\mathrm{Re}\left\{\frac{\underline{A}_{\mathrm{TX}}(t)}{A_{\mathrm{CW}}}\right\}\right) \tag{3.5}$$

$$d_Q(t) = \frac{V_\pi}{\pi}\cos^{-1}\left(-2\,\mathrm{Im}\left\{\frac{\underline{A}_{\mathrm{TX}}(t)}{A_{\mathrm{CW}}}\right\}\right). \tag{3.6}$$

The field transfer functions for the inphase and quadrature part of the MZM output field are shown in Fig. 3.13. We observe that the predistorted field components are nonlinear functions of the drive voltages ($\cos^{-1}$). However, each drive voltage controls either the inphase or quadrature component independently. If the drive voltages are biased at $d_{I,Q}/V_\pi = 0.5$ the transfer characteristics can be approximated as a linear function around this bias, which is marked in Fig. 3.13. This is an important characteristic of the triple MZM: If a linear effect such as chromatic dispersion is to be predistorted a linear filter is sufficient to calculate the drive voltages. Hence, an FIR filter may be used in

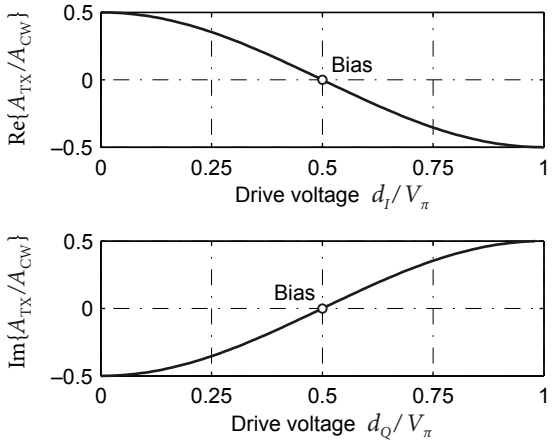

Figure 3.13. *Transfer functions of the triple MZM for the real and imaginary components.*

combination with a triple MZM which also has the advantage of manageable processor memory as explained in the previous section. A single dual-drive MZM would require an additional nonlinear element (without memory) to linearise the transfer characteristic.

Digital-to-Analog Conversion

A digital-to-analog converter (DAC) takes digital samples at the input and outputs analog drive voltages. A typical system-level model of a DAC describes the device by sample rate conversion and quantisation using a finite number of quantisation bits. Since computer simulations are inherently digital, an analog signal is modelled as a sampled signal with a large sampling rate, e.g. 16 or 32 samples per bit. The simulation sampling rate is chosen sufficiently high to avoid aliasing errors. The DAC performs a rate conversion from the lower DAC sampling rate, e.g. 2 samples per bit, to the simulation rate. This technique is referred to as multirate digital signal processing and is implemented using a standard resampling function from the Matlab signal processing toolbox. A comprehensive tutorial can be found in [Crochiere1981].

Fig. 3.14 illustrates the procedure. The drive voltages $d_{I,Q}(i)$ are obtained from the precompensated field $\underline{A}_{\mathrm{TX}}$ through (3.5) and (3.6) sampled at the simulation sampling rate (32 samples per bit period). In order to consider the effect of limited DAC sampling rate, $d_{I,Q}(i)$ are first low-pass filtered to remove

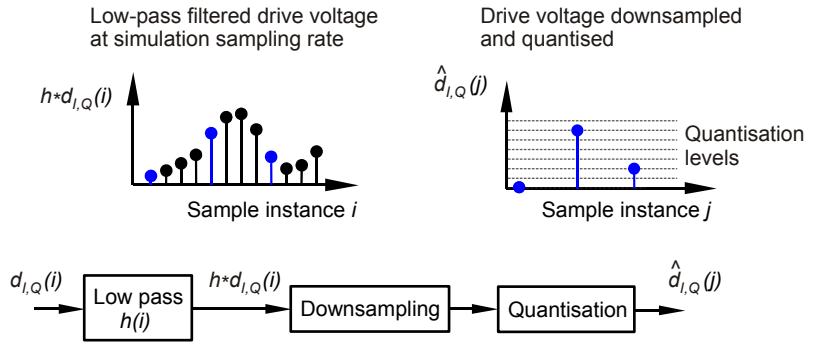

Figure 3.14. *Downsampling of the drive voltages to the lower DAC sampling rate.*

frequency components above the half of the sampling frequency. This is well known from sampling theory as anti-aliasing. The filter impulse response $h(i)$ is a digital FIR filter that approximates the ideal rectangular low-pass characteristic. Then the filtered signal is downsampled to the lower DAC rate. Downsampling by a factor M means that only every Mth sample is kept. In the next step, the samples are quantised using 2^q quantisation levels where q is the number of quantisation bits. Uniform quantisation is used with equally spaced levels ranging from the minimum to the maximum amplitude of the sampled signal. The sampled and quantised signals are denoted by $\hat{d}_{I,Q}(j)$.

The final step of the DAC model is the upsampling of the quantised signal to the simulation sampling rate. The process of increasing the sample rate implies that new samples must be interpolated between the drive signal samples $\hat{d}_{I,Q}(j)$. As illustrated in Fig. 3.15, the new samples are first filled with zeros. Subsequently, a low-pass filter is applied to smooth the waveform. From sampling theory it is known that the low-pass filter eliminates the unwanted periodic images of the baseband signal spectrum [Crochiere1981].

3.3.2. Impact of Finite DAC Sampling Rate and Quantisation

The cost-effective realisation of DAC with sampling rates in the range of 40 to 80 GSa/s tends to be a very critical aspect of EPD implementation at 40 Gbit/s [Roberts2008]. Sampling rates in this range are not yet achievable using currently available DAC devices. However, it should be noted that the current trend towards 100G Ethernet using digital coherent receivers is a strong driver for the development of fast data converters with sampling rates in the

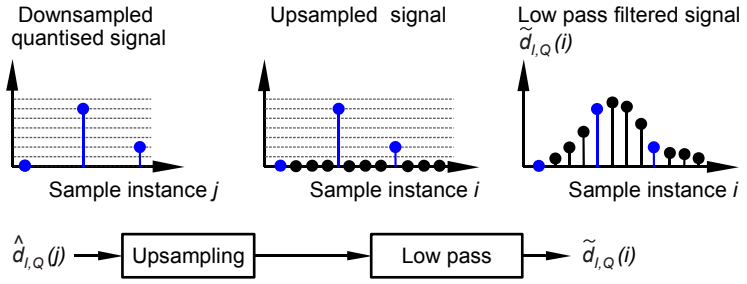

Figure 3.15. *Upsampling of the quantised samples from the DAC rate to obtain the signal at the higher simulation sampling rate.*

range of 50 GSa/s. Recently, Fujitsu Microelectronics Europe announced a 56 GSa/s 8-bit analog-to-digital converter in 65 nm CMOS process technology [Fujitsu2009]. Therefore, the realisation of digital-to-analog converters at such sampling rates is expected in the near future.

In order to analyse the impact of DAC limitations, the sampling rate and quantisation was varied in the EPD transmitter. After transmission, the performance was evaluated using the required OSNR for a BER of 10^{-4}. For the EPD single channel simulations, a DBBS length of 2^{15} bits was used. This was the maximum possible sequence length on the available computers.

First, we tested a DAC sampling rate of 1 sample per bit, i.e. 40 GSa/s, and no quantisation, i.e. continuous drive voltage amplitudes, in back-to-back configuration. This led to penalties of more than 5 dB compared to the results obtained using the ideal EPD transmitter. Using a sampling rate of 1.5 samples per bit, i.e. 60 GSa/s, and 4 quantisation bits causes an acceptable penalty of 0.9 dB. As stated above, a 60 GSa/s DAC is considered within the reach of current technology.

Increasing the rate to 80 GSa/s led to an improvement of only 0.1 dB. It was also verified that a further increase in the number of quantisation bits led to negligible improvements. Therefore, the DAC rate was set to 60 GSa/s with 4-bit quantisation as a good compromise between implementation complexity and performance.

3.3.3. Nonlinear Tolerance of EPD with 60 GSa/s 4-bit DAC

Next, we investigate the impact of intrachannel nonlinearities in a single-channel 800-km EPD system using a 60 GSa/s 4-bit DAC and a triple MZM. The launch power was varied from −4 dBm to 2 dBm. The transmitted signal

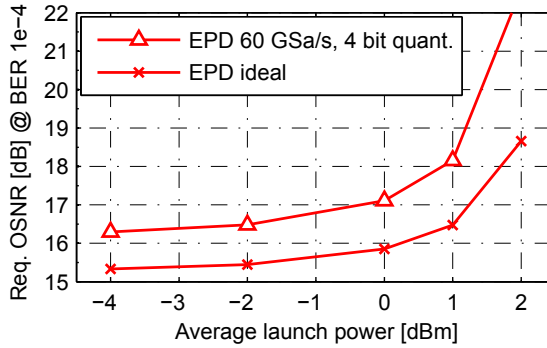

Figure 3.16. *Required OSNR for BER of 10^{-4} in a single channel 40 Gbit/s systems with ideal EPD of chromatic dispersion and with a more realistic EPD transmitter after transmission over 10×80 km SSMF. For the EPD simulations, a sequence length of 2^{15} was used.*

was encoded with a DBBS-15 (32,768 bits). The OSNR requirement for a BER of 10^{-4} versus the launch power is shown in Fig. 3.16. For comparison, the curve for the ideal EPD system without an implementation penalty is also shown.

At lower launch powers, a penalty of 1 dB is paid compared to ideal EPD. We verified that this penalty is mainly due to the limited quantisation of the drive signals, whereas a further increase of the sampling rate only slightly improves the required OSNR. Above a launch power of 0 dBm, the difference in required OSNR between ideal and non-ideal EPD increases rapidly showing that nonlinearities have a stronger impact on the realistic EPD transmission than on ideal EPD. The reason may be that quantisation is a nonlinear operation itself leading to power-dependent quantisation noise.

3.3.4. DCF Loss and Nonlinearity

In order to compare the realistic EPD system performance to that of a realistic ODC system, we need to take into account the additional degradations caused by realistic DCF. In the previous analysis of ODC, the DCFs were assumed lossless and linear, a condition which is only approximately fulfilled in real systems. In reality, the lossy and nonlinear DCFs are placed between the two stages of a dual-stage EDFA, and the input power into the DCF is optimised to reduce the impact of nonlinearities. For a fair comparison between EPD and ODC the additional optical loss and nonlinearity should be taken into account.

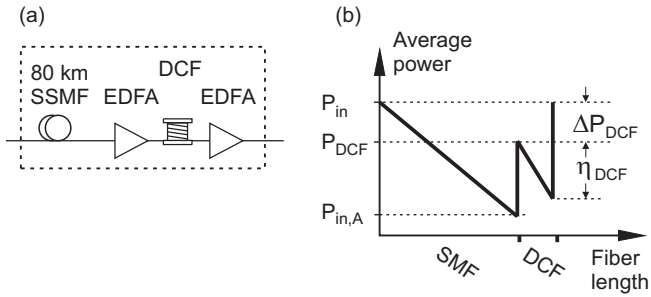

Figure 3.17. *(a) Span design for the ODC system with a DCF and a dual-stage EDFA. (b) Power levels along the span.*

Therefore, we modified the span design of the ODC system as shown in Fig. 3.17(a). The SSMF is followed by a dual-stage EDFA. The DCF is placed between the two amplifier stages. For the following simulations, a DCF attenuation coefficient of $\alpha_{\mathrm{DCF}} = 0.5$ dB/km, a DCF dispersion coefficient of $D_{\mathrm{DCF}} = -100$ ps/nm, and a nonlinearity coefficient of $\gamma_{\mathrm{DCF}} = 3.01\ \mathrm{W^{-1}km^{-1}}$ were assumed. The length of the DCF was adjusted to compensate for the desired amount of dispersion. Here $L_{\mathrm{DCF}} = 12.6$ km was used which is equivalent to 20 ps/nm residual dispersion per span. The gain of the first EDFA is set to obtain a certain DCF input power, P_{DCF}, and the gain of the second EDFA is set to obtain the launch power, P_{in}, into the next span [Fig. 3.17(b)].

First, the required OSNR of the ODC system was calculated for different P_{DCF}. The DCF input power P_{DCF} was chosen lower than the launch power of the system by a certain amount $\Delta P_{\mathrm{DCF}} = P_{in} - P_{\mathrm{DCF}}$ (in dB). Fig. 3.18 shows the results using the realistic DCFs with $\Delta P_{\mathrm{DCF}} = 5$ dB which is a typical value. For comparison, the results using linear and lossless DCFs are also shown. Clearly, the additional impact of DCF nonlinearities reduces the nonlinear threshold of the system compared to the case of the linear lossless DCF.

However, using the lossy DCFs will increase the noise figure and hence reduce the achievable OSNR, cf. Section 2.3.2. The noise figure F_{DCF} of a dual-stage EDFA including a DCF is approximately given by [Essiambre2002]

$$F_{\mathrm{DCF}} = F\left(1 + \frac{\eta_{\mathrm{DCF}} P_{in,A}}{P_{\mathrm{DCF}}}\right) \tag{3.7}$$

where F is the noise figure of each individual EDFA (assumed equal here $F_{[\mathrm{dB}]} = 4$ dB), η_{DCF} is the DCF loss (here $\eta_{\mathrm{DCF[dB]}} = 6.3$ dB), and $P_{in,A}$ is the input power into the first amplifier [Fig. 3.17(b)]. Substituting (3.7) into (2.17) yields

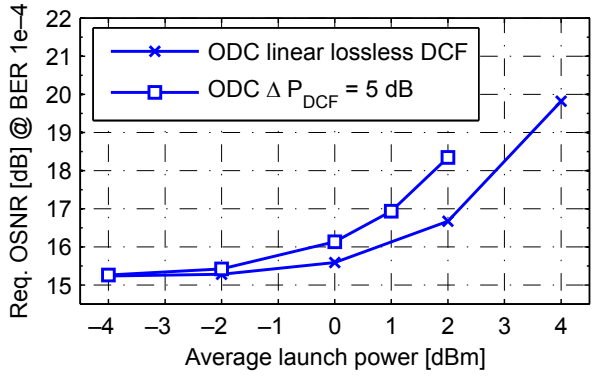

Figure 3.18. *Required OSNR for a BER of 10^{-4} in the single channel 40 Gbit/s ODC system with realistic DCFs after transmission over 10×80 km SSMF. Results for linear and lossless DCFs are shown for comparison.*

the achievable OSNR at the receiver for a transmission link containing dual-stage EDFAs. Using the given parameters yields $F_{\mathrm{DCF[dB]}} - F_{\mathrm{[dB]}} = 1.1$ dB, i.e. the achievable OSNR is reduced by 1.1 dB compared to single-stage EDFA.

3.3.5. Comparison of the OSNR Margin for Single Channel and WDM

In Section 3.2, the required OSNR was sufficient to compare EPD and ODC since the achievable OSNR at the receiver was equal for both systems if the same fibre and amplifier parameters are assumed. However, using the above mentioned modifications for the ODC system, the achievable OSNR is reduced by the DCF loss and the dual-stage EDFA. In this case, the required OSNR is not suitable to compare the system performance of ODC and EPD. Therefore, we compare the performance in terms of OSNR margin, cf. Section 2.8. The OSNR margin is given by the difference between the achievable OSNR and the required OSNR after transmission at the receiver. The achievable OSNR is calculated according to (2.17) using $\alpha L = 0.21$ dB/km $\times$ 80 km, $N = 10$. The amplifier noise figure differs for EPD and ODC because of the additional DCF loss and the dual-stage EDFA in ODC systems as explained in the previous section. $F_{\mathrm{EPD}} = 4$ dB and $F_{\mathrm{ODC}} = 5.1$ dB were used for EPD and ODC, respectively.

Using (2.17), (3.7) and the required OSNR simulation results, the OSNR margin for the realistic ODC and EPD systems was calculated. The results for the single channel case are plotted in Fig. 3.19(a). By varying the value ΔP_{DCF}, the optimum ODC system that achieves the largest maximum OSNR margin was

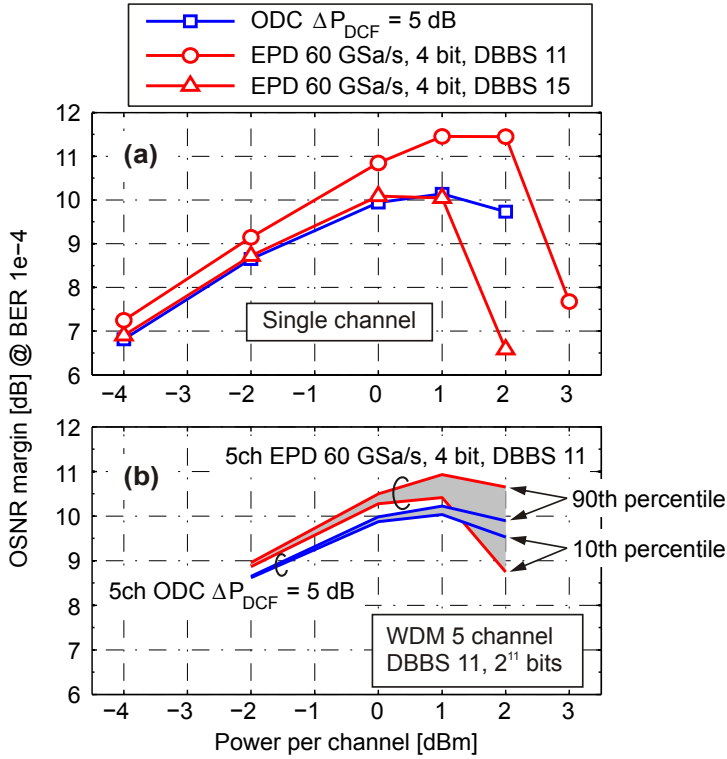

Figure 3.19. *OSNR margin for a BER of 10^{-4} at 40 Gbit/s for realistic EPD and ODC systems after transmission over 10×80 km SSMF: (a) single channel, (b) five-channel WDM*

found for $\Delta P_{\mathrm{DCF}} = 5$ dB. In this case, the maximum margin is 10.1 dB at 1 dBm launch power. The maximum OSNR margin for the EPD system using 60 GSa/s and 4-bit quantisation is 10 dB around 1 dBm launch power if calculated with a DBBS 15. Remarkably, the EPD and ODC systems achieve the same maximum OSNR margin demonstrating that the additional penalty from sampling and quantisation in the EPD system is similar to the penalty due to the DCF loss and the nonlinearities in the ODC system for the configuration used here.

Next, the impact of interchannel effects in realistic ODC and EPD systems was investigated for the WDM case with five channels at 40 Gbit/s per channel using the same simulation technique as in Section 3.2.6. As a result of the required OSNR histogram, the OSNR margin will also exhibit a variation over

a certain range which is characterised by the 10^{th} and 90^{th} percentile as shown in Fig. 3.19(b). The maxima of the OSNR margin percentiles are slightly better for EPD than those of ODC, suggesting an advantage for EPD WDM systems. However, the larger spreading of the EPD percentiles demonstrates that it is stronger degraded by interchannel effects than the ODC system, in particular at the optimum launch power of 1 dBm.

It should also be noted that using a sequence length of 2^{11} will overestimate the OSNR margin for EPD as shown by the comparison of the "DBBS 11" and "DBBS 15" curves in Fig. 3.19(a) for a single channel system. Longer sequences would be desirable for WDM simulations, however, they lead to enormous computation times. Despite the limitations due to the sequence lengths, the true maximum OSNR margin of EPD at 40 Gbit/s is expected to be only slightly worse than that of ODC.

3.4. Conclusions on Electronic Precompensation of Chromatic Dispersion

The impact of intra- and interchannel nonlinearities in 10 and 40 Gbit/s NRZ-OOK systems using EPD systems without inline DCFs was investigated and compared to optimised ODC systems. Using ideal modelling of EPD and ODC systems, the theoretical maximum of the nonlinear tolerance was calculated. At 10 Gbit/s, EPD suffers from large degradations due to intra- and interchannel nonlinearities compared to ODC. As a result, the maximum launch power of the five-channel EPD WDM system is reduced by $\sim$11 dB compared to ODC. At 40 Gbit/s, however, EPD and ODC show a similar nonlinear tolerance for single channel transmission with the nonlinear threshold of EPD being only $\sim$1 dB lower than for ODC. In addition, WDM system simulations at 40 Gbit/s have also shown a similar impact of interchannel nonlinearities for ODC and EPD.

A more realistic comparison at 40 Gbit/s was conducted by including DACs with limited sampling and quantisation, and a field modulator in the EPD transmitter, and by considering the loss and nonlinearities of the DCF in the ODC system. By calculating the OSNR margin of single channel and WDM transmission, it was shown that the 40 Gbit/s EPD system using 60 GSa/s and 4-bit quantisation achieves a performance similar to that of the optimised ODC system. The results presented in this chapter indicate that linear EPD of chromatic dispersion may become more attractive at higher bit rates since limitations due to nonlinearities are less critical than at lower bit rates.

So far we have restricted the investigations to the NRZ-OOK modulation format. The use of more advanced modulation formats may allow a reduced transmitter complexity. In particular, narrow-band formats such as optical duobinary relax the sampling rate requirements to enable 1 sample per bit DAC operation as shown for 10 Gbit/s precompensated transmission [Watts2007]. But this may not be similarly true at 40 Gb/s. In addition, optical duobinary is known to be more sensitive to nonlinear effects than NRZ. Therefore, further study is required for EPD at 40 Gbit/s and above in order to quantify the improvements from using advanced modulation formats.

CHAPTER 4

Electronic Precompensation of Fibre Nonlinearities

EMPLOYING digital signal processing in the transmitter opens the opportunity to not only compensate for chromatic dispersion but also for other impairments, the most important of which are the nonlinear effects of the transmission fibre. As shown in the previous chapter, fibre nonlinearities degrade the performance of dispersion precompensated systems. In principle, all nonlinear effects can be eliminated since they lead to a deterministic perturbation. Assuming that the amplitude and phase information of all wavelength division multiplexing (WDM) channels at the input of the fibre are known, the nonlinear effects are completely described by the nonlinear Schrödinger equation (NLSE) which allows to predistort the field for both chromatic dispersion and nonlinearities.

There are, however, fundamental limitations to such complete compensation of optical nonlinearities. A real transmitter in a current WDM link terminal can only control the limited frequency band of its own channel. While this allows for precompensation of intrachannel nonlinearities, precompensation of interchannel nonlinearities is challenging if not impossible. Under this restriction, the nonlinear interactions from neighbouring channels such as cross-phase modulation (XPM) impose a fundamental limit on the channel launch power since in a practical WDM transmitter, the phase and amplitude of the neighbouring channels are not accessible. This limit will be investigated in this chapter.

Another source of limitations are the imperfections of the transmitter hardware components such as finite digital-to-analog converter (DAC) sampling rate and quantisation or limited processor complexity. In this chapter, we will show how the individual components affect the performance of electronic predistortion (EPD) in 10 and 40 Gbit/s systems. Using a realistic model of an EPD transmitter, the complexity for combined EPD of chromatic dispersion and nonlinearities will be analysed at 10 and 40 Gbit/s. We will show that a simple scaling to 40 Gbit/s is problematic with respect to the real-time realisation. Instead, we propose and analyse electronic predistortion of intrachannel nonlinearities in an optically inline compensated transmission system at 40 Gbit/s.

4.1. Precompensation of Dispersion and Nonlinearities

The first scenario we will discuss is the combined precompensation of chromatic dispersion and intrachannel nonlinearities. In the previous chapter, it was shown that using linear electronic dispersion precompensation instead of optical dispersion compensation (ODC) significantly reduces the nonlinear threshold in 10 Gbit/s transmission due to a stronger impact of intrachannel nonlinearities. If these nonlinearities were precompensated by the EPD transmitter, an increase of the nonlinear threshold would be expected. This has already been theoretically and experimentally demonstrated for 10 Gbit/s transmission [Killey2006, Roberts2006]. In [Killey2006], the authors present numerical simulations of precompensated transmission over 1200 km standard single mode fibre (SSMF). It is demonstrated that the nonlinear threshold of -2 dBm for linear dispersion compensation is increased to 1 dBm using additional nonlinearity compensation based on a 13-bit look-up table (LUT). In an experiment reported in [Roberts2006], a similar increase of the launch power was observed. After 1280 km SSMF transmission, the nonlinear threshold could be increased from 0 dBm with linear compensation to 3 dBm with nonlinear compensation.

In 40 Gbit/s transmission, the reduction of the nonlinear threshold between ODC and EPD is less pronounced as discussed in the previous chapter. Additional precompensation of intrachannel nonlinearities may further improve the nonlinear threshold of EPD, thus, even outperforming ODC.

In order to investigate the potential improvements from simultaneous EPD of dispersion and intrachannel nonlinearities, we start with an ideal model which achieves perfect precompensation and show the fundamental limitations in single channel and WDM transmission. Subsequently, we analyse the hardware requirements of such nonlinearity precompensation in 10 and 40 Gbit/s systems and discuss the feasibility.

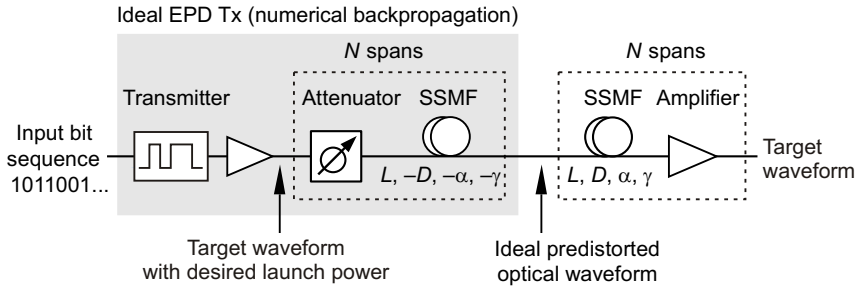

Figure 4.1. *System model used for ideal backpropagation to calculate the ideal predistorted field.*

4.1.1. Ideal Backpropagation

The transmitter needs to calculate and synthesise the predistorted waveform. This requires a model that reverses the unwanted propagation effects of the channel. As early as 1979, the effect of optical phase conjugation was found to fully compensate for chromatic dispersion by four-wave mixing nonlinear interaction [Yariv1979]. The concept of optical phase conjugation is the theoretical basis of today's electronic predistortion as explained in Section 2.6. By placing a phase conjugating element in the middle of a transmission link, the dispersion and nonlinearity induced signal distortions of the first half of the link are reversed in the second half under the condition that the two parts have identical parameters and the power profile is symmetric with respect to the middle of the link as shown in Fig. 2.15 on page 40. For electronic predistortion, the transmission over the first half and the phase conjugation is performed using digital signal processing in the transmitter.

Instead of taking the complex conjugate it is more convenient for the numerical simulation to use negative link parameters for the dispersion D, the fibre attenuation α and for the nonlinearity coefficient γ. This method is often referred to as backpropagation since it describes the propagation in the negative z direction from the receiver to the transmitter. It was first proposed in [Pare1996].

Fig. 4.1 shows the setup used for ideal backpropagation. The shaded box represents the backpropagation part which is, essentially, a model for an ideal EPD transmitter. The second part of the setup is the actual transmission link. The undistorted target waveform is generated inside the backpropagation part by a conventional transmitter for the desired modulation format. The fibre spans of the backpropagation part are designed to obtain a symmetric power profile us-

ing attenuators whose attenuation is given by the gain of the corresponding amplifiers in the actual transmission link. As mentioned above, the backpropagation fibre parameters for the chromatic dispersion D, the fibre attenuation α and for the nonlinearity coefficient γ are chosen negative to those of the transmission fibre. The EPD transmitter model generates the ideal predistorted waveform which is then launched into the transmission link. While propagating through the link the waveform evolves to the target signal at the receiver. Obviously, the transmitter must be programmed for a nominal target distance and launch power.

Fibre propagation is modelled using the NLSE, cf. (2.39) in Section 2.4.1. It is solved numerically using the split step Fourier algorithm [Agrawal2001]. If the backpropagation is calculated without limiting the step size, the bandwidth and the processor memory, any amount of nonlinearity can be predistorted. For the simulations presented in this thesis, the step size of the split step method was chosen in each step such that the maximum acceptable nonlinear phase shift induced in one step is less than 1 mrad. This method is often referred to as the nonlinear phase-rotation method and is widely used in fibre-optic transmission simulations [Sinkin2003]. If the same step size and simulation bandwidth[1] is used for backpropagation as for the forward propagation, the nonlinearity compensation will be ideal in the simulation under the assumption of a noiseless channel.

This technique is used to investigate the launch power limitations in an 10×80 km SSMF transmission link if both chromatic dispersion and intrachannel nonlinearities are ideally predistorted. By neglecting limitations due to electronics and transmitter hardware, the theoretically maximum achievable performance is considered.

This method is fundamentally limited by the finite transmitter bandwidth and by additional non-deterministic effects that cannot be pre-calculated, e.g. interchannel nonlinearities, polarisation mode dispersion (PMD) and nonlinear interactions of amplified spontaneous emission (ASE) noise with the signal. Such effects will disturb the perfect channel inversion. The impact of some of these effects will be studied in the following.

4.1.2. Fundamental Bandwidth Limitations of Nonlinear Predistortion

We first investigate the nonlinear tolerance of a single channel using ideal predistortion of chromatic dispersion and self-phase modulation (CD+SPM EPD). This may seem unnecessary since the setup in Fig. 4.1 is designed to generate the

[1] The simulation bandwidth is determined by the number of signal samples per bit period used for the signal representation.

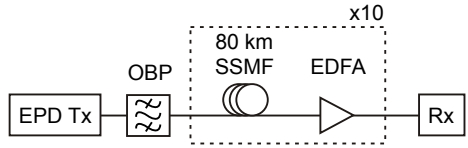

Figure 4.2. *EPD system setup to investigate the bandwidth limitation. OBP: optical band-pass.*

ideal predistorted field which will result in the undistorted target waveform at the receiver independent of the launch power. However, in a real transmission system with multiple wavelength channels, this ideal condition is fundamentally disturbed since each WDM channel is optically filtered in the multiplexer. Even if no implementation penalty exists due to the EPD hardware constraints, there will still be the bandwidth limitation due to the band-pass filter. In this section, we will quantify the limitation due to transmitter-side optical band-pass filtering.

For this purpose, we use the setup shown in Fig. 4.2. The optical band-pass represents the filter inside a WDM multiplexer. The ideal predistorted field obtained from the setup in Fig. 4.1 is used for the central channel. This signal is optically filtered by a second-order Gaussian band-pass with a 3-dB bandwidth of 20 GHz which was found to be the optimum in 50 GHz DWDM operation using 10 Gbit/s/channel. All filter and system parameters are the same as used for the WDM simulations in Chapter 3. The nonlinear tolerance of single channel transmission is analysed by calculating the required optical signal-to-noise ratio (OSNR) for a bit error rate (BER) of 10^{-4} versus the launch power.

The simulation results for CD+SPM EPD are plotted in Fig. 4.3. For comparison, the results for ideal linear dispersion precompensation (CD EPD) already discussed in Section 3.2.1 are also included in the graph. Clearly, the additional SPM compensation increases the nonlinear tolerance. Up to a launch power of 6 dBm, no nonlinearity induced penalty is observed for the CD+SPM EPD configuration. Above 6 dBm, however, the required OSNR increases rapidly due to bandwidth limitations imposed by the optical band-pass filter.

In fact, the ideal nonlinear predistortion generates new frequency components which lead to a power-dependent bandwidth increase of the predistorted signal spectrum. This is illustrated in Fig. 4.4 for the two launch power values of 6 and 8 dBm. It shows the spectrum of the optical signal before and after the transmitter band-pass filter. Increasing the launch power broadens the signal spectrum before the filter. The physical reason for this phenomenon

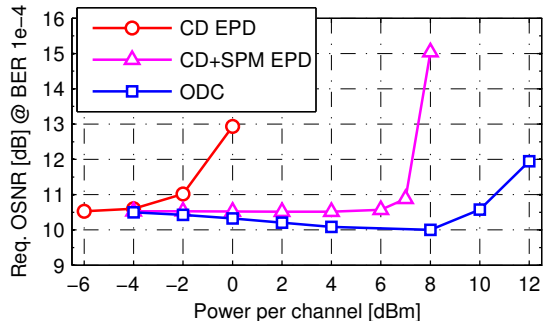

Figure 4.3. *Required OSNR for a BER of 10^{-4} in a 10 Gbit/s single channel system for ideal predistortion of chromatic dispersion and self-phase modulation.*

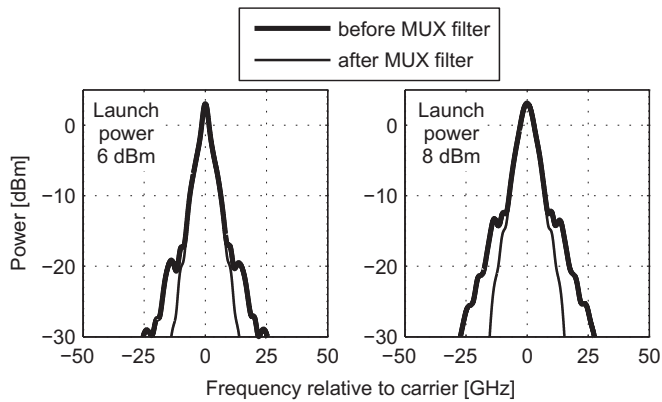

Figure 4.4. *Spectra of the predistorted optical 10 Gbit/s signals before and after the optical band-pass filter in the EPD transmitter for an average launch power of 6 and 8 dBm.*

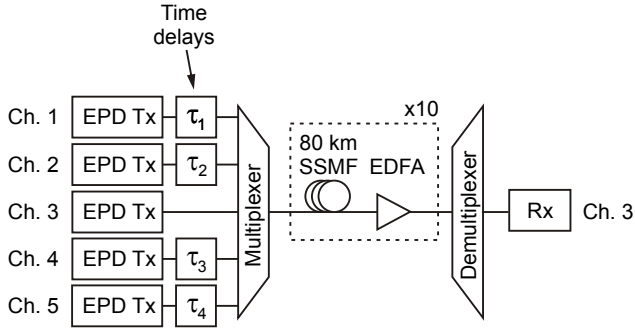

Figure 4.5. *EPD WDM system setup with five channels which are individually predistorted for intrachannel nonlinearities of the inline dispersion compensated link. The time delay elements are used to analyse the XPM statistics in WDM operation.*

is the SPM-induced chirping which leads to spectral broadening as described in [Agrawal2001, pp. 97–100].

By removing frequency components which are relevant for ideal predistortion, the optical band-pass filter distorts the ideal conditions. Thus, the finite multiplexer bandwidth required for dense WDM operation is a source of degradations in EPD systems. Note that the ODC system does not suffer from such spectral broadening at large launch power since the transmitted signal is an undistorted NRZ-OOK waveform whose spectral width is independent of the launch power.

4.1.3. Fundamental XPM Limitations at 10 Gbit/s

Interchannel interactions such as XPM will impose a limit on the maximum launch power if intrachannel nonlinearities are compensated. In order to quantify the impact of interchannel effects, a five-channel WDM system is simulated as shown in Fig. 4.5. All channels are individually predistorted for dispersion and intrachannel nonlinearities using the ideal backpropagation described in Section 4.1.1. Parallel polarisation of the channels along the entire link has been assumed since this is the worst-case. The target modulation format is NRZ-OOK. Prior to multiplexing, the neighbouring channels are delayed by a random time τ_i ($i = 1, \ldots, 4$) to account for the situation in a real WDM system where the relative timing of the channels cannot be controlled [Essiambre2005a]. In order to account for the statistical nature of the

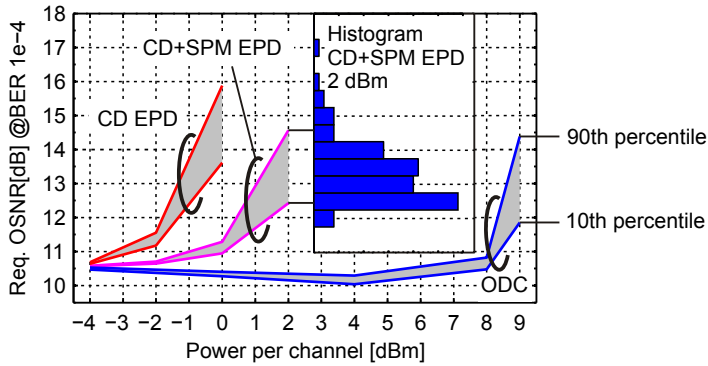

Figure 4.6. *Required OSNR distributions for BER of 10^{-4} in 5×10 Gbit/s WDM systems as a function of the average launch power per channel after 800 km with ODC, linear EPD of chromatic dispersion (CD EPD), and nonlinear EPD of chromatic dispersion and self-phase modulation (CD+SPM EPD). The 10^{th} and 90^{th} percentiles of the distributions are shown as a result of 100 simulations with random time delays between WDM channels. Inset: Histogram of the required OSNR for CD+SPM EPD at 2 dBm power per channel.*

interchannel effects, most importantly XPM, we calculate the required OSNR using 100 random realisations of different time shifts between the channels for a range of launch powers per channel. Since the fibre type is standard single mode fibre (SSMF), the dominant interchannel effect is XPM while four-wave mixing (FWM) can be ruled out in SSMF[2] due to the high local dispersion (cf. Section 2.4.6 and [Essiambre2005a]). The system parameters for the EPD systems at 10 Gbit/s are summarised in Table 3.1 on page 52. The same simulation technique was used in the previous chapter. It is based on the fact that XPM depends on the intensity of neighbouring WDM channels and that a wide range of temporal waveform alignments between WDM channels is required to accurately capture the effect of XPM.

In each of the 100 iterations, the required OSNR for a BER of 10^{-4} of the central channel is calculated using a De Bruijn binary sequence (DBBS) of order 10 (2^{10} bits). From the resulting histograms of the required OSNR, the 10^{th} and 90^{th} percentiles are determined and plotted versus the launch power. The larger the difference between the two percentiles the stronger is the impact of XPM.

Fig. 4.6 shows the results for the combined EPD of chromatic dispersion and intrachannel nonlinearities in a five-channel WDM system using 50 GHz chan-

[2]Note that the simulation using the split-step algorithm generally includes all interchannel effects.

nel spacing. The penalty spreading is characterised by the 10^{th} and 90^{th} percentile curves labeled "CD+SPM EPD"[3]. For comparison, the results discussed in Section 3.2.5 for linear EPD of chromatic dispersion only ("CD EPD") and for optical inline dispersion compensation ("ODC") are also shown. Using CD+SPM EPD allows for an increase in the launch power per channel by approximately 2 dB compared to CD EPD. The maximum launch power before significant spreading occurs is increased to about 0 dBm. Above a launch power of 0 dBm the required OSNR increases and spreads significantly which is due to interchannel nonlinearities, in particular XPM. This fluctuation of the required OSNR was already found at a single launch power in [Essiambre2005a]. The physical reason for this effect is the same as discussed in Section 3.2.5. The combination of high intensity variations in the predistorted waveform and the large uncompensated dispersion causes strong XPM-induced degradations [Essiambre2006, Schüppert2009].

As a result, the additional compensation of intrachannel nonlinearities allows for an increase of the launch power by about 2 dB compared to linear dispersion compensation. However, the fundamental limitation due to XPM still occurs at significantly lower launch power than for a conventional ODC system.

The ODC system does not show large fluctuations of the required OSNR below 8 dBm launch power. The difference in maximum launch power between ODC and CD+SPM EPD is more than 8 dB. This clearly shows the major drawback of EPD in 10 Gbit/s WDM systems [Essiambre2005a]. In the ODC system, XPM is suppressed by the choice of the dispersion map.

EPD transmission in a dense WDM system with 50 GHz channel spacing and 10 Gbit/s per channel has been experimentally demonstrated over 20×80 km SSMF by Birk et al. in a collaboration of AT&T and Nortel [Birk2006]. In the experiment, 72 channels were transmitted including seven electronically precompensated channels at adjacent wavelengths which are driven by Nortel's commercially manufactured eDCO transmitter system. Although the paper states that no error on the central precompensated channel was observed over the 135-hour measurement time, it is not discussed why a launch power of -2.5 dBm was chosen instead of a launch power of -1 dBm which gave the maximum OSNR margin. This could be due to XPM problems.

Our simulation results also show that in the investigated scenario (10 Gbit/s per channel, 50 GHz channel spacing, 20 GHz multiplexer bandwidth) the launch power limitations due to interchannel effects dominate over limitations due to

[3] We use the term self-phase modulation (SPM) here to be consistent with published literature [Essiambre2005a, Essiambre2006a]. However, the effect is different from intrapulse SPM since a number of pulses overlap and interact through nonlinearity which is similar to intrachannel nonlinearities in systems at 40 Gbit/s and above.

the optical multiplexer band-pass filter covered in the previous Section. However, this issue was studied in [Fischer2009] for a range of different multiplexer filter bandwidths, bit rates and channel spacings. The authors found that there are also configurations where degradations due to optical filtering dominate over interchannel nonlinearities.

4.1.4. Fundamental XPM Limitations at 40 Gbit/s

In Chapter 3, we have demonstrated that the impact of nonlinearities in 40 Gbit/s transmission differs significantly from 10 Gbit/s. In fact, the linear electronic predistortion of dispersion appears to be a more promising candidate to replace optical inline dispersion compensation at the higher bit rate since the nonlinear tolerance and, thus, the maximum launch power is not significantly reduced when migrating from ODC to linear EPD of dispersion. In addition to dispersion, the combined effect of dispersion and intrachannel nonlinearities (CD+SPM EPD)[4] can also be predistorted in the same way as shown for 10 Gbit/s in the previous section. This section will discuss the theoretical limitations due to interchannel nonlinearities in WDM EPD systems operating at 40 Gbit/s per channel. For this analysis,we assume ideal EPD transmitter hardware with sufficient complexity. The complexity issue for 40 Gbit/s EPD transmission is separately dealt with in Section 4.1.9.

The simulated WDM system setup is the same as for 10 Gbit/s, Fig. 4.5. In order to quantify the impact of interchannel effects, most importantly XPM, the same simulation technique as in the previous section was used, namely 100 iterations with random time delay between the channels. Each channel was loaded with a DBBS 10 (2^{10} bits) and was individually predistorted using the ideal nonlinear backpropagation explained in Section 4.1.1. The system parameters for the EPD system at 40 Gbit/s are summarised in Table 3.1 on page 52. Note that the channel spacing of 100 GHz leads to a spectral efficiency of 0.4 bit/s/Hz which is higher than that of the 10 Gbit/s systems where 0.2 bit/s/Hz was used (50 GHz channel spacing).

Fig. 4.7 shows the 10^{th} and 90^{th} percentiles of the required OSNR distributions versus the launch power for combined predistortion of dispersion and nonlinearities (CD+SPM EPD). For comparison, the results from Chapter 3 for linear EPD of chromatic dispersion (CD EPD) and ODC are also shown. Using CD+SPM EPD improves the nonlinear tolerance compared to linear CD EPD. The maximum launch power before significant spreading occurs is in-

[4] Again, we use the term self-phase modulation (SPM) here although the effect is different from intrapulse SPM since a number of pulses overlap and interact through nonlinearity which is also referred to as intrachannel nonlinearities in systems at 40 Gbit/s and above.

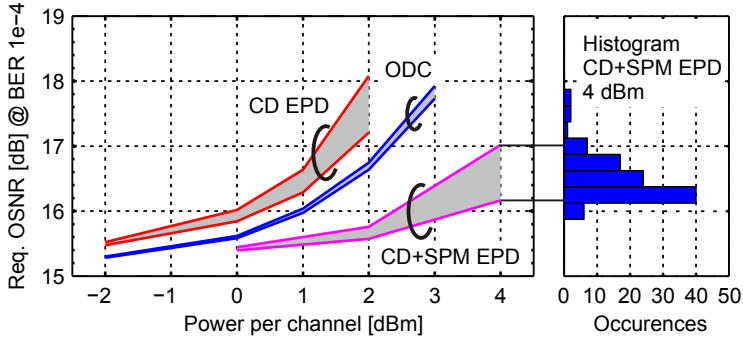

Figure 4.7. *Required OSNR distributions for BER of 10^{-4} in 5×40 Gbit/s WDM systems as a function of the average launch power per channel after 800 km with ODC, linear EPD of chromatic dispersion (CD EPD), and nonlinear EPD of chromatic dispersion and self-phase modulation (CD+SPM EPD). The 10^{th} and 90^{th} percentiles of the distributions are shown as a result of 100 simulations with random time delays between WDM channels. Inset: Histogram of the required OSNR at 4 dBm launch power for CD+SPM EPD.*

creased by approximately 2 dB. Remarkably, the CD+SPM EPD technique also outperforms optical dispersion compensation. However, the required OSNR histogram for CD+SPM EPD shown in the inset in Fig. 4.7 reveals large penalty spreading indicating the fundamental limitation due to XPM.

Note that the WDM systems are simulated using a DBBS 10 which we found to underestimate the required OSNR in the single channel case (cf. Section 3.2.3). Although longer sequences would be desirable, a DBBS 10 was chosen as a compromise to keep simulation times acceptable. The true nonlinear tolerance of WDM EPD systems at 40 Gbit/s is expected to be slightly worse than shown in Fig. 4.7 since there may be bit patterns in longer DBBS which cause a stronger impact of XPM.

It should also be remembered that the CD+SPM EPD technique for 40 Gbit/s is only theoretically considered in this section without taking into account realistic hardware components. In fact, we will show later that the nonlinearity compensation is rather unrealistic in 40 Gbit/s NRZ-OOK systems when we consider the required hardware complexity associated with nonlinear filtering. In order to estimate the required hardware complexity, we will develop a realistic model of an EPD transmitter capable of nonlinear precompensation in the following sections.

4.1.5. Transmitter Design for Nonlinear EPD

After EPD has been studied under ideal system conditions, we will discuss the design of a real-time EPD transmitter for compensation of dispersion and nonlinearities and study the system impact of realistic components such as digital-to-analog converters (DAC) or look-up table (LUT) based nonlinear filters. Some of these practical implementation issues will be addressed in the following.

The block diagram of the realistic EPD transmitter is depicted in the shaded box in Fig. 4.8. This structure which simultaneously predistorts the transmitted signal for chromatic dispersion and intrachannel nonlinearities was first proposed in [Killey2006]. The transmitted bits are fed into the digital signal processing unit which consists of a nonlinear filter such as a LUT and a linear filter such as a finite impulse response (FIR) filter. The motivation for the dual-stage filter structure is the required filter complexity of the look-up table (LUT) for nonlinearity precompensation and of the linear filter for dispersion precompensation. Here, the term complexity is used to describe the filter size such as the number of FIR filter taps or the memory requirement of a LUT. A linear FIR filter can precompensate for linear effects, such as chromatic dispersion. The required filter size given by the number of taps scales linearly with the amount of precompensated chromatic dispersion. However, intrachannel nonlinear effects cannot be compensated using linear filters. This requires the calculation of the nonlinearly predistorted waveform using, e.g., the backpropagation method described in Section 4.1.1. Since this calculation is too time consuming for real-time implementation, an alternative method for fast nonlinear filtering is required. This may be realised by a fast look-up table (LUT) based on random access memory (RAM) [Killey2005]. As we will discuss in the next section, the memory requirement for a look-up table scales exponentially with the memory depth, m, of the optical channel since the table needs to store one data entry for all 2^m possible combinations of m bits. In fact, the total memory requirement in bits is given by $2 \times 2^m \times k \times q$ (2: in-phase/quadrature parts, k is the number of samples per bit, and q is the number of quantisation bits of the DAC) [Winzer2005].

Due to the exponential scaling, compensation of nonlinearities combined with a large amount of dispersion is increasingly difficult to implement using a LUT. This problem led to the filter structure in Fig. 4.8 where the dispersion compensation is separated from the nonlinearity compensation. The physical motivation behind this structure is the fact that the dominant nonlinear interaction on a certain bit slot is caused by a number of neighbouring pulses which may be smaller than the total number of overlapping bits. Therefore, the mem-

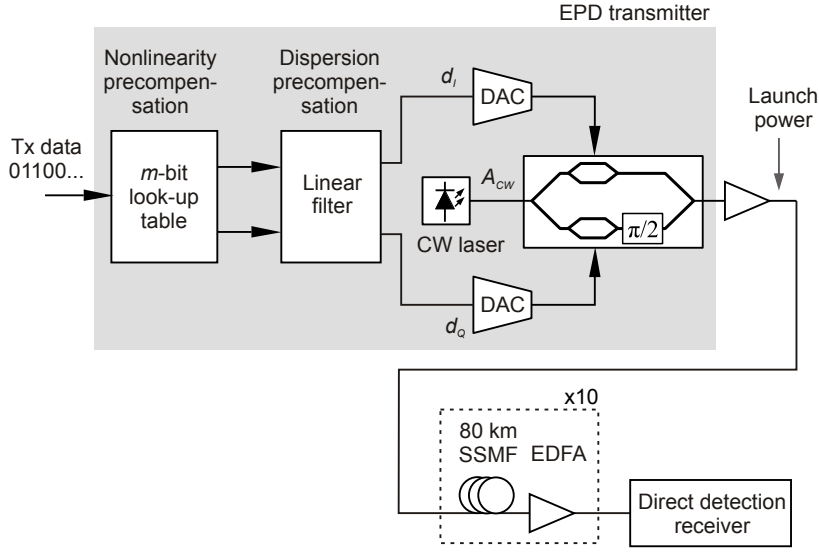

Figure 4.8. *System setup for realistic combined precompensation of chromatic dispersion and nonlinearities.*

ory depth for nonlinearity compensation may be chosen smaller than the number of bits for dispersion compensation [Killey2006]. Before we study the efficiency of this technique in 10 and 40 Gbit/s using numerical simulations we will give a detailed description of the look-up table in the next section.

4.1.6. Look-up Table Based Nonlinear Filtering

A look-up table (LUT) may be used to implement a nonlinear filtering operation in real-time. It stores the digitised samples of the predistorted waveform in a fast memory table. The size of the LUT is limited by the memory capabilities. Each entry of the LUT is addressed using an m-bit word giving a total number of 2^m addresses.

Fig. 4.9 shows the operation principle of an m-bit look-up table inside the EPD transmitter ($m = 3$ in the illustration). From the incoming bit stream, in each time step, m bits are grouped which would be implemented using an m-bit shift register. Those m bits are used to address the table entry which stores the digitised samples for the in-phase and quadrature component. For one time step, k samples per bit with a resolution of q quantisation bits are read out of the

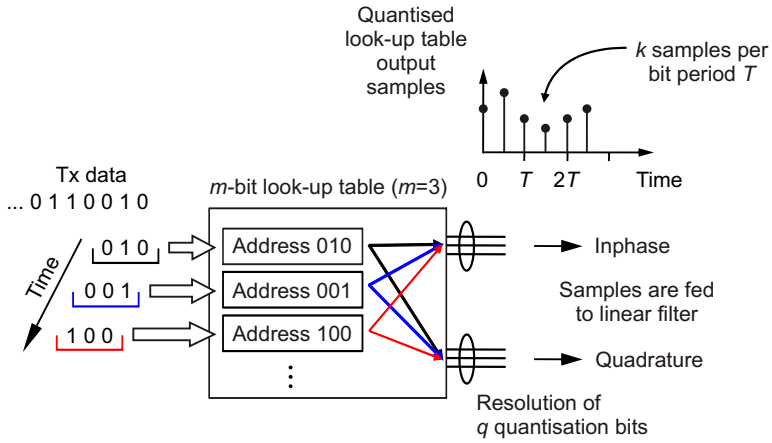

Figure 4.9. *Principle of a look-up table based nonlinear precompensating transmitter [Winzer2005, Killey2005].*

table. In the next time step, the input bit stream is advanced by one bit and the samples corresponding to the following m-bit sequence are read out. By running this algorithm, the sampled and quantised predistorted signal is generated continuously and fed to the linear dispersion precompensating filter which follows the LUT in the EPD transmitter (Fig. 4.8).

4.1.7. Calculation of LUT Entries

The samples stored in the LUT are calculated using the backpropagation method described in Section 4.1.1. The procedure is illustrated in Fig. 4.10 for an m-bit LUT (here $m = 3$). For the complete table, 2^m iterations are carried out to include all possible combinations of m bits. The figure illustrates the algorithm for the bit sequence "1 0 1".

In the first step, the target signal is generated encoding the current bit sequence. At this stage of the algorithm, the desired target modulation format has to be chosen. Here, the signal is NRZ-OOK modulated. The signal predistortion is calculated using the nonlinear Schrödinger equation with negative link parameters as described in Section 4.1.1. The link design for the backpropagation is shown by the shaded box in Fig. 4.10. The amplifier in front of the transmission spans sets the desired average power of the transmitted signal since the values stored in the LUT depend on the launch power of the EPD system. Note the dispersion compensating fibre (DCF) that follows the transmission

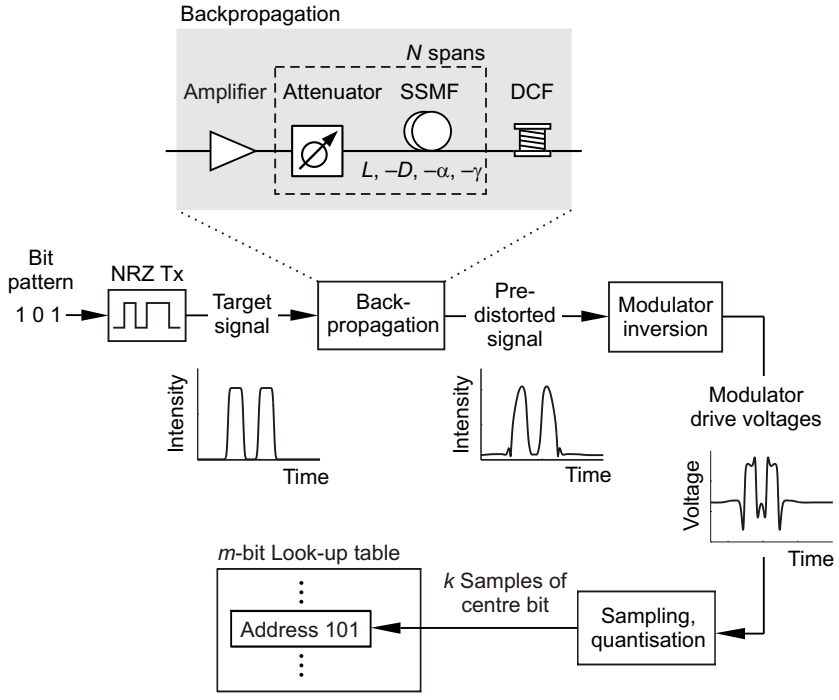

Figure 4.10. *Calculation of the LUT entries.*

spans. It compensates for the entire accumulated dispersion of the link such that only the nonlinear pulse distortions are left. The DCF is necessary since the dispersion compensation and the nonlinearity compensation are separated in the EPD transmitter as described in the previous section. While the LUT only stores the nonlinear predistorted samples, the linear dispersion compensation will be carried out using a separate linear filter.

In the next step, the modulator drive voltages required to generate the desired waveform are calculated depending on the used modulator type. In the following sections, we will use a triple dual-drive Mach–Zehnder modulator (MZM) whose in-phase and quadrature drive voltages are given by (3.5) and (3.6) in Section 3.3.1.

The voltage waveform of the centre bit is samples and quantised using k samples per bit and a resolution of q quantisation bits. The center bit slot contains the distortions caused by the neighbouring bits since intersymbol interference due to chromatic dispersion spreads symmetrically. Those central samples are stored in the LUT entry under the address given by the current bit pattern ("1 0 1" in example shown in Fig. 4.10). By calculating the predistorted samples for all combinations of m bits, the EPD transmitter can synthesise the predistorted signal for arbitrary patterns in real-time by a simple memory read operation.

4.1.8. Single Channel Transmission using LUT-based EPD Transmitter at 10 Gbit/s

In order to quantify the efficiency of the LUT-based nonlinearity predistortion technique, the transmission over 800 km SSMF was analysed using the setup shown in Fig. 4.8 at a bit rate of 10 Gbit/s. The predistorted signal was precalculated for LUT sizes ranging from 5 to 11 bit assuming a DAC with 2 samples per bit, i.e. 20 GSa/s, and using a quantisation resolution of 4 bit. These DAC parameters were chosen to resemble a commercially available 22 GSa/s DAC manufactured by Nortel [Schvan2005].

The dispersion precompensation filter is implemented using the ideal inverse transfer function of a linear lossless fibre in the frequency domain given by (3.1) in Section 3.1.2. A real-time implementation is possible using a finite impulse response (FIR) filter with a sufficient number of filter taps. As discussed in Section 3.3.1, the required number of filter taps is given by the linear channel memory, m_{L}, i.e. the number of overlapping pulses due to chromatic dispersion. This has also been studied in [Winzer2005]. It was found that precompensation of an 800 km SSMF link at 10 Gbit/s requires a memory depth of 17 bits which means 34 FIR filter taps, assuming two taps per bit. Therefore, we did not fur-

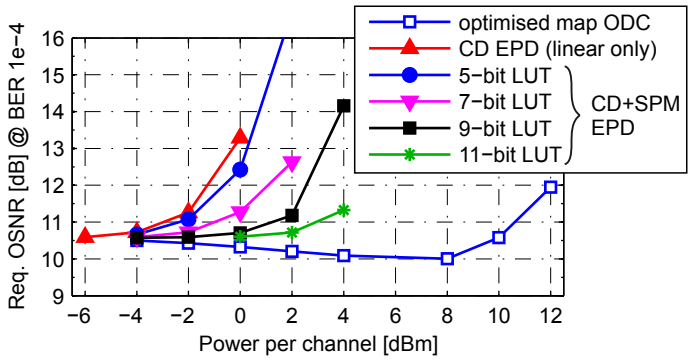

Figure 4.11. *Required OSNR versus the launch power after transmission over 10×80 km SSMF for a range of 10 Gbit/s single channel EPD system configurations, including linear EPD of chromatic dispersion (CD EPD) and combined precompensation of chromatic dispersion and self-phase modulation (CD+SPM EPD) using different LUT sizes. The DAC operated at 20 GSa/s with 4-bit quantisation. For comparison, the ODC results are shown.*

ther analyse this issue for our investigations and simply used the ideal filter. Filter tap counts in this range are possible using current digital signal processing technology at 10 Gbit/s. The processor memory required for the linear filter is negligible compared to the LUT size.

The required OSNR results for a BER of 10^{-4} are plotted versus the launch power in Fig. 4.11. For comparison, the results for the optimised ODC system and for linear precompensation without using a LUT [labeled "CD EPD (linear only)"] are also shown. If only linear precompensation is used the nonlinear threshold is reached at -1.7 dBm. In contrast, the ODC system has a nonlinear threshold of 11.3 dBm which is $\sim$ 10 dB larger. The LUT-based EPD transmitter improves the nonlinearity tolerance for the precompensated systems with increasing LUT size. An 11-bit LUT with a memory size[5] of $2 \times 2 \times 4 \times 2^{11}$ bit $=$ 4 kByte increases the nonlinear threshold to 4 dBm. However, it should be noted that the WDM simulations have shown a launch power limit of only approximately 0 dBm for CD+SPM EPD due to XPM.

The results confirm the assumption expressed in Section 4.1.5, namely that in 10 Gbit/s on-off keying (OOK) transmission, the dominant nonlinear interaction on a certain bit slot is caused by the pulses in nearby neighbouring bit slots. The impact of bit slots further away may be neglected which is supported by the

[5] 2: the in-phase and quadrature part, $k = 2$ samples per bit, $q = 4$ quantisation bits

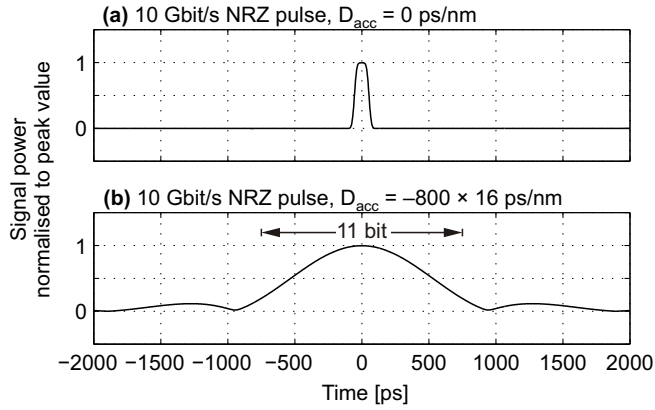

Figure 4.12. *Single 10 Gbit/s NRZ-OOK pulse ($T = 100$ ps). (a) Without accumulated dispersion. (b) Linearly precompensated for an accumulated dispersion of $D_{acc} = -800 \times 16$ ps/nm.*

efficient nonlinearity compensation even if smaller LUT are used. Therefore, the memory depth for nonlinearity compensation may be chosen smaller than the number of bits for dispersion compensation. Fig. 4.12 illustrates the waveforms of a 10 Gbit/s single pulse. The plot on the top shows the undistorted NRZ pulse having a duration of $T = 100$ ps. The plot on the bottom shows the signal linearly dispersion-precompensated for an accumulated dispersion equivalent to 800 km SSMF with $D = 16$ ps/nm. The double-headed arrow marks the time duration of 11 bit. This time duration shows the nonlinear channel memory captured by an 11-bit LUT. Clearly, the pulse has broadened beyond 11 bit, but the signal amplitude is small outside the 11-bit window. This explains why the dominant nonlinear interactions are effectively captured by an 11-bit LUT.

In conclusion, these results demonstrate that using the combination of a linear filter with the complete channel memory and a LUT with a reduced memory depth achieves efficient nonlinearity compensation in 10 Gbit/s single channel EPD transmission. Our results agree with a published study by Killey et al. [Killey2006], confirming the validity of our models. The presented technique reduces the required complexity of the EPD transmitter. In contrast, if only LUT is used for both chromatic dispersion and nonlinearity precompensation as proposed in [Winzer2005], the LUT would have to be designed to account for the full channel memory. For 800 km SSMF, a LUT memory depth of $m = 17$ was found which would increase the required memory to $\sim$ 256 kByte.

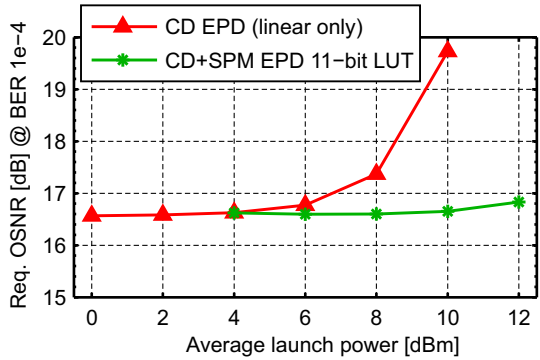

Figure 4.13. *Required OSNR versus the launch power after transmission over 50 km SSMF for 40 Gbit/s single channel EPD systems with only linear EPD of chromatic dispersion (CD EPD) and with combined precompensation of dispersion nonlinearities (CD+SPM EPD) using an 11-bit LUT and 80 GSa/s 4-bit DAC.*

4.1.9. Single Channel Transmission using LUT-based EPD Transmitter at 40 Gbit/s

Increasing the bit rate by a factor of 4 will increase the channel memory by a factor of 16 since the linear memory due to dispersion scales with $D_{\mathrm{acc}}B^2$ (cf. Section 2.3.4). As a consequence, if the same FIR filter and LUT size of the 10 Gbit/s 800 km system are used for 40 Gbit/s, the transmission distance scales down to only 50 km. Although of limited practical relevance, we simulated the transmission over 50 km SSMF at 40 Gbit/s using the realistic EPD transmitter presented in Section 4.1.5 to verify the theoretical considerations. A LUT size of 11 bit and the linear dispersion compensating filter were programmed for 50 km SSMF transmission using the technique described in Section 4.1.7. The DAC operates at 2 samples per bit, i.e. 80 GSa/s, with a resolution of 4 bit. The linear dispersion compensating filter performs ideal dispersion compensation such that at low launch power the only source of degradation are the limited DAC sampling rate and quantisation resolution of the modulator drive voltages in the EPD transmitter.

The required OSNR versus the average launch power after transmission over one span of 50 km SSMF is shown in Fig. 4.13 for linear EPD of chromatic dispersion (CD EPD) and for the simultaneous EPD of dispersion and intrachannel nonlinearities (CD+SPM EPD). The “CD EPD” curve is obtained using the ideal linear dispersion compensating filter in the transmitter but with a finite DAC

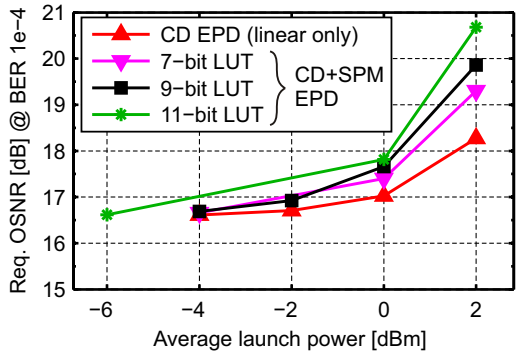

Figure 4.14. *Simulation results for 40 Gbit/s EPD transmission over 10×80 km SSMF using a look-up table based transmitter for simultaneous precompensation of dispersion and nonlinearities.*

sampling rate and quantisation. Hence, the result at a low launch power characterises the back-to-back performance without transmission impairments. The back-to-back required OSNR of 16.5 dB is about 1.2 dB higher than the back-to-back value obtained for the ideal transmitter used, e.g., in Section 4.1.4. This penalty is attributed to the impact of sampling and quantisation of the modulator drive voltages.

If only chromatic dispersion is compensated, fibre nonlinearities degrade the received signal at larger launch power values. As expected, by employing the additional nonlinearity compensation using an 11-bit LUT, the nonlinear tolerance is significantly improved. This demonstrates that, for the same memory size in the transmitter, the 10 Gbit/s transmission distance may be scaled to 40 Gbit/s by a factor of 16, as theoretically predicted.

Transmission over 50 km SSMF would not justify such a complex EPD transmitter. Nevertheless, this scenario may be beneficial in transmission over fibres with smaller dispersion parameter, such as non-zero dispersion shifted fibre (NZDSF). In this case, the achievable transmission distance using an 11-bit LUT would increase compared to SSMF.

In the next step, we extend the investigation to multiple SSMF spans to study the efficiency of combined dispersion and nonlinearity compensation at 40 Gbit/s. We simulated single channel transmission over 10 $\times$ 80 km SSMF using look-up tables with sizes ranging from 7 to 11 bit. The results are shown in Fig. 4.14. As a reference, the graph also includes the results obtained using linear EPD of chromatic dispersion only (curve labeled “CD EPD”). At larger

launch powers the required OSNR increases as a result of the intrachannel nonlinearities which limit the performance. The LUT-based EPD of both dispersion and intrachannel nonlinearities (CD+SPM EPD) should improve the nonlinear tolerance. However, the curves labeled "CD+SPM EPD" show that this attempt fails. On the contrary, increasing the LUT size even seems to degrade the performance.

This is explained by the fact that the 11-bit LUT is by far too small to capture significant nonlinear intrachannel interactions of neighbouring bits at this value of $D_{\mathrm{acc}}B^2$. Fig. 4.15(a) and (b) show the waveforms of a single NRZ pulse with a pulse width of $T = 25$ ps, $B = 40$ Gbit/s (a) with $D_{\mathrm{acc}} = 0$ ps/nm and (b) linear dispersion-precompensated for $D_{\mathrm{acc}} = -800 \times 16$ ps/nm, respectively. The bottom graph demonstrates the strong pulse broadening in 40 Gbit/s transmission. For comparison, the time duration of 11×25 ps $= 275$ ps captured by an 11-bit LUT is also shown in Fig. 4.15(b). Clearly, no efficient nonlinearity compensation may be expected since a significant amount of pulse energy has spread beyond the 11-bit time interval.

The straightforward solution would be to use larger look-up tables. However, the plot in Fig. 4.15(b) suggests that the LUT size would have to be significantly increased before nonlinearity compensation becomes efficient. Rescaling the LUT size requirements of 11-bit at 10 Gbit/s by a factor of 16, an estimated size of >100 bit is required at 40 Gbit/s. Realising look-up tables in this order of magnitude is not possible since the memory requirement scales exponentially with the number of address bits. A 30-bit LUT, for example, requires approximately 1 GByte of memory which would have to be read out at several tens of gigasamples per second.

Another method to estimate the required LUT size is the nonlinear channel memory, m_{NL}, according to (2.43). For the EPD system considered in this section, we have $m_{\mathrm{NL}} = 165$ bits using $|D_{\mathrm{acc}}| = D_{\mathrm{SMF}} \times 800$ km, $B = 40$ Gbit/s, $\Delta f = 40$ GHz. Although (2.43) does not give the exact required LUT size, it is useful to determine the order of magnitude, thereby illustrating the enormous nonlinear memory of the considered EPD system.

In conclusion, the EPD transmitter with linear filtering and LUT based nonlinear filtering is not efficient in precompensating for intrachannel nonlinearities of 40 Gbit/s NRZ transmission due to the enormous channel memory. Possible electronic signal processing alternatives which might improve the nonlinear tolerance of transmission at 40 Gbit/s and above are the optimisation of the modulation format or the design of a novel transmitter architecture. A higher order modulation format, such as differential quadrature phase shift keying (DQPSK) which encodes two bits per symbol, reduces the optical bandwidth compared to OOK modulation. Consequently, the channel memory is reduced

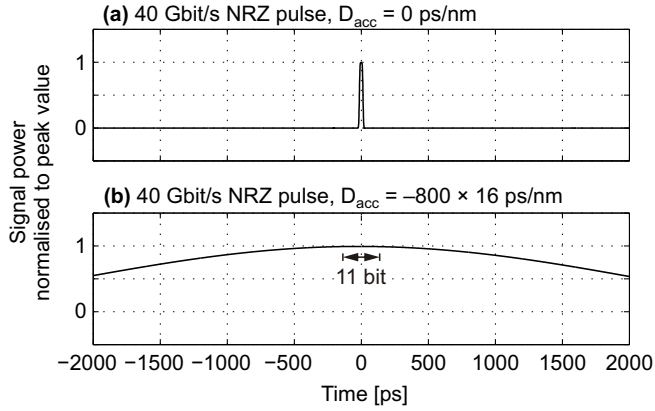

Figure 4.15. *Single 40 Gbit/s NRZ-OOK pulse ($T = 25$ ps). (a) Without accumulated dispersion. (b) Linearly precompensated for an accumulated dispersion of $D_{acc} = -800 \times 16$ ps/nm.*

allowing for smaller LUT sizes and reduced DAC sampling rate. The DAC quantisation resolution, however, should be increased. Higher order modulation to relax the memory requirements for electronic dispersion precompensation was also suggested in [Winzer2005].

Furthermore, it has been proposed to utilise simplified versions of the backpropagation method described in Section 4.1.1 for real-time nonlinearity compensation at the transmitter [Liu2006] or using coherent reception [Li2008, Ip2008]. The idea of these approaches is to realise a coarse split-step Fourier algorithm using high-speed parallel signal processing to solve the nonlinear Schrödinger equation. In [Ip2008], it was found that in 10 Gsymbol/s RZ-QPSK transmission over 25×80 km, a step size equal to the length of a fibre span is a good compromise between performance and computational complexity. However, the backpropagation approaches have also been criticised since they "rely very heavily on often non-realistic computations speeds" [Shtaif2008]. This becomes even more problematic at higher bit rates.

Another scenario with a moderate channel memory is the conventional inline dispersion compensated transmission link, e.g., using dispersion compensating fibre. It is possible to combine EPD using moderately-sized look-up tables and optical dispersion compensation to electronically compensate for nonlinearities, thus increasing the nonlinear tolerance. This approach will be elaborated further in the next sections.

4.2. EPD of Intrachannel Nonlinearities in 40 Gbit/s Systems with Inline DCF

One way to reduce the channel memory is to limit the maximum accumulated dispersion by using, e.g., inline DCF modules. This may at first appear contradictory to the purpose of electronic precompensation which aims to remove the DCF, but the scheme still has some advantages since it reduces the channel memory and, thus, relaxes the transmitter complexity allowing for electronic nonlinearity compensation. In such systems, DCFs compensate for chromatic dispersion whereas electronic predistortion mitigates the distortions due to intrachannel nonlinearities. This scheme would be particularly beneficial in high bit rate systems where the short pulse widths and high launch power cause increased signal degradation due to intrachannel nonlinearities.

4.2.1. System Design

We propose to use a simple link design that consists of a cascade of identical 100% inline dispersion postcompensated spans [Weber2006]. Using identical spans significantly simplifies network planning and management [Hanik2004] compared to using optimised dispersion maps. At 40 Gbit/s, the transmission link is operated in the pseudolinear regime where intrachannel nonlinear effects are the main source of degradation. We will show that by using an EPD transmitter based on LUT with feasible size enables significantly improved compensation of intrachannel nonlinearities.

A schematic of the system setup is shown in Fig. 4.16. We consider a single-channel system of 800 km length (10×80 km spans) with each span comprising an SSMF, a DCF and an erbium-doped fibre amplifier (EDFA). An SSMF with dispersion $D = 16$ ps/(nm·km), nonlinearity coefficient $\gamma = 1.31$ W^{-1}km^{-1} and loss $\alpha = 0.2$ dB/km was considered. The accumulated dispersion of the SSMF is fully postcompensated by the DCF as shown by the dispersion map diagram in Fig. 4.17. The DCF were assumed linear and lossless. The amplifier gain equals the span loss. The launched predistorted electric field[6] $\underline{A}_{\mathrm{TX}}(t)$ is generated such as to produce the target electric field $\underline{A}_{\mathrm{RX}}(t)$ after nonlinear propagation along the transmission link in the absence of noise.

The shaded box in Fig. 4.16 shows the predistorting transmitter. The design is similar to the EPD transmitter presented in Section 4.1.5. The difference here is that no linear filter for dispersion compensation is required since dispersion is optically compensated. The intrachannel nonlinearity predistortion device in

[6] The term "electric field" here refers to the slowly varying field envelope, cf. (2.26) in Section 2.3.3.

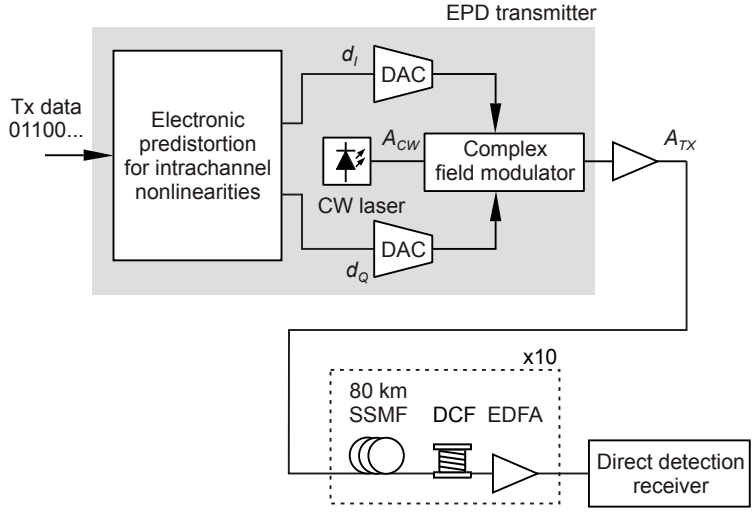

Figure 4.16. *System setup for electronic predistortion of intrachannel nonlinearities in systems using optical dispersion compensation.*

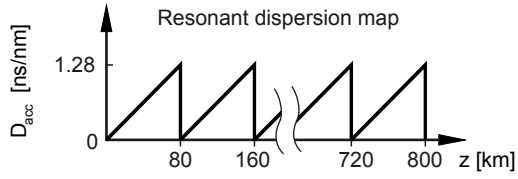

Figure 4.17. *Dispersion map of the investigated transmission system.*

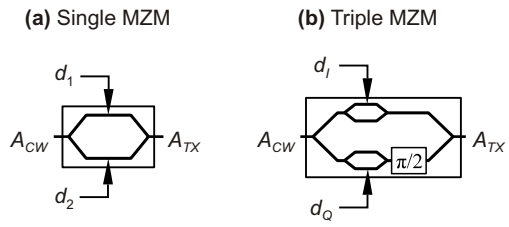

Figure 4.18. *Possible realisations of a complex field modulator: (a) Single dual-drive MZM, (b) triple MZM, also referred to as nested MZM or I/Q modulator (I: in-phase, Q: quadrature).*

Fig. 4.16 delivers the digital drive voltages for the optical field modulator. In the following, we distinguish between two models of the predistortion device:

- The investigations in Sections 4.2.2 and 4.2.5 will be carried out by calculating the perfectly predistorted field using the ideal backpropagation introduced in Section 4.1.1. This emulates a nonlinear filter with sufficient memory to fully capture all intrachannel nonlinear effects, i.e. the impact of limited processor memory is neglected.
- In Section 4.2.3, we will extend the EPD transmitter model by including the effects of a finite LUT size. The refined model is suitable for real-time implementation since the LUT may be realised using fast RAM [Killey2005].

If ideal backpropagation is used, the full nonlinear channel memory is accounted for in the transmitter which is equivalent to a LUT with unrestricted address size. Ideal backpropagation is useful to obtain the theoretical maximum of the performance. The principle of the backpropagation technique and LUT operation is the same as presented in Sections 4.1.1 and 4.1.6 with the differences that the backpropagation link includes inline DCF and no linear dispersion compensating filter is required after the LUT.

The modulator drive voltages required to obtain the predistorted waveform are calculated from the field transfer function of the complex field modulator. Two different modulators were investigated: a single dual-drive MZM [Fig. 4.18(a)] and a triple dual-drive MZM [Fig. 4.18(b)]. The theory for the single dual-drive MZM was introduced in Section 2.2.1. The transfer function of the MZM is given by (2.5). Inserting (2.3) into (2.5) and substituting $\underline{A}_{out} = \underline{A}_{\mathrm{TX}}$ and $\underline{A}_{in} = A_{\mathrm{CW}}$ into (2.5) yields the output field as a function of

the drive voltages

$$\underline{A}_{\mathrm{TX}}(t) = A_{\mathrm{CW}} \cos\left(\frac{\pi[d_1(t) - d_2(t)]}{2V_\pi}\right) \exp\left(\frac{j\pi[d_1(t) + d_2(t)]}{2V_\pi}\right) \tag{4.1}$$

where d_1 and d_2 are the modulator drive voltages, V_π is the voltage required for a π phase shift in one arm of the MZM and A_{CW} is the light of the continuous wave laser. The drive voltages $d_1(t)$ and $d_2(t)$ as a function of the predistorted field $\underline{A}_{\mathrm{TX}}(t) = |\underline{A}_{\mathrm{TX}}(t)| \exp(j\varphi(t))$ are given by (2.7) and (2.8) in Section 2.2.1 using $\underline{A}_{out} = \underline{A}_{\mathrm{TX}}$ and $\underline{A}_{in} = A_{\mathrm{CW}}$.

From (2.7) and (2.8), it can be seen that the drive voltages are nonlinear functions of the predistorted field. If only a linear effect such as chromatic dispersion is precompensated, a memoryless nonlinear element or a nonlinear filter, e.g. a LUT, would be required for the single MZM [Killey2005], also cf. Section 3.3.1. For nonlinearity compensation, however, where a nonlinear filter is a necessity, the single MZM might provide a low-cost alternative to the triple MZM for complex field modulation.

The equations for the triple MZM drive voltages $d_I(t)$ and $d_Q(t)$ are given by (3.5) and (3.6) in Section 3.3.1. We will compare the performance of the two modulators for nonlinear predistortion.

The drive signals are quantised using uniform quantisation and subsequently sampled to account for the limited sample rate of DAC, cf. Section 3.3.1. At the end of the link, the optical signal is filtered by a second-order Gaussian optical band-pass, detected using an ideal photodiode, and filtered by an electrical low-pass fifth-order Bessel filter, having a 3-dB bandwidth of 28 GHz. The 3-dB bandwidth of the optical band-pass was 80 GHz.

4.2.2. Impact of the DAC and the Modulator

First, we will investigate the EPD technique without accounting for a limited memory in the transmitter, i.e. using the ideal backpropagation. This is equivalent to assuming an unrestricted LUT size. Neglecting the memory effects will reveal the ultimate limitations imposed by the finite digital-to-analog converter (DAC) sampling rate and quantisation, as well as, the impact of the field modulator.

In order to analyse the impact of DAC limitations, the sample rate was varied between one and four samples per bit, corresponding to a range from 40 to 160 GSa/s at 40 Gbit/s. For each sample rate, different numbers of quantisation bits were used. The average launch power was fixed at +2 dBm. The required OSNR for a BER of 10^{-4} after transmission over 800 km using the single MZM based transmitter is plotted in Fig. 4.19(a). One sample per bit is not sufficient

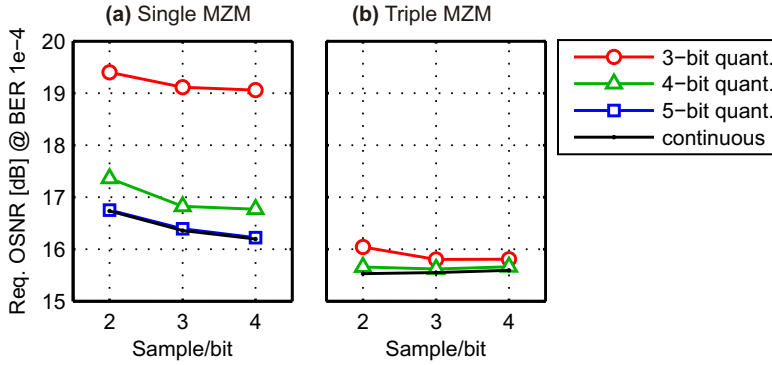

Figure 4.19. *Required OSNR after transmission over 800 km as a function of the DAC sample rate using (a) the single MZM and (b) triple MZM for different quantisation resolutions and for the continuous case. The average launch power was set at +2 dBm.*

and leads to a completely closed eye diagram regardless of the quantisation. At 2 sample/bit (80 GSa/s) and using three quantisation bits, an OSNR of 19.4 dB is required for a BER of 10^{-4} which corresponds to a penalty of more than 4 dB compared to the ideal case without DAC limitations. Increasing to 4-bit quantisation reduces the required OSNR by 2 dB. More than 5-bit quantisation has negligible effect since the 5-bit curve already converges to the case of continuous drive voltage amplitudes. Increasing the sample rate above 2 sample/bit slightly reduces the required OSNR depending on the quantisation.

The results for the triple MZM are shown in Fig. 4.19(b). At 2 samples per bit and 3-bit quantisation, a required OSNR of 16.0 dB is achieved. Using more than 2 samples per bit or more than 4 quantisation bits did not further reduce the required OSNR. The results show that the triple MZM relaxes the sampling rate and quantisation requirements. However, this comes at the cost of a more complex optical structure involving two nested MZM which, of course, is also more expensive than a single MZM.

The difference between the two MZM is illustrated qualitatively by the quantisation error plots in Fig. 4.20. For each sample, the difference between the ideal predistorted complex field and the field resulting from 4-bit quantised drive signals is plotted as a dot in the complex plane normalised to the peak-to-peak amplitude of the field of the nonpredistorted signal. The single MZM [Fig. 4.20(a)] has a larger error distribution than the triple MZM [Fig. 4.20(b)] demonstrating that the triple MZM is more tolerant to limited quantisation than

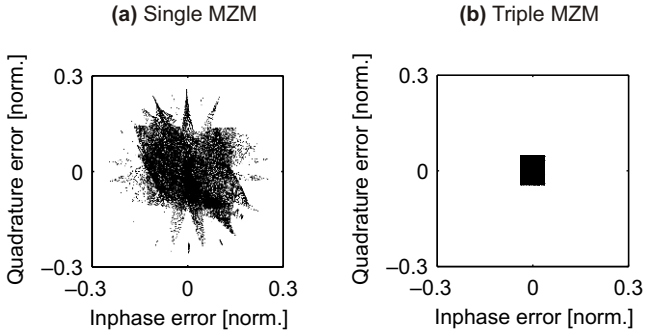

Figure 4.20. *Normalised quantisation error for 4-bit quantisation in the complex field plane using (a) the single MZM and (b) the triple MZM.*

the single MZM. The physical reason is that the complex field at the output of the single MZM depends on the sum and the difference of the drive signals as shown by (4.1), whereas in the triple MZM, each drive signal controls one component of the field independently as discussed in Section 3.3.1. In the case of the single MZM, quantisation errors of the drive signals can, therefore, constructively add up.

The precompensation technique was investigated for a range of signal launch powers. For each launch power, the appropriate predistorted optical field was calculated using ideal backpropagation. The DAC was set to a sample rate of 80 GSa/s (two samples per bit) and 4-bit quantisation.

Fig. 4.21(a) shows the required OSNR for a BER of 10^{-4} versus the average launch power after transmission over 800 km. The achievable OSNR calculated according to (2.15) for an amplifier noise figure of 4 dB and a total span loss of 22.4 dB is also shown by the dashed line. The difference between the required OSNR and the achievable OSNR characterises the OSNR margin at the given input power. In addition, the results are shown for a lower BER of 10^{-9} in Fig. 4.21(b). Systems at 40 Gbit/s tend to operate at BER in the range of 6×10^{-5} to 2×10^{-3} using state-of-the-art forward error correction (FEC). The two graphs show that although the penalties at a certain launch power may change the relative comparison between the system does not change from the higher to the lower BER. However, the OSNR margin decreases significantly when lowering the target BER. The following discussion of the results will concentrate on a BER of 10^{-4}.

The required OSNR for conventional ODC systems with a resonant dispersion map, i.e. full inline compensation per span, and with an optimised map

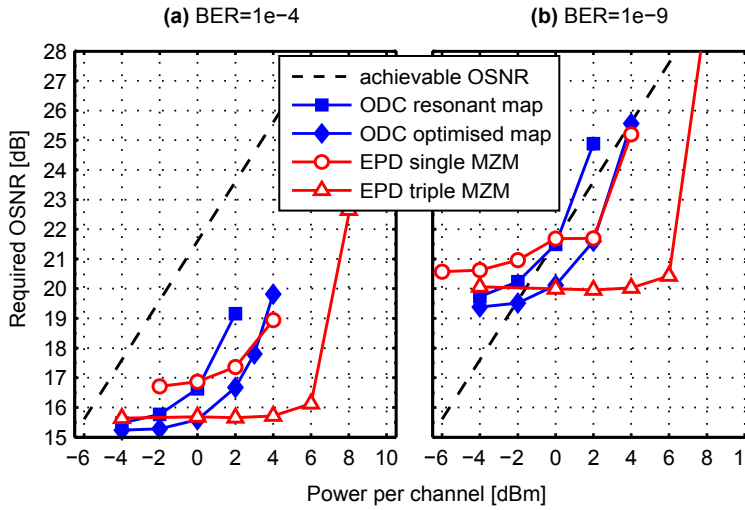

Figure 4.21. *Required OSNR for (a) BER of* 10^{-4} *and (b) BER of* 10^{-9} *after transmission over 800 km as a function of the input power for ODC and EPD systems. EPD refers to precompensation of intrachannel nonlinearities in a resonant dispersion map. A 80 GSa/s, 4-bit DAC and unrestricted LUT size were used. The target format was 40 Gbit/s NRZ-OOK.*

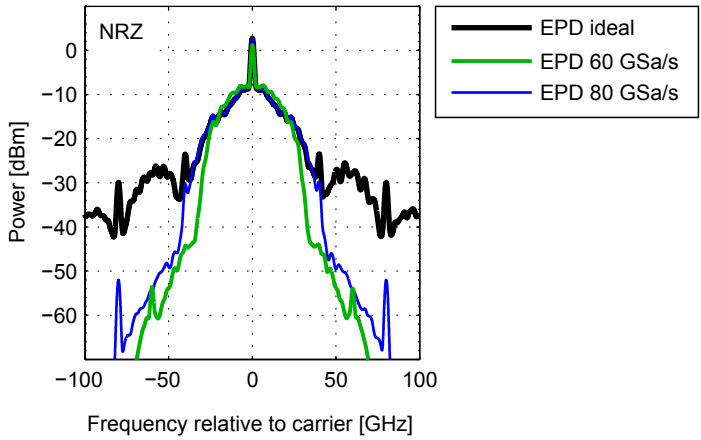

Figure 4.22. *Optical spectra at the output of the EPD transmitter for ideal digital-to-analog conversion and using limited sampling rates for 40 Gbit/s NRZ target format. The launch power was set at +6 dBm.*

are shown for reference in Fig. 4.21(a). The dispersion map is often referred to as "resonant" since, at the end of each span, the accumulated dispersion is reset to zero. Clearly, the resonant map leads to a strong impact of intrachannel nonlinearities since nonlinear perturbations add up constructively at the beginning of each span. The nonlinear threshold[7] in this case is limited to −1 dBm.

EPD using the single MZM only slightly improves the nonlinear tolerance. The single MZM causes a relatively large implementation penalty as explained above and does not achieve a better performance than the ODC system with an optimised map. In contrast, employing EPD with a triple MZM for the resonant map significantly improves the tolerance to nonlinearities of the system even compared to the optimised ODC system. The required OSNR remains approximately constant at around 16 dB up to 6 dBm launch power. This indicates that the transmission in this case is only limited by ASE noise and not by intra-channel nonlinear effects. The nonlinear threshold is increased to 6 dBm whereas the optimised ODC system only reaches $\sim$ 1 dBm.

Above 6 dBm, the EPD performance using the triple MZM is limited by the finite DAC sample rate and quantisation. The finite quantisation may be considered as an additional source of amplitude noise added at the transmitter. The

[7] The back-to-back OSNR of the ODC system (15.2 dB) was used as a reference for the determination of the nonlinear threshold for both EPD and ODC systems. This ensures that the implementation penalty of the EPD system is taken into account for the nonlinear threshold.

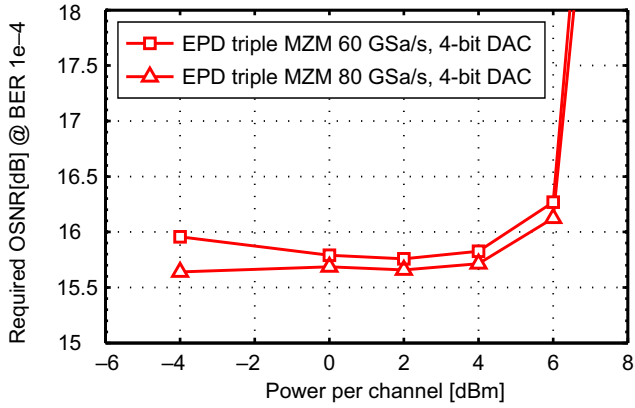

Figure 4.23. *Required OSNR for (a) BER of* 10^{-4} *after transmission over 800 km versus the launch power. EPD refers to precompensation of intrachannel nonlinearities in a resonant dispersion map. A 60 and 80 GSa/s, 4-bit DAC and unrestricted LUT size were used. The target format was 40 Gbit/s NRZ-OOK.*

limited sampling rate in combination with an anti-aliasing filter leads to a suppression of the frequency components above the Nyquist limit of 40 GHz (corresponding to 80 GSa/s). As explained in Section 4.1.2, increasing the launch power results in a spectral broadening of the predistorted signal. Removing frequency components disturbs the nonlinearity compensation. Fig. 4.22 shows the optical spectra using ideal digital-to-analog conversion and using 80 GSa/s, thus, demonstrating the suppression of higher frequency components.

The realisation of a 80 GSa/s DAC with 4 bit is challenging. Devices at this speed are not yet available. As stated in the previous chapter, however, the recent trend towards 100G Ethernet is a driver for fast data converters. During the course of the thesis work, a 56 GSa/s analog-to-digital converter (ADC) became available [Fujitsu2009]. Therefore, we repeated some selected simulations using the lower DAC rate of 60 GSa/s to account for the recent advances. Fig. 4.22 illustrates the optical signal spectrum obtained using the lower DAC rate. Clearly, the signal bandwidth is narrower than at 80 GSa/s. Next, we repeated the simulations of 40 Gbit/s single channel transmission using a pair of 60 GSa/s 4-bit DAC in the EPD transmitter. Fig. 4.23 compares the required OSNR for a BER of 10^{-4} versus the launch power for sample rates of 60 and 80 GSa/s. The 80 GSa/s results are replotted from Fig. 4.21. The results show that decreasing the rate from 80 to 60 GSa/s causes only a small penalty of approximately 0.1 dB. In conclusion, the 60 GSa/s DAC achieves approximately

the same nonlinear tolerance as the 80 GSa/s while also relaxing the hardware requirements for an EPD transmitter. Nevertheless, it should be remembered that further reducing the rate to 40 GSa/s is not possible since it leads to completely closed eye diagrams as stated above.

To sum up the discussion, the combination of optical dispersion compensation based on a non-optimised resonant dispersion map and electronic predistortion for intrachannel nonlinearities achieves a significant increase in the nonlinear threshold of about 5 dB compared to optimised ODC. For the above discussion, an unrestricted LUT length was assumend. The limit in this case is set by the DAC sampling rate. We found that a 60 GSa/s, 4-bit DAC is required. In the following, we will extend the analysis and study the LUT requirements.

4.2.3. Finite LUT Size

In the previous sections, an unrestricted LUT was assumed by calculating the modulator drive voltages from the ideally backpropagated signal. While this allows to isolate DAC impairments, the impact of a finite LUT is of practical interest for a real-time realisation of EPD. In fact, the original motivation of our approach to combine optical and electronic compensation was to reduce the channel memory of the link to enable moderate LUT sizes. Therefore, it will be analysed in this section to what extent this approach is valid.

The operation of the LUT and the calculation of the samples stored in the LUT was carried out using the same technique described in Sections 4.1.6 and 4.1.7. The only two differences are that the backpropagation link includes inline DCF which fully compensate the span dispersion, and no linear dispersion compensating filter is required after the LUT.

The simulation results for the required OSNR of 800 km SSMF transmission are shown in Fig. 4.24 for different LUT sizes ranging from 3 to 11 bit. For comparison, the curve obtained using unrestricted LUT size, i.e. using the ideal backpropagation, and the results for the optimised ODC system are also shown. Clearly, increasing the LUT size improves the nonlinear tolerance. Even a relatively small table with 9 address bits achieves a better nonlinear threshold than the optimised ODC system.

The graph in Fig. 4.25 summarises the resulting nonlinear threshold values versus the LUT address size including the nonlinear thresholds obtained by the optimised ODC system and the EPD system with unrestricted LUT. Increasing the LUT size will also increase the nonlinear threshold. The 11-bit LUT achieves a nonlinear threshold of 4.8 dBm which is nearly 4 dB better than an optimised dispersion map. This demonstrates the expected effectiveness of a real-time realisation of the LUT based predistortion for intrachannel nonlinearities.

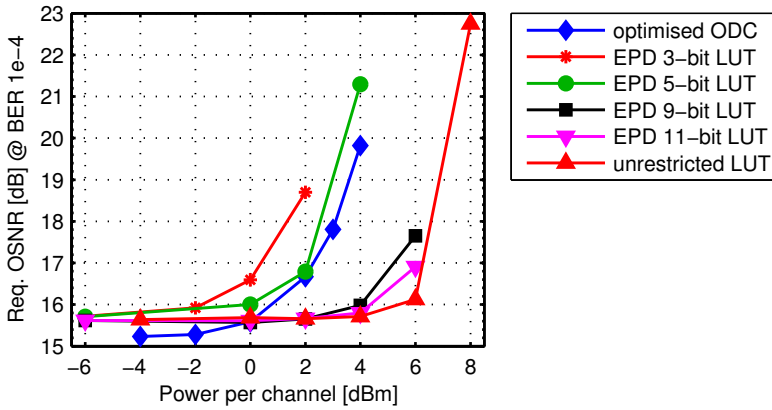

Figure 4.24. *Required OSNR versus the launch power for different LUT address sizes after transmission over 10×80 km SSMF. Optimised ODC results are also shown. The triple MZM was used with an 80 GSa/s 4-bit DAC. The target format was 40 Gbit/s NRZ-OOK.*

The maximum nonlinear threshold obtained using the 11-bit LUT is only about 1 dB less than the upper limit at 6 dBm obtained using the unrestricted LUT, i.e. using the ideal backpropagation and 80 GSa/s 4-bit DAC. This upper limit is given by the finite sampling rate and quantisation of the DAC. The results for finite LUT sizes confirm that the nonlinear channel memory of the transmission link due to pulse overlap is indeed reduced using the inline DCF. The physical reason is that the periodic dispersion compensation does not allow pulses to spread significantly, thus, limiting the number of nonlinearly interacting pulses. In conclusion, an 11-bit LUT in the EPD transmitter with a pair of DAC operated at a quantisation resolution of 4 bit and 80 GSa/s achieves effective compensation of intrachannel nonlinearities in the proposed transmission system[8]. The nonlinear threshold is increased by 6 dB compared to the ODC system with a resonant map and by 4 dB compared to ODC with an optimised map.

The results confirm the more general design rule that the memory length of nonlinearities determines the transmitter complexity. The nonlinear channel memory, m_{NL}, estimated according to (2.43) is $m_{\mathrm{NL}} = 5.3$ bits using $D_{\mathrm{acc}} = D_{\mathrm{SMF}} \times L_{\mathrm{eff}}$, $B = 40$ Gbit/s, $\Delta f = 40$ GHz. Although (2.43) does not give the

[8] According to the results of the previous section (Fig. 4.23), we expect that the sampling rate may be reduced to 60 GSa/s without significantly changing the nonlinear threshold.

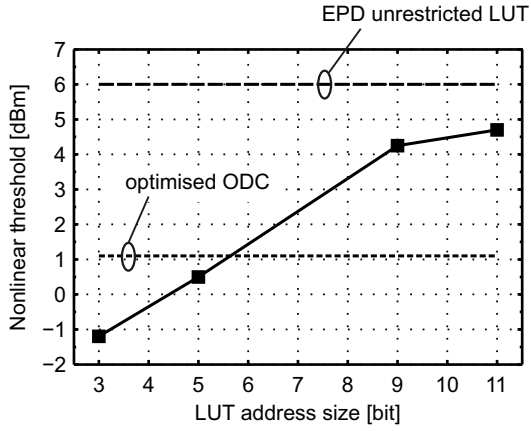

Figure 4.25. *Nonlinear threshold versus the LUT address sizes. The triple MZM was used with an 80 GSa/s 4-bit DAC.*

exact required LUT size, it is useful to determine the order of magnitude when scaling to higher bit rates or different accumulated dispersion.

After the combination of EPD and ODC was first proposed [Weber2006], the effectiveness of this technique has been confirmed by several other authors [Xie2006, Hellerbrand2007]. In [Xie2006], the authors demonstrate electronic predistortion of intrachannel nonlinearities in 40 Gbit/s systems using optical inline dispersion compensation for a transmission link consisting of 20 km TrueWave fibre with a dispersion coefficient of $D = 6$ ps/nm/km. The authors applied the nonlinear predistortion to a link with an optimised dispersion map. Predistortion achieves an increase in the maximum launch power into the system of about 3 dB. The limit in this case was given by interchannel effects such as XPM and FWM. Although these effects are expected to be less degrading in SSMF transmission, we will carry out a detailed analysis of WDM EPD transmission in the next section.

4.2.4. Fundamental XPM Limitations

In the previous sections, it was shown that the combination of conventional inline dispersion compensation using DCF and EPD for compensation of intrachannel nonlinearities improves the nonlinear threshold of single channel predistorted 40 Gbit/s NRZ transmission by approximately 5 dB compared to an optimised ODC system without predistortion. Nonlinear interactions between neighbouring individually predistorted channels have been neglected so

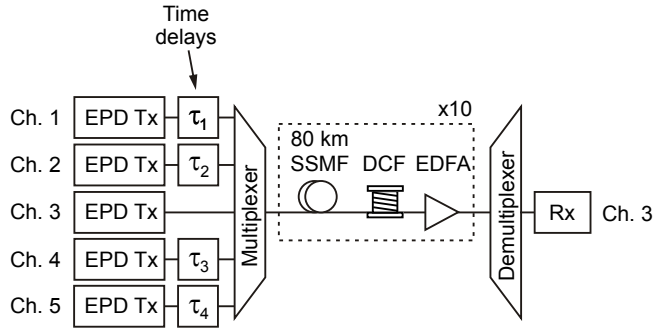

Figure 4.26. *WDM system setup with five individually predistorted channels at 40 Gbit/s. The time delay elements are used to analyse the XPM statistics in WDM operation.*

far. However, our previous discussions on 40 Gbit/s dispersion precompensation in Section 3.2.6 and nonlinearity precompensation in Section 4.1.4 have revealed that those EPD systems tend to suffer from stronger interchannel nonlinearities in WDM operation than ODC systems. Therefore, studying the nonlinear tolerance of the proposed EPD technique in a WDM system is of great practical interest to analyse if the advantage is maintained in the presence of interchannel nonlinearities.

The impact of interchannel nonlinearities, most importantly XPM, will be analysed using the five-channel transmission system setup shown in Fig. 4.26. The optical transmission path is the same as presented in Section 4.2.1. It consists of 10×80 km SSMF spans each of which is fully inline postcompensated using a DCF resulting in a resonant map. The term resonant is used to express the fact that, at the end of each span, the accumulated dispersion is reset to zero. The fibre parameters are the same as stated in Section 4.2.1.

Each channel was loaded with a DBBS 10. The intrachannel nonlinearities within each channel were individually predistorted using a realistic EPD transmitter that consists of a triple MZM, driven by two 80 GSa/s, 4-bit DAC and an 11-bit LUT. This allows to quantify the penalties in a realistic EPD system including the major degrading effects of imperfect hardware components.

Five electronically predistorted channels with a channel spacing of 100 GHz are multiplexed at the transmitter using a second-order Gaussian band-pass filter for each channel whose center frequency is the carrier frequency of the channel. The multiplexer filter 3-dB bandwidth was 120 GHz. After transmission,

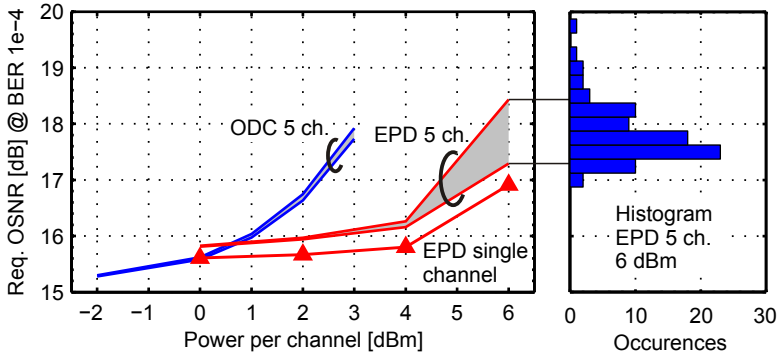

Figure 4.27. *Required OSNR distributions for BER of 10^{-4} in 5×40 Gbit/s WDM systems versus the power per channel after 800 km for optimised ODC and EPD of intrachannel nonlinearities in a resonant dispersion map. An 11-bit LUT, an 80 GSa/s, 4-bit DAC and a triple MZM were used in the EPD transmitter. The 10^{th} and 90^{th} percentiles of the distributions are shown as a result of 100 simulations with random time delays between WDM channels. Inset: Histogram of the required OSNR for EPD at 6 dBm power per channel.*

the central channel is demultiplexed using a 44 GHz band-pass filter[9]. The filter bandwidths are the result of a numerical optimisation detailed in Appendix A. The electrical postdetection filter is a fifth-order Bessel low-pass having a 3-dB cut-off bandwidth of 28 GHz.

The simulation technique used to quantify the impact of XPM is the same as in Sections 3.2.5 and 4.1.3. The required OSNR for a BER of 10^{-4} of the central channel was calculated for 100 random realisations of different time shifts between the channels and for a range of launch powers per channel in the 40 Gbit/s EPD system. From the resulting histograms of the required OSNR, the 10^{th} and 90^{th} percentiles are calculated.

The results are plotted versus the launch power in Fig. 4.27. The larger the difference between the two percentiles the stronger is the impact of XPM. For comparison, the ODC results and the EPD single channel results using an 80 GSa/s, 4-bit quantisation and 11-bit LUT are also shown[10]. The first observation with

[9] Note that the demultiplexer filter is narrower than the optical receiver filter in the previous single channel simulations where a bandwidth of 80 GHz was used. The filter bandwidth was reduced to avoid coherent crosstalk between channels in the receiver.

[10] Note that the EPD single channel curve is different from the single channel results plotted in Fig. 4.24 in the previous chapter due to the narrower receiver band-pass filter bandwidth of 44 GHz as opposed to 80 GHz.

EPD is that five channel transmission only slightly degrades the required OSNR of the EPD system compared to the single channel case up to a launch power of 4 dBm. In addition, the EPD WDM results show negligible spreading of the required OSNR up to 4 dBm indicating negligible impact of XPM. At powers larger than 4 dBm, however, the required OSNR starts to spread as a result of XPM. A comparison with the EPD single channel curve shows that the power at which XPM becomes a problem coincides with the power at which single channel degradations start to occur.

The inset in Fig. 4.27 shows the histogram of the required OSNR of the central channel at 6 dBm launch power. Clearly, significant spreading occurs with required OSNR values ranging from 17 to 20 dB. In contrast, the ODC system shows no signs of XPM. Instead, the maximum launch power is limited by intrachannel nonlinearities with a nonlinear threshold at about 1 dBm. The nonlinear threshold of the EPD WDM system is about 3 dB better than for ODC.

To sum up the discussion, the system using a resonant dispersion map and electronic predistortion for intrachannel nonlinearities at 40 Gbit/s achieves an effective increase in the nonlinear tolerance even in a WDM system with five predistorted neighbouring channels. The maximum launch power may be in increased by about 3 dB compared to the optimised ODC system. These results already include the implementation penalties of an EPD transmitter with a triple MZM, two 80 GSa/s, 4-bit DAC and an 11-bit LUT. In the investigated system, the launch power is limited to 4 dBm. Above this power, the system performance is degraded by the imperfect EPD transmitter hardware (DAC and LUT) and by XPM of neighbouring WDM channels.

4.2.5. Advanced Modulation Formats

In ODC systems, the modulation format is generated at the transmitter whose structure and complexity depends on the employed format. This has been detailed in Section 2.2 where the most important modulation formats have been introduced. In contrast, in EPD systems, the modulation format is not generated at the transmitter. Instead, the EPD transmitter must be capable of generating arbitrary complex fields to reverse the degrading effects leading to the target modulation format after propagation at the receiver. Limitations arise due to finite DAC sampling and quantisation. Given a fixed transmitter complexity, the target modulation format at the receiver can be used as a degree of freedom to optimise the system performance since only the programming of the digital predistortion device needs to be modified. The potential improvements of the EPD technique by utilising advanced modulation formats has also been assessed in [Xie2007, Hellerbrand2007]. We will investigate the predistortion

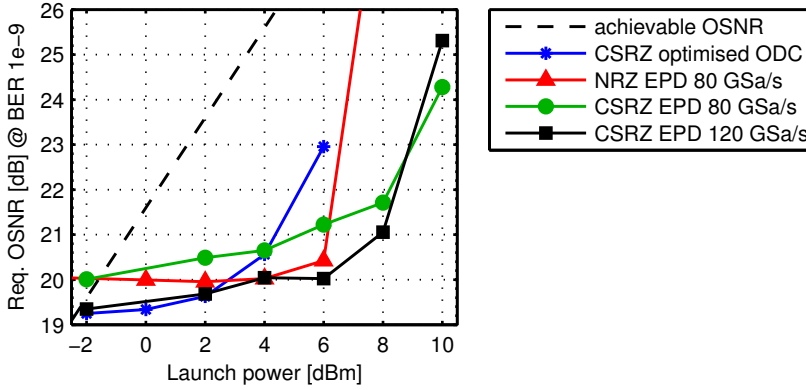

Figure 4.28. *Required OSNR versus the launch power for EPD and ODC using different modulation formats including CSRZ-OOK. EPD refers to predistortion of intrachannel nonlinearities in a resonant dispersion map. For EPD, the triple MZM was used with an 80 GSa/s 4-bit DAC and unrestricted LUT size.*

technique for different target modulation formats in systems using full inline optical dispersion compensation.

Carrier-Suppressed Return-to-Zero (CSRZ)

It is known for conventional ODC systems that return-to-zero (RZ) formats generally obtain a better performance in high-speed transmission than NRZ. In particular, the transmission characteristics of carrier-suppressed return-to-zero (CSRZ) benefit from the carrier suppression compared to other RZ formats [Sano2001, Gnauck2004]. However, it is not clear to what extent this advantage is maintained in electronically predistorted transmission.

Therefore, we chose CSRZ as the target format for the transmission system shown in Fig. 4.16 and reprogrammed the predistortion block for CSRZ modulation. A triple MZM was employed. The predistortion block was implemented using the ideal backpropagation, i.e. unrestricted processor memory is assumed and the impact of finite LUT size is neglected. The modulator drive voltages were obtained using (3.5) and (3.6). All other parameters remain unchanged to previous NRZ transmission, i.e. the DAC sampling rate was set at 80 GSa/s, 4-bit quantisation.

The graph in Fig. 4.28 compares the required OSNR for a BER of 10^{-9} for various system scenarios [11]. The results for conventional CSRZ ODC transmission, i.e. without EPD and using the optimised dispersion map, confirm the well-known fact that CSRZ improves the nonlinear tolerance at 40 Gbit/s compared to nonreturn-to-zero (NRZ). The nonlinear threshold is increased to nearly 4 dBm.

Unfortunately, employing the CSRZ predistortion at 80 GSa/s causes a considerable implementation penalty of about 1 dB at low launch powers compared to the CSRZ ODC system. This leads to required OSNR performance that is worse than NRZ. The reason for this behaviour becomes clear when we analyse the optical spectrum at the EPD transmitter for 80 GSa/s DAC and for an ideal DAC, shown in Fig. 4.29. Sampling with 80 GSa/s leads to a significant clipping of higher frequency components in the main lobe of the spectrum. Increasing the sampling rate to 120 GSa/s, i.e. 3 samples per bit, restores the main lobe. This is confirmed by the required OSNR performance using a 120 GSa/s DAC plotted in Fig. 4.28. CSRZ clearly shows an advantage in nonlinear tolerance. However, the practical relevance is doubtful due to the enormous DAC speed and the relatively small improvement.

Based on these observations, a narrow-band format such as optical duobinary may be a promising candidate since it would suffer less from sampling rate limitations. Although I did not carry out simulations using duobinary, I co-authored a study on advanced modulation formats for EPD of intrachannel nonlinearities which included optical duobinary [Hellerbrand2007]. A periodically inline compensated 10×80 km SSMF transmission link with a resonant dispersion map was considered. Indeed, it is shown that the performance of duobinary is tolerant to sampling rate reduction. However, duobinary requires a back-to-back OSNR that is more than 2 dB higher than that of NRZ at a BER of 10^{-9}. This penalty cannot be compensated for by EPD. In addition, EPD using duobinary target format has a smaller nonlinear threshold than NRZ. These results indicate that the poor nonlinear performance of duobinary outweighs the advantages from the narrow bandwidth.

Differential Phase Shift Keying (DPSK)

Another advanced modulation format that has attracted considerable interest for high-speed transmission is differential phase shift keying (DPSK), cf. Section 2.2.3. In order to exploit the advantages of DPSK, balanced detection using

[11] Note that a BER of 10^{-9} is used instead of 10^{-4} as in the previous sections. The reason is that these simulations were performed earlier, amidst the growing use of FEC in optical communication where higher BER can be tolerated. However, as demonstrated by Fig. 4.21, the relative comparison between systems remains valid at lower BER.

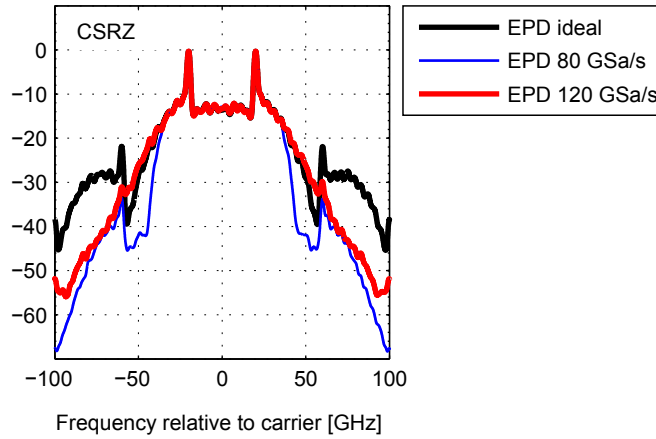

Figure 4.29. *Optical spectra at the EPD transmitter for ideal digital-to-analog conversion and using limited sampling rate for CSRZ modulation format. The launch power was set at +6 dBm.*

a delay interferometer and two photo diodes is necessary. The balanced DPSK receiver used for the following simulations was introduced in Section 2.7.2. A block diagram is shown in Fig. 2.17. The 3-dB bandwidth of the second order Gaussian optical band-pass is 80 GHz. The electrical filter is a fifth-order Bessel low-pass with a 3-dB cut-off frequency of 28 GHz. The target modulation format is DPSK using 67%-RZ pulses.

For the semi-analytical BER estimation, the saddle point approximation is applied instead of the Gaussian approximation used in the previous sections. As detailed in Section 2.7.3, the saddle point approximation yields accurate results for the BER DPSK signals.

We compare the nonlinear tolerance of a conventional DPSK transmission, i.e. without EPD, over a resonant non-optimised dispersion map to the EPD DPSK system. The predistortion was reprogrammed to transmit signals that will evolve into the DPSK format at the receiver. The EPD transmitter uses a triple MZM and 80 GSa/s, 4-bit DAC and unrestricted LUT size.

The resulting required OSNR for a BER of 10^{-9} versus the launch power is shown in Fig. 4.30. First, a significantly improved required OSNR performance is observed for DPSK compared to NRZ at low launch powers. This is the well-known 3-dB OSNR advantage of DPSK that is obtained by balanced detection [Gnauck2005]. In this case, the difference to NRZ EPD is even about

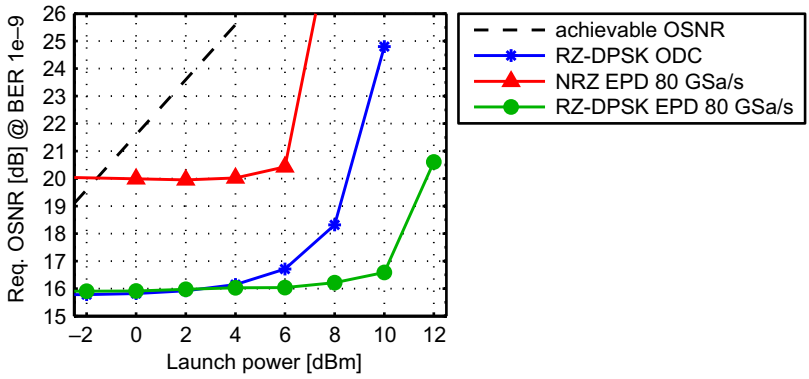

Figure 4.30. *Required OSNR versus the launch power for EPD and ODC using NRZ-OOK and 67% RZ-DPSK. EPD refers to predistortion of intrachannel nonlinearities in a resonant dispersion map. For EPD, the triple MZM was used with an 80 GSa/s 4-bit DAC and unrestricted LUT size.*

4 dB due to the additional implementation penalty of the NRZ EPD transmitter. Interestingly, the DPSK EPD transmission using 80 GSa/s and 4-bit quantisation shows a negligible implementation penalty demonstrating the robustness of the DPSK format to digitised drive voltages.

The nonlinear threshold is improved by about 3 dB compared to DPSK ODC which is only a moderate improvement compared to those obtained with NRZ. The reason is that the DPSK format is inherently less susceptible to intrachannel nonlinearities than NRZ. In fact, a major source of degradation in DPSK transmission which is neglected here is nonlinear phase noise. Intensity noise from amplifier's ASE is converted to phase noise through SPM, which is also referred to as the Gordon-Mollenauer effect [Gordon1990]. Since caused by noise, it is a non-deterministic effect and cannot be predistorted. For the semi-analytical BER estimation to be accurate, nonlinear phase noise must be negligible. This condition may not be fulfilled at larger launch powers and may lead to additional penalties [Ohm2005].

The discussion of DPSK transmission also reveals an inherent drawback of the transmitter-side predistortion technique, namely that only perfectly deterministic processes can be predistorted if no feedback channel is used. Even chromatic dispersion varies with time (albeit slowly) and may require adaptive compensation. Therefore, practical realisations of EPD rely on an adaptive feedback channel to optimise the parameters of the precompensation. Nortel's commercially available EPD solution (eDCO transmitter) uses feedback messages in

the overhead of G.709 OTU-2 frames[12] to scan the dispersion of the link [Nortel2006]. The feedback channel may allow to adaptively compensate for slow variations such as variations in the dispersion of the link. However, rapidly varying effects cannot be adaptively compensated using predistortion such as polarisation mode dispersion on the time scale up to 40 kHz [Krummrich2004] or the Gordon-Mollenauer effect which varies on even shorter time scales. Such degradations may be compensated more effectively using receiver-side digital signal processing after coherent detection. For instance, partial nonlinear phase noise cancellation has been shown using digital signal processing (DSP) based postprocessing [Kikuchi2006].

[12] G.709 refers to an ITU-T recommendation which defines the functionality of the optical transport networks (OTN) above the physical layer. The standard defines that several overhead sections and FEC information are added to the client signal to form an optical transport unit (OTU).

CHAPTER 5

Summary and Conclusions

THE FINAL CHAPTER of this thesis summarises the results and discusses their significance. In addition, the perspectives of electronic predistortion (EPD) and possible alternatives for future high bit rate systems are examined.

The aim of the thesis was to investigate long-haul fibre-optic transmission systems that employ electronic precompensation of chromatic dispersion and fibre nonlinearities at high bit rates of 10 and 40 Gbit/s. In Chapter 3, only linear precompensation was considered whereas nonlinear precompensation was investigated in Chapter 4.

5.1. Linear EPD of Dispersion

The effectiveness of EPD was studied using an 800 km transmission system consisting of 10 $\times$ 80 km standard single mode fibre spans which is introduced in Chapter 3. First, we studied ideal precompensation of the entire accumulated chromatic dispersion of the link in 10 and 40 Gbit/s transmission. For this purpose, the EPD transmitter was modelled to perfectly invert the effect of chromatic dispersion by emulating a linear filter with sufficient memory. Unconstrained transmitter hardware complexity and accuracy were assumed. In this case, transmission is fundamentally limited by fibre nonlinearities. In order to assess the potential benefits or disadvantages of EPD over conventional optical dispersion compensation (ODC) systems, we also considered a 10 $\times$ 80 km

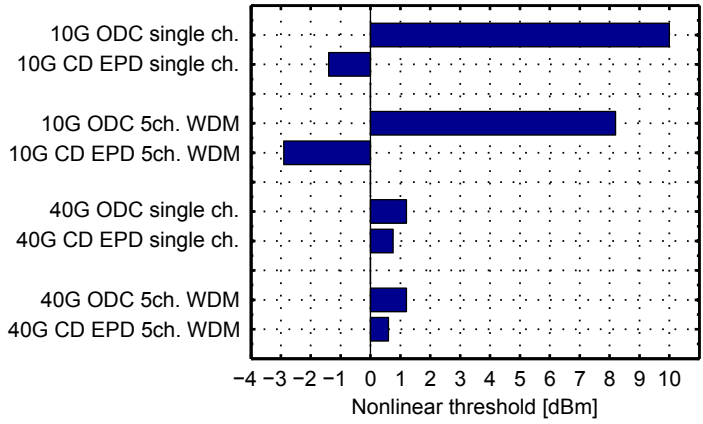

Figure 5.1. *Nonlinear threshold (calculated for a BER of 10^{-4}) of the ODC and EPD reference systems (800 km SSMF) at 10 and 40 Gbit/s for single channel and WDM operation. "CD EPD" refers to linear precompensation of chromatic dispersion (CD) under ideal conditions, i.e. without transmitter hardware constraints.*

ODC system with an optimised dispersion map which employs inline dispersion compensating fibre (DCF) for dispersion compensation. The nonlinear tolerance of EPD and ODC is expressed by the nonlinear threshold which is defined as the maximum launch power leading to a required optical signal-to-noise ratio (OSNR) penalty of 1 dB. The required OSNR was calculated for a bit error rate (BER) of 10^{-4}.

Fig. 5.1 summarises the nonlinear threshold results of the investigated system scenarios of Chapter 3 that were simulated using the ideal modelling. The modulation format was NRZ-OOK. Nonlinearities are examined separately for single channel and five-channel WDM systems to identify the relative impact of intra- and inter-channel effects. For WDM systems, a statistical simulation technique has been adopted to investigate the performance fluctuation due to cross-phase modulation (XPM) which was first observed in [Essiambre2005a]. The nonlinear threshold refers to the mean of the required OSNR distribution.

For the 10 Gbit/s single channel and WDM case (using 50 GHz channel spacing), we observe in Fig. 5.1 that the nonlinear threshold of EPD is significantly lower than for ODC indicating that EPD suffers severely from intra- and inter-channel nonlinearities compared to ODC. In contrast, at a bit rate of 40 Gbit/s transmission, the nonlinear thresholds of EPD and ODC are approximately equal with a difference of less than 1 dB for both single channel and WDM (us-

ing 100 GHz channel spacing). This demonstrates that in the relative comparison between electronic (all at the transmitter) and optical (distributed along the line) dispersion compensation, EPD benefits from the highly dispersive pseudolinear transmission regime, i.e. using a fibre with high local dispersion at high bit rates. Remarkably, the nonlinear threshold for 40 Gbit/s EPD single channel transmission is larger than that of 10 Gbit/s.

The role of the channel memory for the simulation of EPD systems at higher bit rates was pointed out. In particular, the enormous memory due to chromatic dispersion in 40 Gbit/s on-off keying (OOK) modulated channels presents difficulties for the accurate calculation of the required OSNR. The required bit sequence length exceeds the capabilities of the computer hardware used for the simulations. For the single channel simulations, the maximum sequence length was 2^{15} whereas, for the WDM simulations, a length of 2^{11} was used. As a consequence, the nonlinear threshold of the 40 Gbit/s EPD WDM system is slightly overestimated.

In addition to fundamental limitations, we addressed the implementation penalties caused by hardware constraints such as the digital signal processor memory and the digital-to-analog converter (DAC) sampling rate and quantisation. The most critical aspect of a 40 Gbit/s EPD transmitter is the DAC. Therefore, a realistic EPD transmitter model including a pair of DACs and a triple Mach–Zehnder modulator (MZM) was implemented to estimate the requirements based on the penalty after transmission. A DAC sampling rate of 60 GSa/s and quantisation of 4-bit was found sufficient for an implementation penalty smaller than 1 dB. Although such devices are not available at the time of writing, we expect data converters at such speeds in the near future since the applications of digital signal processing (DSP) in fibre-optic transmission are a strong driver.

Next, we investigated the nonlinear tolerance and the maximum achievable OSNR margin of 40 Gbit/s EPD using the realistic transmitter model. For a more realistic comparison between EPD and ODC, the loss and nonlinearity of the inline DCF and a dual-stage amplifier were considered in the ODC system. Consequently, the achievable OSNR of ODC is lower than that of EPD.

In the 40 Gbit/s single channel case, the maximum OSNR margin of the EPD and ODC 800 km system was approximately equal at 10 dB. The optimum launch power is 1 dBm. However, using EPD with five neighbouring predistorted 40 Gbit/s channels revealed a small penalty fluctuation first reported for 10 Gbit/s in [Essiambre2005a]. Nevertheless, the OSNR margin results of single channel and WDM transmission show that the 40 Gbit/s EPD system using 60 GSa/s and 4-bit quantisation achieves a performance which is similar or only slightly worse than that of ODC.

It was finally discussed in Chapter 3 that linear EPD of chromatic dispersion may become more attractive at higher bit rates since limitations due to nonlinearities are less critical than at lower bit rates. However, the realisation of the required electronics hardware for 40 Gbit/s EPD is a considerable challenge.

5.2. Nonlinear EPD

The control of the phase and amplitude using an optical field modulator combined with high-speed electronics in the transmitter allows additional precompensation of nonlinear fibre effects. Strategies for nonlinear predistortion at high bit rates were introduced and discussed in Chapter 4.

First, the combined predistortion of dispersion and intrachannel nonlinearities (CD+SPM EPD) was studied under the assumption of an ideal transmitter with unconstrained complexity for 800 km SSMF transmission. The ideal nonlinear predistortion was realised by backpropagation using the split-step algorithm. It was further argued that only intrachannel nonlinearities can potentially be predistorted. The information of neighbouring WDM channels which are required for predistortion of interchannel nonlinearities, are not accessible in a practical system. Therefore, interchannel nonlinearities such as XPM impose a fundamental limit on the nonlinear tolerance. At 10 Gbit/s, the additional predistortion of intrachannel nonlinearities increases the nonlinear threshold by approximately 3 dB compared to linear dispersion compensation. At 40 Gbit/s, the nonlinear threshold is improved by about 2.5 dB. The launch power is limited by XPM degradations. Furthermore, the statistical WDM simulations reveal fluctuations of the required OSNR depending on the launch power for both 10 and 40 Gbit/s.

Second, we investigated the hardware requirements for CD+SPM EPD for 10 and 40 Gbit/s. The nonlinear predistortion in a real-time realisation could be implemented using a combination of look-up table (LUT) based filtering for nonlinearities and a linear filter for dispersion. We find that at 10 Gbit/s, an EPD transmitter using an 11-bit LUT, a pair of 20 GSa/s, 4-bit DACs, and a triple MZM achieves a nonlinear threshold increase of nearly 6 dB compared to linear dispersion compensation only. By analysing the nonlinear channel memory, we discuss that simply scaling this technique to 40 Gbit/s is not feasible since the LUT memory requirement of more than 100 address bits is impractical.

Finally, we consider electronic predistortion of intrachannel nonlinearities at 40 Gbit/s in an optically dispersion compensated transmission link. In this case, the nonlinear channel memory of the 40 Gbit/s link is reduced by the periodic compensation of dispersion enabling LUT based nonlinear filtering in the transmitter. Electronic nonlinearity compensation allows to simplify the link design

and to use identical 100% postcompensated spans, i.e. a resonant dispersion map, without the need to optimise the dispersion map. We showed for single channel transmission that using an 11-bit LUT, a pair of 80 GSa/s, 4-bit DACs, and a triple MZM, the nonlinear threshold is increased by 6 dB compared to the ODC system with a resonant map and by 4 dB compared to ODC with an optimised map. Further, we considered a five-channel WDM system where each channel is predistorted for intrachannel nonlinearities. In this case, the maximum launch power of 4 dBm is limited by interchannel effects achieving a 3-dB increase compared to the optimised five-channel WDM system without EPD.

5.3. Perspectives of EPD

The availability of high-speed DSP has led to a new paradigm in optical transmission system design. Electronics are increasingly used in the transmitters and receivers to perform mitigation of optical impairments. In the following, the similarities and differences of EPD and receiver side techniques will be discussed and recommendations for future work are given.

Signal processing in direct detection receivers can also perform compensation. However, the photo current after direct detection is a nonlinear function of the optical field amplitude and does not contain information on the optical phase. Hence, nonlinear equalisers are required. Although nonlinear mitigation techniques such as maximum likelihood sequence estimation (MLSE) or nonlinear feed-forward equaliser (FFE)-decision feedback equaliser (DFE) are promising for dispersion and nonlinearity compensation at 10 Gbit/s [Poggiolini2007, Xia2007], scaling to higher bit rates is a considerable challenge since the processing complexity and/or memory requirement of nonlinear equalisers scales exponentially with the channel memory.

In coherent receivers, the optical signal is mixed with the light of a local oscillator laser through an optical hybrid, which allows to recover the inphase and quadrature component of the optical field in the electronic domain. If the complex optical field can be either controlled (EPD) or measured (coherent reception), then the compensation of chromatic dispersion becomes a relatively straightforward linear filtering task. Linear filters can be readily scaled to higher bit rates. In this case, the critical component is the DAC for EPD and the analog-to-digital converter (ADC) for receiver based techniques. One of the most important advantages of transmitter or receiver based electronic compensation is the ability to adaptively reconfigure the compensator to account for a dynamically changing channel. Nortel's commercial EPD solution uses feedback messages in the overhead of G.709 OTU-2 frames to scan the dispersion of the link [Nortel2006]. Dynamic reconfiguration becomes increasingly im-

portant for compensation of polarisation mode dispersion (PMD) which can change as fast as 40 kHz [Krummrich2004]. Adaptive compensation of such effects requires a sufficiently fast feedback signal which becomes challenging for precompensation over long distances. Clearly, digital coherent receivers have an advantage in the compensation of dynamically changing processes. Investigations on the impact of PMD in EPD systems have not been published so far.

In principle, compensation of nonlinearities is possible using both EPD and digital coherent receivers. Coherent receivers must use some form of backpropagation calculation of the received distorted field to reverse the nonlinear effects [Li2008]. The backpropagation approaches have been criticised since they "rely very heavily on often non-realistic computation speeds" [Shtaif2008]. For EPD it was discussed in Chapter 4 that combined predistortion of dispersion and nonlinearities at 40 Gbit/s requires impractically large LUT sizes. However, this study only considered NRZ-OOK as the target modulation format which is not the optimum choice. Multi-level modulation formats such as quadrature phase shift keying (QPSK) or quadrature amplitude modulation (QAM) reduce the symbol rate and the channel memory compared to OOK formats of the same bit rate. In addition, QPSK is currently considered a promising candidate for future 100 Gbit/s transmission systems, see [Winzer2007] and references therein. Further research is recommended to analyse potential improvements by optimising the target modulation format.

Using predistortion with multi-level modulation formats such as QPSK requires a more complex receiver. In this case, it could be an attractive option to use an electronic predistortion transmitter in conjunction with a digital coherent receiver (see, e.g., [Ip2009]). In fact, it has been shown that sharing the dispersion compensation equally between the transmitter and the receiver is the optimum strategy for minimising the impact of both intra- and interchannel fibre nonlinearities [Savory2006]. In addition, the overall complexity of the compensation processing is reduced if shared between both terminals due to the exponential complexity scaling for nonlinearity compensation. In the current demand for more capacity, it is expected that next-generation high speed fibre-optic transmission systems will make extensive use of electronic signal processing both in the transmitter and in the coherent receiver to compensate for impairments, to enable novel modulation formats and to increase spectral efficiency.

APPENDIX A

Optimisation of Multiplexer and Demultiplexer Filter Bandwidths

The filter bandwidth in the multiplexer and demultiplexer affects the required OSNR of the transmission. The optimum bandwidth values depend on a number of parameters such as the modulation format, channel spacing and bit rate. We performed a numerical optimisation of the filter bandwidths using a three-channel transmission system in back-to-back configuration as shown in Fig. A.1. Three channels are individually modulated using NRZ-OOK and filtered using the multiplexer band-pass filters. The channels are combined to form the optical field. No transmission fibre is considered since the filters are optimised in back-to-back configuration. The block diagram of the receiver is the same as described in Section 2.7.

In order to determine the filter bandwidths for the 10 and 40 Gbit/s systems presented in Chapter 3 and 4, we performed a numerical optimisation by simply varying the bandwidths of the optical band-pass filters in the multiplexer and demultiplexer and evaluating the required OSNR for a BER of 10^{-4} at each bandwidth pair.

For the 40 Gbit/s system, a channel spacing of 100 GHz was used. Fig. A.2 shows contours of constant OSNR penalty as a function of the multiplexer (MUX) and demultiplexer (DMUX) band-pass filter bandwidth. We observe that the multiplexer bandwidth has a wide optimum range from 80 GHz up to well above 100 GHz. We chose 120 GHz. The demultiplexer bandwidth in

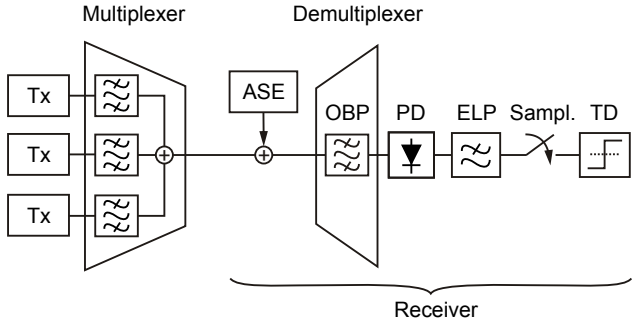

Figure A.1. *System setup used for the optimisation of the filter bandwidths of the optical band-pass filters in the multiplexer and demultiplexer. OBP: optical band-pass filter, PD: photo diode, ELP: electrical low-pass filter, Sampl.: Sampling, TD: threshold decision.*

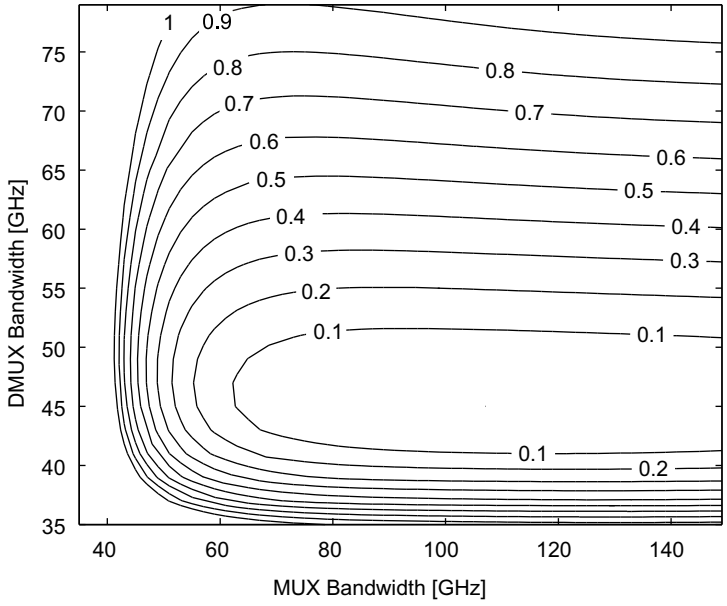

Figure A.2. *Contour plot of the required OSNR penalty (BER of 10^{-4}) as a function of the bandwidths of the optical band-pass filters in the multiplexer (MUX) and demultiplexer (DMUX) using 40 Gbit/s NRZ-OOK. Three wavelength channels with a channel spacing of 100 GHz were transmitted.*

the receiver is more critical. For nonreturn-to-zero (NRZ)-modulated signals, the optimum bandwidth is a trade-off between amplified spontaneous emission (ASE) noise rejection and intersymbol interference (ISI) [Winzer2001]. The optimum was found at 44 GHz.

The same simulations were carried out for 10 Gbit/s using 50 GHz channel spacing. The optimum values for 10 and 40 Gbit/s are summarised in Table 3.1 on page 52.

The predistortion WDM systems were simulated using the same filter bandwidths as the conventional ODC systems. For nonlinear predistortion, the optimum filter bandwidths may change depending on the spectral broadening for larger launch powers observed in Section 4.1.2. However, in order to compare ODC and EPD, the same filters were used for both scenarios.

APPENDIX B

Optimised Dispersion Map

THE IMPACT of inter- and intrachannel nonlinearities on conventional ODC transmission can be minimised by optimising the dispersion map. We restrict our analysis of ODC on SSMF fibre spans which are periodically inline compensated using DCF modules as shown in Fig. 3.1(a) on page 51. A common approach for optimising the map is to introduce a dispersion precompensation, D_{pre}, at the transmitter and a residual dispersion per span, D_{res} [Killey2000, Essiambre2002]. This leads to a saw-tooth shaped tilted map, as shown by Fig. Fig. 3.1(b) on page 51. Additionally, a net residual dispersion, D_{nrd}, at the receiver may be used.

The optimisation was carried out by varying the dispersion precompensation and the residual dispersion per span and locating the optimum. Keeping the pair (D_{pre}, D_{res}) fixed, the net residual dispersion at the receiver is then varied to further optimise the signal.

For 40 Gbit/s, a single channel was transmitted which is sufficient to optimise the map at this bit rate as confirmed by [Killey2000]. Fig. B.1 shows contour lines of constant required OSNR for a BER of 10^{-9} versus dispersion precompensation and residual dispersion per span after transmission over the 10×80 km link. The launch power was set to 3 dBm which is sufficiently high to cause noticeable intrachannel nonlinearities. As a result, the optimum precompensation and the optimum residual dispersion per span were found at $D_{\text{pre}} = -300$ ps/nm and $D_{\text{res}} = 20$ ps/nm, respectively. The optimum net

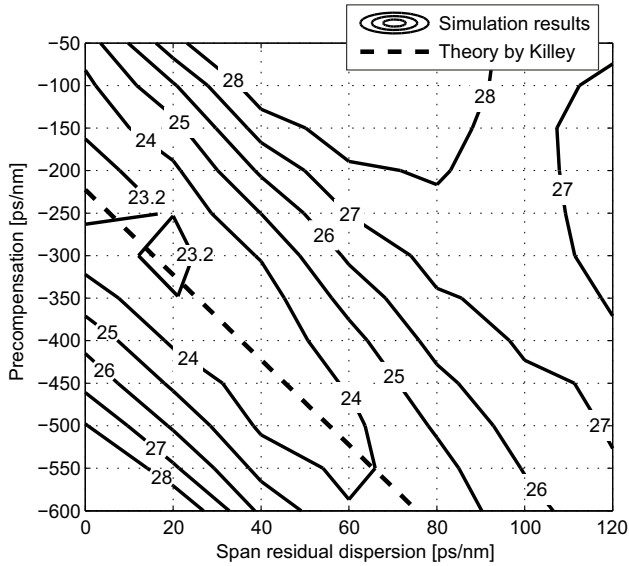

Figure B.1. *Contour lines of constant required OSNR for a BER of* 10^{-9} *versus dispersion precompensation and residual dispersion per span after transmitting a single 40 Gbit/s NRZ-modulated channel over a* 10×80 *km SSMF link. The launch power was set at 3 dBm. The dashed line is calculated according to [Killey2000, eq. (3)]*

residual dispersion was 0 ps/nm. The dashed line in Fig. B.1 shows an analytical design rule derived in [Killey2000, eq. (3)]. Good agreement between simulations and the theory is found. It is also typical for the pseudolinear transmission regime, as e.g. transmission of 40 Gbit/s OOK signals over SSMF, that the net residual dispersion before the receiver is zero [Essiambre2002].

Optimisation of the dispersion map at 10 Gbit/s was carried out using five WDM channels spaced 50 GHz with 2 dBm launch power per channel. Taking multiple channels into account is necessary since the dispersion map severely affects the strength of interchannel nonlinear interactions at this bit rate and channel spacing. Apart from this modification, the same simulation technique as for 40 Gbit/s was used. The following optimum parameters were found: $D_{\mathrm{pre}} = -1000$ ps/nm, $D_{\mathrm{res}} = 100$ ps/nm, $D_{\mathrm{nrd}} = 150$ ps/nm.

It should be noted that although the optimum net residual dispersion before the receiver in 10 Gbit/s OOK transmission depends on the launch power we used 150 ps/nm for all launch powers, possibly operating sub-optimum at larger

launch powers. However, the conclusions regarding the comparison between EPD and ODC drawn in Chapters 3 and 4 remain valid.

List of Abbreviations

ADC	analog-to-digital converter
ASE	amplified spontaneous emission
ASK	amplitude-shift keying
BER	bit error rate
CMOS	complementary metal–oxide–semiconductor
CSRZ	carrier-suppressed return-to-zero
CW	continuous-wave
DAC	digital-to-analog converter
DBBS	De Bruijn binary sequence
DCF	dispersion compensating fibre
DFE	decision feedback equaliser
DPSK	differential phase shift keying
DQPSK	differential quadrature phase shift keying
DSP	digital signal processing
EDFA	erbium-doped fibre amplifier
EPD	electronic predistortion
FEC	forward error correction
FFE	feed-forward equaliser

FFT	fast Fourier transform
FIR	finite impulse response
FWM	four-wave mixing
GSa/s	Gigasample per second
IFWM	intrachannel four-wave mixing
IM	intensity-modulation
ISI	intersymbol interference
IXPM	intrachannel cross-phase modulation
LUT	look-up table
MLSE	maximum likelihood sequence estimation
MZM	Mach–Zehnder modulator
NLSE	nonlinear Schrödinger equation
NRZ	nonreturn-to-zero
NZDSF	non-zero dispersion shifted fibre
ODC	optical dispersion compensation
OOK	on-off keying
OSNR	optical signal-to-noise ratio
pdf	probability density function
PM	phase-modulation
PMD	polarisation mode dispersion
Pol-SK	polarisation shift keying
PRBS	pseudo-random binary sequence
PSK	phase shift keying
QAM	quadrature amplitude modulation
QPSK	quadrature phase shift keying
RAM	random access memory
RZ	return-to-zero
SBS	stimulated Brillouin scattering
SPM	self-phase modulation
SRS	stimulated Raman scattering

SSMF standard single mode fibre

WDM wavelength division multiplexing

XPM cross-phase modulation

References

[Abbott2008] S. Abbott, "Review of 20 years of undersea optical fiber transmission system development and deployment since TAT-8," in *Proc. European Conference on Optical Communication (ECOC 2008)*, Brussels, Belgium, 2008, paper Mo.4.E.1.

[Agrawal2001] G. P. Agrawal, *Nonlinear Fiber Optics*, 3rd ed. San Diego, CA: Academic Press, 2001.

[Agrawal2002] ——, *Fiber-Optic Communication Systems*, 3rd ed. New York, NY: John Wiley & Sons, 2002.

[Antona2008] J.-C. Antona, E. Grellier, A. Bononi, S. Petitrenaud, and S. Bigo, "Revisiting binary sequence length requirements for the accurate emulation of highly dispersive transmission systems," in *Proc. European Conference on Optical Communication (ECOC 2008)*, Brussels, Belgium, 2008, paper W.1.E.3.

[Bayvel2002] P. Bayvel and R. I. Killey, "Nonlinear optical effects in WDM transmission," in *Optical Fiber Telecommunications*, I. P. Kaminov and T. Li, Eds. San Diego, CA: Academic, 2002, vol. IVb, ch. 13, pp. 611–641.

[Berntson1996] A. Berntson, D. Anderson, M. Lisak, M. L. Quiroga-Teixciro, and M. Karlsson, "Self-phase modulation in

dispersion compensated optical fibre transmission systems," *Optics Communications*, vol. 130, no. 1-3, pp. 153 – 162, 1996.

[Birk2006] M. Birk, X. Zhou, M. Boroditsky, S. H. Foo, D. Bownass, M. Moyer, and M. O'Sullivan, "WDM technical trial with complete electronic dispersion compensation," in *Proc. European Conference on Optical Communication (ECOC 2006)*, Cannes, France, paper Th2.5.6.

[Bosco2006] G. Bosco and P. Poggiolini, "Long-distance effectiveness of MLSE IMDD receivers," *IEEE Photon. Technol. Lett.*, vol. 18, no. 9, pp. 1037–1039, 2006.

[Boyd1992] R. W. Boyd, *Nonlinear Optics*. San Diego, CA: Academic, 1992.

[Breuer1996] D. Breuer, C. Kurtzke, and K. Petermann, "Upgrading the embedded standard-fibre network by optical-phase conjugation," *IEE Proc.-Optoelectron.*, vol. 143, no. 3, pp. 205–208, 1996.

[Bülow2002] H. Bülow, "Electronic equalization of transmission impairments," in *Proc. Conference on Optical Fiber Communication (OFC 2002)*, paper TuE4.

[Carena2008] A. Carena, V. Curri, P. Poggiolini, and F. Forghieri, "Optical vs. electronic chromatic dispersion compensation in WDM coherent PM-QPSK systems at 111 Gbit/s," in *Proc. Conference Optical Fiber Communications (OFC 2008)*, San Diego, CA, paper JThA57.

[Cartledge2009] J. Cartledge, D. Krause, K. Roberts, C. Laperle, D. McGhan, H. Sun, K.-T. Wu, M. O'Sullivan, and Y. Jiang, "Electronic signal processing for fiber-optic communications," *IEEE LEOS Newsletter*, pp. 11–15, February 2009.

[Chandrasekhar2006] S. Chandrasekhar, C. R. Doerr, and L. L. Buhl, "Demonstration of 100% precompensated DWDM transmission over 1280 km of SSMF with no inline dispersion compensation using interconnected recirculating loops," *IEEE Photon. Technol. Lett.*, vol. 18, no. 1, pp. 256–258, 2006.

[Chandrasekhar2008] S. Chandrasekhar and X. Liu, "Experimental study on 42.7-Gb/s forward-error-correction performance under burst errors," *IEEE Photon. Technol. Lett.*, vol. 20, no. 11, pp. 927–929, 2008.

[Crochiere1981] R. E. Crochiere and L. R. Rabiner, "Interpolation and decimation of digital signals—A tutorial review," *Proc. IEEE*, vol. 69, no. 3, pp. 300–331, 1981.

[DiGiovanni2002] D. J. DiGiovanni, S. K. Das, L. L. Blyler, W. White, R. K. Boncek, and S. E. Golowich, "Design of optical fibers for communications systems," in *Optical Fiber Telecommunications*, I. P. Kaminov and T. Li, Eds. San Diego, CA: Academic, 2002, vol. IVa, ch. 2, pp. 17–79.

[ElSaid2005] M. M. El Said, J. Sitch, and M. I. Elmasry, "An electrically pre-equalized 10-Gb/s duobinary transmission system," *J. Lightwave Technol.*, vol. 23, no. 1, pp. 388–400, 2005.

[Essiambre1999] R.-J. Essiambre, B. Mikkelsen, and G. Raybon, "Intra-channel cross-phase modulation and four-wave mixing in high-speed TDM systems," *Electron. Lett.*, vol. 35, no. 18, pp. 1576–1578, 2 Sept. 1999.

[Essiambre2002] R.-J. Essiambre, R. Gregory, and B. Mikkelsen, "Pseuolinear transmission of high-speed TDM signals: 40 and 160 Gb/s," in *Optical Fiber Telecommunications*, I. P. Kaminov and T. Li, Eds. San Diego, CA: Academic, 2002, vol. IVb, ch. 6, pp. 232–304.

[Essiambre2005a] R.-J. Essiambre and P. J. Winzer, "Fibre nonlinearities in electronically pre-distorted transmission," in *Proc. European Conference on Optical Communication (ECOC 2005)*, Glasgow, UK, paper Tu3.2.2.

[Essiambre2006] ——, "Impact of fiber nonlinearities on advanced modulation formats using electronic pre-distortion," in *Proc. Conference Optical Fiber Communications (OFC 2006)*, Anaheim, CA, paper OWB1.

[Essiambre2006a] R.-J. Essiambre, P. J. Winzer, X. Q. Wang, W. Lee, C. A. White, and E. C. Burrows, "Electronic predistortion and fiber nonlinearity," *IEEE Photon. Technol. Lett.*, vol. 18, no. 17, pp. 1804–1806, 2006.

[Färbert2004] A. Färbert, S. Langenbach, N. Stojanovic, C. Dorschky, T. Kupfer, C. Schulien, J. P. Elbers, H. Wernz, H. Griesser, and C. Glingener, "Performance of a 10.7 Gb/s receiver with digital equaliser using maximum likelihood sequence estimation," in *Proc. European Conference on Optical Communication (ECOC 2004)*, Stockholm, Sweden, paper PD-Th4.1.5.

[Fischer2009] J. K. Fischer and K. Petermann, "Scaling of nonlinear threshold in WDM transmission systems using electronic precompensation of intrachannel nonlinearities," in *Proc. European Conference on Optical Communication (ECOC 2009)*, Vienna, Austria, paper P4.05.

[Fisher1983] R. A. Fisher, B. R. Suydam, and D. Yevick, "Optical phase conjugation for time-domain undoing of dispersive self-phase-modulation effects," *Opt. Lett.*, vol. 8, no. 12, pp. 611–613, 1983.

[Forestieri2000] E. Forestieri, "Evaluating the error probability in lightwave systems with chromatic dispersion, arbitrary pulse shape and pre- and postdetection filtering," *J. Lightwave Technol.*, vol. 18, no. 11, pp. 1493–1503, 2000.

[Forghieri1997] F. Forghieri, R. W. Tkach, and A. R. Chraplyvy, "Fiber nonlinearities and their impact on transmission systems," in *Optical Fiber Telecommunications*, I. P. Kaminov and T. Li, Eds. San Diego, CA: Academic, 1997, vol. IIIa, ch. 8, pp. 196–264.

[Fujitsu2009] Fujitsu Microelectronics Europe GmbH, "Fujitsu launches ultrafast 56 GSa/s 8-bit ADC technology for 100G coherent receivers and high-performance test equipment," *Press release*, February 2009. [Online]. Available: http://www.chais.info

[Gnauck1997] A. H. Gnauck and R. M. Jopson, "Dispersion compensation for optical fiber systems," in *Optical Fiber Telecommunications*, I. P. Kaminov and T. Li, Eds. San Diego, CA: Academic, 1997, vol. IIIa, ch. 7, pp. 162–195.

[Gnauck2004] A. H. Gnauck, X. Liu, X. Wei, D. M. Gill, and E. C. Burrows, "Comparison of modulation formats for 42.7-

Gb/s single-channel transmission through 1980 km of SSMF," *IEEE Photon. Technol. Lett.*, vol. 16, no. 3, pp. 909–911, 2004.

[Gnauck2005] A. H. Gnauck and P. J. Winzer, "Optical phase-shift-keyed transmission," *J. Lightwave Technol.*, vol. 23, no. 1, pp. 115–130, 2005.

[Gordon1990] J. P. Gordon and L. F. Mollenauer, "Phase noise in photonic communications systems using linear amplifiers," *Opt. Lett.*, vol. 15, no. 23, pp. 1351–1353, 1990.

[Green2001] P. Green, "Progress in optical networking," *IEEE Commun. Mag.*, vol. 39, no. 1, pp. 54–61, Jan. 2001.

[Griffin2002] R. A. Griffin and A. C. Carter, "Optical differential quadrature phase-shift key (oDQPSK) for high capacity optical transmission," in *Proc. Conference on Optical Fiber Communication (OFC 2002)*, paper WX6.

[Hanik2004] N. Hanik, A. Ehrhardt, A. Gladisch, C. Peucheret, P. Jeppesen, L. Molle, R. Freund, and C. Caspar, "Extension of all-optical network-transparent domains based on normalized transmission sections," *J. Lightwave Technol.*, vol. 22, no. 6, pp. 1439–1453, 2004.

[Hellerbrand2007] S. Hellerbrand, C. Weber, N. Hanik, and K. Petermann, "Advanced modulation formats for electronic predistortion of intra-channel nonlinearities at 40 Gbit/s," in *Proc. European Conference on Optical Communication (ECOC 2007)*, Berlin, Germany, paper We6.2.4.

[Hill1977] D. R. Hill, A. Jessop, and P. J. Howard, "A 140 Mbit/s field demonstration system," in *Proc. 3rd European Conference on Optical Communication (ECOC 1977)*, Munich, Germany, paper pp. 240-242.

[Hlawatsch1992] F. Hlawatsch and G. F. Boudreaux-Bartels, "Linear and quadratic time-frequency signal representations," *IEEE Signal Processing Mag.*, vol. 9, no. 2, pp. 21–67, 1992.

[Huurdeman2003] A. A. Huurdeman, *The Worldwide History of Telecommunications*. Hoboken, NJ: John Wiley & Sons, 2003.

[Ip2008] E. Ip and J. M. Kahn, "Compensation of dispersion and nonlinear impairments using digital backpropagation," *J. Lightwave Technol.*, vol. 26, no. 20, pp. 3416–3425, 2008.

[Ip2009] ——, "Fiber impairment compensation using coherent detection and digital signal processing," *J. Lightwave Technol.*, p. to be published, 2009.

[Jansen2005] S. L. Jansen, D. van den Borne, A. Schöpflin, E. Gottwald, P. M. Krummrich, G. D. Khoe, and H. de Waardt, "26x42.8-Gbit/s DQPSK transmission with 0.8-bit/s/Hz spectral efficiency over 4,500-km SSMF using optical phase conjugation," in *Proc. European Conference on Optical Communication (ECOC 2005)*, Glasgow, UK, paper Th 4.1.5.

[Jansen2007] S. L. Jansen, I. Morita, D. van den Borne, G. D. Khoe, H. de Waardt, and P. M. Krummrich, "Experimental study of XPM in 10-Gb/s NRZ precompensated transmission systems," in *Proc. Conference Optical Fiber Communications (OFC 2007)*, Anaheim, CA, paper OThS6.

[Kikuchi1997] N. Kikuchi, K. Sekine, and S. Sasaki, "Analysis of cross-phase modulation (xpm) effect on WDM transmission performance," *Electron. Lett.*, vol. 33, no. 8, pp. 653–654, 1997.

[Kikuchi2006] K. Kikuchi, "Phase-diversity homodyne detection of multilevel optical modulation with digital carrier phase estimation," *Selected Topics in Quantum Electronics, IEEE Journal of*, vol. 12, no. 4, pp. 563–570, 2006.

[Killey2000] R. I. Killey, H. J. Thiele, V. Mikhailov, and P. Bayvel, "Reduction of intrachannel nonlinear distortion in 40-Gb/s-based WDM transmission over standard fiber," *IEEE Photon. Technol. Lett.*, vol. 12, no. 12, pp. 1624–1626, 2000.

[Killey2005] R. I. Killey, P. M. Watts, V. Mikhailov, M. Glick, and P. Bayvel, "Electronic dispersion compensation by signal predistortion using digital processing and a dual-

drive Mach-Zehnder modulator," *IEEE Photon. Technol. Lett.*, vol. 17, no. 3, pp. 714–716, 2005.

[Killey2005b] R. I. Killey, P. M. Watts, M. Glick, and P. Bayvel, "Electronic precompensation techniques to combat dispersion and nonlinearities in optical transmission," in *Proc. European Conference on Optical Communication (ECOC 2005)*, Glasgow, UK, paper Tu4.2.1.

[Killey2006] ——, "Electronic dispersion compensation by signal predistortion," in *Proc. Conference Optical Fiber Communications (OFC 2006)*, Anaheim, CA, paper OWB3.

[Klekamp2006] A. Klekamp, F. Buchali, M. Audoin, and H. Bulow, "Nonlinear limitations of electronic dispersion precompensation by intrachannel effects," in *Proc. Conference Optical Fiber Communications (OFC 2006)*, Anaheim, CA, 2006, paper OWR1.

[Koch1985] T. Koch and R. Alferness, "Dispersion compensation by active predistorted signal synthesis," *J. Lightwave Technol.*, vol. 3, no. 4, pp. 800–805, 1985.

[Krummrich2004] P. Krummrich and K. Kotton, "Extremely fast (microsecond scale) polarization changes in high speed long haul WDM transmission systems," in *Proc. Conference on Optical Fiber Communication (OFC 2004)*, Los Angeles, CA, paper FI3.

[Li2003] G. L. Li and P. K. L. Yu, "Optical intensity modulators for digital and analog applications," *J. Lightwave Technol.*, vol. 21, no. 9, pp. 2010–2030, 2003.

[Li2008] X. Li, X. Chen, G. Goldfarb, E. Mateo, I. Kim, F. Yaman, and G. Li, "Electronic post-compensation of WDM transmission impairments using coherent detection and digital signal processing," *Optics Express*, vol. 16, no. 2, pp. 880–888, 2008.

[Liu2006] X. Liu and D. A. Fishman, "A fast and reliable algorithm for electronic pre-equalization of SPM and chromatic dispersion," in *Proc. Conference Optical Fiber Communications (OFC 2006)*, Los Angeles, CA, paper OThD4.

[Marcuse1991] D. Marcuse, "Calculation of bit-error probability for a lightwave system with optical amplifiers and post-detection Gaussian noise," *J. Lightwave Technol.*, vol. 9, no. 4, pp. 505–513, April 1991.

[McGhan2006] D. McGhan, M. O'Sullivan, C. Bontu, and K. Roberts, "Electronic dispersion compensation," in *Proc. Conference Optical Fiber Communications (OFC 2006)*, Anaheim, CA, paper Tutorial OWK1.

[McNicol2005] J. McNicol, M. O'Sullivan, K. Roberts, A. Comeau, D. McGhan, and L. Strawczynski, "Electrical domain compensation of optical dispersion," in *Proc. Conference Optical Fiber Communications (OFC 2005)*, Anaheim, CA, paper OThJ3.

[Nelson2009] L. E. Nelson, S. L. Woodward, S. Foo, X. Zhou, M. D. Feuer, D. Hanson, D. McGhan, H. Sun, M. Moyer, M. O. Sullivan, and P. D. Magill, "Performance of a 46-Gbps dual-polarization QPSK transceiver with real-time coherent equalization over high PMD fiber," *J. Lightwave Technol.*, vol. 27, no. 3, pp. 158–167, 2009.

[Nortel2006] Nortel Networks, "Breaking the physical barriers with electronic dynamically compensating optics (eDCO)," *White Paper*, April 2006.

[Ohm2005] M. Ohm, R. J. Essiambre, and P. J. Winzer, "Nonlinear phase noise and distortion in 42.7-Gbit/s RZ-DPSK systems," in *Proc. European Conference on Optical Communication (ECOC 2005)*, paper Tu1.2.1.

[O'Sullivan2005] M. S. O'Sullivan, K. Roberts, and C. Bontu, "Electronic dispersion compensation techniques for optical communication systems," in *Proc. European Conference on Optical Communication (ECOC 2005)*, Glasgow, UK, paper Tu3.2.1.

[Pare1996] C. Paré, A. Villeneuve, P.-A. Bélanger, and N. J. Doran, "Compensating for dispersion and the nonlinear Kerr effect without phase conjugation," *Opt. Lett.*, vol. 21, no. 7, pp. 459–461, Apr. 1996.

[Poggiolini2007] P. Poggiolini, G. Bosco, M. Visintin, S. J. Savory, Y. Benlachtar, P. Bayvel, and R. I. Killey, "MLSE-EDC versus optical dispersion compensation in a single-channel SPM-limited 800 km link at 10 Gbit/s," in *Proc. European Conference on Optical Communication (ECOC 2007)*, Berlin, Germany, 2007, paper Th9.1.3.

[Poggiolini2009] P. Poggiolini, A. Carena, V. Curri, and F. Forghieri, "Evaluation of the computational effort for chromatic dispersion compensation in coherent optical PM-OFDM and PM-QAM systems," *Opt. Express*, vol. 17, no. 3, pp. 1385–1403, 2009.

[Randel2005] S. Randel, "Analyse faseroptischer Übertragungssysteme mit Wellenlängenmultiplex bei 160 Gbit/s Kanaldatenrate," Ph.D. dissertation, Technische Universität Berlin, 2005.

[Roberts2005] K. Roberts, "Advanced optical technologies for data intensive applications," in *iGrid2005*, San Diego, CA. [Online]. Available: www.igrid2005.org

[Roberts2006] K. Roberts, C. Li, L. Strawczynski, M. O'Sullivan, and I. Hardcastle, "Electronic precompensation of optical nonlinearity," *IEEE Photon. Technol. Lett.*, vol. 18, no. 2, pp. 403–405, 2006.

[Roberts2008] K. Roberts, "Digital compensation of the optical line: Pre-distortion Tx & coherent Rx," in *Digest of the IEEE/LEOS Summer Topical Meetings*, July 2008, paper WD2.2, pp. 245–246.

[Sano2001] A. Sano and Y. Miyamoto, "Performance evaluation of prechirped RZ and CS-RZ formats in high-speed transmission systems with dispersion management," *J. Lightwave Technol.*, vol. 19, no. 12, pp. 1864–1871, 2001.

[Savory2005] S. J. Savory, A. Napoli, B. Thomsen, P. Bayvel, and R. I. Killey, "Robust optical systems using maximum likelihood sequence estimators," in *IEE Seminar on Optical Fibre Communications and Electronic Signal Processing*, Dec. 2005.

[Savory2006] S. J. Savory, "Optimum electronic dispersion compensation strategies for nonlinear transmission," *Electronics Letters*, vol. 42, no. 7, pp. 407–408, 2006.

[Savory2007] S. J. Savory, G. Gavioli, R. I. Killey, and P. Bayvel, "Electronic compensation of chromatic dispersion using a digital coherent receiver," *Opt. Express*, vol. 15, no. 5, pp. 2120–2126, 2007.

[Savory2007a] S. J. Savory, "Coherent detection – why is it back?" in *Proc. Annual Meeting of the IEEE Lasers and Electro-Optics Society (LEOS 2007)*, paper TuH1, pp. 212–213.

[Schüppert2009] M. Schüppert, *Einfluss der Fasernichtlinearitäten in WDM-OOK-Übertragungssystemen mit elektronischer Dispersionsvorkompensation*. Diploma thesis, Technische Universität Berlin, Fachgebiet Hochfrequenztechnik, July 2009.

[Schvan2005] P. Schvan, D. Pollex, and T. Bellingrath, "A 22 GS/s 6b DAC with integrated digital ramp generator," in *Proc. Digest of Technical Papers Solid-State Circuits Conference (ISSCC 2005)*, 2005, pp. 122–588 Vol. 1.

[Serena2007] P. Serena, A. Orlandini, and A. Bononi, "The memory of optimized dispersion-managed periodic optical links," in *Proc. European Conference on Optical Communication (ECOC 2007)*, Berlin, Germany, paper P093.

[Shake1998] I. Shake, H. Takara, K. Mori, S. Kawanishi, and Y. Yamabayashi, "Influence of inter-bit four-wave mixing in optical TDM transmission," *Electron. Lett.*, vol. 34, no. 16, pp. 1600–1601, 1998.

[Shtaif2008] M. Shtaif, "The changing paradigm of terrestrial long-haul transmission system design," in *Proc. International Conference on Transparent Optical Networks (ICTON 2008)*, Athens, Greece, paper Mo.D1.3.

[Sinkin2003] O. V. Sinkin, R. Holzlöhner, J. Zweck, and C. R. Menyuk, "Optimization of the split-step Fourier method in modeling optical-fiber communications systems," *J. Lightwave Technol.*, vol. 21, no. 1, pp. 61–68, 2003.

[Sun2008] H. Sun, K.-T. Wu, and K. Roberts, "Real-time measurements of a 40 Gb/s coherent system," *Opt. Express*, vol. 16, no. 2, pp. 873–879, 2008.

[Warm2008] S. Warm, C.-A. Bunge, T. Wuth, and K. Petermann, "Electronic dispersion precompensation using a directly modulated laser," in *Proc. European Conference on Optical Communication (ECOC 2008)*, Brussels, Belgium, paper P.4.07.

[Watanabe1993] S. Watanabe, T. Naito, and T. Chikama, "Compensation of chromatic dispersion in a single-mode fiber by optical phase conjugation," *IEEE Photon. Technol. Lett.*, vol. 5, no. 1, pp. 92–95, 1993.

[Watts2005] P. M. Watts, V. Mikhailov, S. Savory, P. Bayvel, M. Glick, M. Lobel, B. Christensen, P. Kirkpatrick, S. Shang, and R. I. Killey, "Performance of single-mode fiber links using electronic feed-forward and decision feedback equalizers," *IEEE Photon. Technol. Lett.*, vol. 17, no. 10, pp. 2206–2208, 2005.

[Watts2007] P. M. Watts, M. Glick, P. Bayvel, and R. I. Killey, "Performance of electronic predistortion systems with 1 sample/bit processing using optical duobinary format," in *Proc. European Conference on Optical Communication (ECOC 2007)*, Berlin, Germany, paper Tu3.1.6.

[Watts2007a] P. M. Watts, R. Waegemans, M. Glick, P. Bayvel, and R. I. Killey, "An FPGA-based optical transmitter design using real-time DSP for advanced signal formats and electronic predistortion," *J. Lightwave Technol.*, vol. 25, no. 10, pp. 3089–3099, Oct. 2007.

[Weber2006] C. Weber, J. K. Fischer, C.-A. Bunge, and K. Petermann, "Electronic precompensation of intrachannel nonlinearities at 40 Gb/s," *IEEE Photon. Technol. Lett.*, vol. 18, no. 16, pp. 1759–1761, 2006.

[Weber2006a] ——, "Electronic precompensation of intra-channel nonlinearities at 40 Gbit/s," in *Proc. European Conference on Optical Communication (ECOC 2006)*, Cannes, France, paper We1.5.4.

[Weber2007] C. Weber, "Electronic mitigation of chromatic dispersion and fibre nonlinearities," in *Proc. 2nd Sino-German Symposium on Optical Communication Networks (SOCN)*, Berlin, Germany, Sept. 11-16 2007.

[Weber2008] C. Weber and K. Petermann, "Impact of fibre nonlinearities in electronic dispersion compensation systems at 40 Gb/s," in *Proc. European Conference on Optical Communication (ECOC 2008)*, Brussels, Belgium, paper P.4.10.

[Weber2009] C. Weber, C.-A. Bunge, M. Winter, and K. Petermann, "Fibre nonlinearities in 10 and 40 Gb/s electronically dispersion precompensated WDM transmission," in *Proc. Conference on Optical Fiber Communication (OFC 2009)*, San Diego, CA, paper OTuD2.

[Weber2009a] C. Weber, C.-A. Bunge, and K. Petermann, "Fiber nonlinearities in systems using electronic predistortion of dispersion at 10 and 40 Gbit/s," *J. Lightwave Technol.*, vol. 27, no. 16, pp. 3654–3661, Aug. 2009.

[Wickham2004] L. K. Wickham, R.-J. Essiambre, A. H. Gnauck, P. J. Winzer, and A. R. Chraplyvy, "Bit pattern length dependence of intrachannel nonlinearities in pseudolinear transmission," *IEEE Photon. Technol. Lett.*, vol. 16, no. 6, pp. 1591–1593, 2004.

[Winzer2001] P. J. Winzer, M. Pfennigbauer, M. M. Strasser, and W. R. Leeb, "Optimum filter bandwidths for optically preamplified NRZ receivers," *J. Lightwave Technol.*, vol. 19, no. 9, pp. 1263–1273, 2001.

[Winzer2005] P. J. Winzer and R.-J. Essiambre, "Electronic predistortion for advanced modulation formats," in *Proc. European Conference on Optical Communication (ECOC 2005)*, Glasgow, UK, 2005, paper Tu4.2.2.

[Winzer2006] ——, "Advanced optical modulation formats," *Proc. IEEE*, vol. 94, no. 5, pp. 952–985, May 2006.

[Winzer2007] P. J. Winzer and G. Raybon, "100G ethernet a review of serial transport options," in *Digest of the IEEE/LEOS Summer Topical Meetings 2007*, July 2007, pp. 7–8.

[Xia2007] C. Xia and W. Rosenkranz, "Nonlinear electrical equalization for different modulation formats with optical filtering," *J. Lightwave Technol.*, vol. 25, no. 4, pp. 996–1001, April 2007.

[Xie2006] C. Xie and R.-J. Essiambre, "Intra-channel nonlinearity compensation in 40-Gb/s systems by combining electronic pre-distortion and optical dispersion compensation," in *Proc. European Conference on Optical Communication (ECOC 2006)*, Cannes, France, 2006, paper We3.P.82.

[Xie2007] C. Xie, "Performance of electronic pre-distortion in 40-Gb/s systems with optical dispersion compensation for different modulation formats and transmission fibres," in *Proc. European Conference on Optical Communication (ECOC 2007)*, Cannes, France, 2007, paper Tu3.1.5.

[Yang2006] H. Yang, C. Peucheret, T. Tokle, and P. Jeppesen, "Comparison of practical implementation limitations for different electronic pre-distortion transmitter structures," in *Proc. European Conference on Optical Communication (ECOC 2006)*, Cannes, France, 2006, paper We1.5.2.

[Yariv1979] A. Yariv, D. Fekete, and D. M. Pepper, "Compensation for channel dispersion by non-linear optical phase conjugation," *Optics Letters*, vol. 4, no. 2, pp. 52–54, 1979.